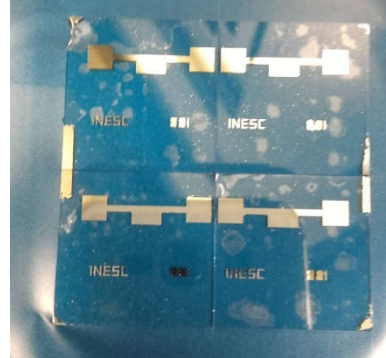
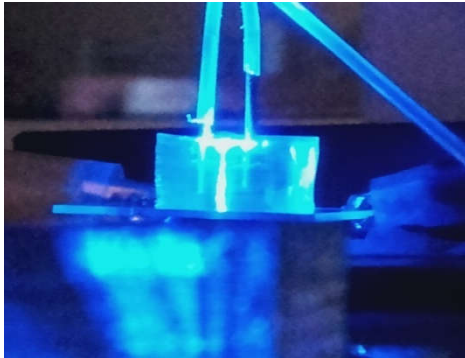


UNIVERSIDADE DE LISBOA
INSTITUTO SUPERIOR TÉCNICO



Microfluidic separation using aqueous two phase systems

Daniel Filipe Camarneiro Silva

Supervisor: Doctor Maria Raquel Múrias dos Santos Aires Barros
Co-supervisor: Doctor Virginia Chu

Thesis approved in public session to obtain the PhD Degree in
Biotechnology and Biosciences

Jury final classification: Pass with distinction

2018

UNIVERSIDADE DE LISBOA
INSTITUTO SUPERIOR TÉCNICO

Microfluidic separation using aqueous two phase systems

Daniel Filipe Camarneiro Silva

Supervisor: Doctor Maria Raquel Múrias dos Santos Aires Barros
Co-supervisor: Doctor Virginia Chu

Thesis approved in public session to obtain the PhD Degree in
Biotechnology and Biosciences

Jury final classification: Pass with distinction

Jury

Chairperson: Doctor João Pedro Estrela Rodrigues Conde, Instituto Superior Técnico, Universidade de Lisboa

Members of the committee:

Doctor José António Couto Teixeira, Escola de Engenharia, Universidade do Minho

Doctor Maria Raquel Múrias dos Santos Aires Barros, Instituto Superior Técnico, Universidade de Lisboa

Doctor João Pedro Estrela Rodrigues Conde, Instituto Superior Técnico, Universidade de Lisboa

Doctor Pedro Carlos de Barros Fernandes, Instituto Superior Técnico, Universidade de Lisboa

Doctor Abel Martín González Oliva, Instituto de Tecnologia Química e Biológica António Xavier, Universidade Nova de Lisboa

Funding institution

Fundação para a ciência e a tecnologia

2018

I Resumo

O despertar do estilo de vida moderno nas últimas décadas aumentou enormemente a importância e necessidade de uma grande variedade de biomoléculas. Como tal, a sua produção foi, ao longo dos anos, muito melhorada para aumentar a disponibilidade de biomoléculas. Todavia, certos sectores, como o da medicina, requerem alto teor de pureza e, como tal, existe actualmente uma crescente demanda por técnicas de separação e purificação que sejam eficientes, escaláveis e económicas. Os sistemas aquáticos bifásicos (ATPS) em particular, têm mostrado um potencial interessante para o processamento de biomoléculas.

A primeira fase deste trabalho tem como objectivo o desenvolvimento de um dispositivo microfluidico integrado para a purificação de anticorpos a partir de um meio complexo, usando ATPS como instrumento para acelerar a etapa de concepção de forma económica. Imunoglobulina G (IgG) purificada foi usada como sistema modelo. A partição de IgG marcada com isotiocianato de fluoresceína (FITC) num ATPS composto de polietilenoglicol(PEG) e tampão de fosfatos com cloreto de sódio (NaCl) foi testada em vários dispositivos microfluidicos. A estrutura final usada foi um microcanal com 16,8 cm de comprimento com três entradas e três saídas. Difusão completa foi atingida com velocidades menores que 1 $\mu\text{L}/\text{min}$, mas o fluxo dentro do microcanal era instável. Obter o rendimento do processo não foi possível devido a um erro de quantificação, mas valores teóricos atingem os 90% e o coeficiente de partição (K_p), obtido a partir de valores de fluorescência dentro do microcanal, foi de 2,15. Adicionalmente, o sistema provou ser fácil de simular

Durante o trabalho desta tese, também tentamos caracterizar o comportamento de ATPS dentro de um dispositivo microfluidico. Assim, microscopia confocal foi usada para determinar como a interface de um ATPS se comporta dentro de um canal microfluidico. Microscopia confocal é uma técnica de microscopia fluorescente que pode isolar planos horizontais de vista e, usando programas informáticos apropriados, reconstruir os planos obtidos num modelo 3D da amostra a ser estudada. Microscopia confocal é uma técnica que necessita fluorescência na amostra e, como tal, insulina marcada com FITC foi usada para este propósito. Devido ao K_p da insulina nos ATPS usados, à volta de 13 para o ATPS de PEG/tampão de fosfatos e à volta de 4 para o ATPS de PEG/dextrano, a adição de insulina-FITC ao ATPS cria um contraste agudo entre as duas fases quando usada em microscopia confocal. Microscopia confocal permitiu-nos ver a interface em condições microfluidicas e determinar que não se trata de uma barreira direita mas sim uma curva que favorece a interação entre a fase rica em PEG e a parede de polidimetilsiloxano(PDMS).

Devido ao aumento da importância de ATPSs em processos de separação e purificação, caracterização de ATPS também se tornou numa parte essencial do uso de

ATPSs. Para facilitar o uso de ATPS, desenvolveu-se um dispositivo microfluidico com o objectivo de eficiente e rapidamente caracterizar a curva binodal de ATPSs. Soluções padrão contendo PEG, tampão de fosfatos e dextrano foram usados para testar o dispositivo microfluidico. O dispositivo microfluidico era um canal com 20,5 cm de comprimento, 150 μm de largura e 20 μm de altura com três entradas. Para cada ATPS usados como teste, duas das soluções de padrão apropriadas foram inseridas junto com água milli-Q no dispositivo microfluidico. A mistura cria uma solução cuja composição é dependente da velocidade volumétrica das soluções padrão e da água milli-Q. As imagens microscópicas obtidas mostram uma clara distinção entre as soluções que formam uma interface e as soluções que não formam interfaces. Adicionalmente, a curva binodal que foi determinada usando este método é semelhante à curva binodal determinada usando o método de titração turbidometrico.

O passo seguinte na caracterização de ATPS foi desenvolver um método para rapidamente determinar K_p num dispositivo microfluidico. O método desenvolvido para este objectivo tem muitas similaridades com o método usado para a determinação de curvas binodais. A determinação de K_p foi feita para insulina-FITC, IgG-FITC, Proteína A(Prot-A)-FITC, Albumina de Soro Bovino(BSA)-FITC e Proteína Fluorescente Verde(GFP). GFP não necessita de um marcador de FITC já que a GFP já é fluorescente por si mesma. Consequentemente, no fim do microcanal onde a difusão deverá estar completa, microscopia fluorescente é usada para determinar o K_p da biomolécula que está a ser testada. Este método provou ser capaz de facilmente determinar valores de K_p . Além disso, os valores de K_p obtidos usando este método são semelhantes aos valores de K_p obtidos usando métodos de determinação em macroescala.

O trabalho final desenvolvido no âmbito desta tese foi estudar a possibilidade de integração de outros métodos de separação já estabelecidos com o uso de microATPS. O método escolhido para ser integrado foi a electroforese. Electroforese é uma técnica que envolve o estabelecimento de um campo eléctrico que é aplicado a uma solução. O campo eléctrico irá influenciar o movimento de solutos com carga eléctrica. Integrado com o uso de ATPS em dispositivos microfluidicos, a electroforese irá aumentar ou diminuir os valores de K_p de biomoléculas. Os eléctrodos são eléctrodos de Alumínio(Al) gravados num substrato de vidro que é usado para selar o dispositivo microfluidico. Os eléctrodos são inicialmente gravados sem uma lacuna entre os dois eléctrodos que é depois gravada fluindo uma solução de gravação de Al. As biomoléculas usadas para este estudo foram a Prot-A, IgG, BSA e insulina, todas marcadas com FITC, para que a sua difusão pudesse ser seguida usando microscopia de fluorescência. A gravação *in situ* da lacuna entre os eléctrodos é um método rápido e fiável para replicar o alinhamento entre o microcanal e os eléctrodos. Adicionalmente, a integração de electroforese provou ser efectiva, pois foram observadas alterações nos valores de K_p quando o campo eléctrico foi aplicado.

Palavras-Chave: Soluções aquosas bifasicas, microfluidos, separação e purificação de biomoléculas, microscopia de fluorescência, determinação de coeficientes de partição

II Abstract

The advent of the modern life in the last few decades have brought a greatly increased need for a wide variety of biomolecules. Production of said biomolecules have, thus, been greatly refined to increase their availability. However, certain fields, such as the medical field, require materials with high purity. Thus there is an increasing demand for efficient, scalable and cost-effective techniques for separation and purification of biomolecules. In particular, aqueous two phase systems (ATPS) have shown interesting potential for downstream processing.

The first stage of this work has the aim to develop an integrated lab-on-a-chip microfluidic device for antibody purification from complex medium, using ATPS, as a tool to accelerate bioprocess design in a cost-effective manner. Pure immunoglobulin G (IgG) was used as a model system. The partition of IgG tagged with fluorescein isothiocyanate (FITC) in Polyethyleneglycol (PEG)/phosphate buffer with NaCl in ATPS was investigated in a microfluidic device. The final structure was a 16,8 cm microchannel with three inlets and three outlets. Complete diffusion was achieved at volumetric rates lower than $1\mu\text{L}/\text{min}$. Obtaining the process's yield was not possible due to a quantification error, but theoretical values reach 90% and the partition coefficient (K_p) was calculated from the fluorescent values at 2,15. Additionally, the system has proven to be easily predictable with simulations from Comsol or other means.

During the work of this thesis, we also attempted to characterize the behavior of the ATPS in the microfluidic setting. In order to do this, confocal microscopy was used to determine how the ATPS interface behaves in the microfluidic channel. Confocal microscopy is a fluorescence microscopy technique that can isolate horizontal planes of view and, using appropriate software, reconstruct the planes into a 3D model of the sample. Confocal microscopy requires fluorescence in the sample, therefore insulin marked with FITC was used. Due to the coefficient partition of insulin in the ATPSs used, the introduction of insulin-FITC into the ATPS creates a sharp contrast between the two phases. Confocal microscopy allowed us to see the interface and to determine that it is not a straight barrier but that is curved in a way that favors the interaction between the PEG-rich phase and the PolyDiMethylSiloxane (PDMS) wall.

Due to the rising importance of ATPS in separation and purification processes, characterization of said ATPS has also become an essential part of ATPS use. For this purpose a microfluidic platform was devised to quickly characterize the ATPS binodal curve. Stock solutions containing PEG, phosphate buffer and dextran were used to test the microfluidic platform. The microfluidic platform was a 20,5 cm microchannel with a width of $150\mu\text{m}$ and a height of $20\mu\text{m}$ and three inlets. For each ATPS used as test, two of the appropriated stock solutions were inserted along with milli-Q water into the microchannel. The mixture will create a solution whose composition is dependent of the loading rate of the solutions. The microscopy images show that there is a clear distinction between the solutions that form a interface from the

solutions that do not. Furthermore, the binodal curve determined using this method is similar to the binodal curve determined using the turbidometric titration method.

The next step of ATPS characterization was to develop a method to rapidly determine K_p in a microfluidic setting. The method developed for this purpose has many similarities with the method used for binodal curve determination with the same microchannel and solutions. The determination of the K_p was performed for insulin-FITC, IgG-FITC, Protein A (Prot-A)-FITC, Bovine Serum Albumin(BSA)-FITC and Green Fluorescent Protein(GFP). GFP does not need a FITC marker since GFP is already fluorescent by itself. Thus, at the end of the microchannel, where diffusion would be complete, fluorescent microscopy is used to be able to determine the K_p of the biomolecule that is being tested. This method has proved capable to predict values of K_p easily. Furthermore, the K_p values obtained using this method is similar to the K_p values obtained using a macroscale and more established method.

The final work of the thesis was to study the possibility of integration of microfluidic ATPS with other established methods of biomolecules separation and purification. The method chosen to be integrated is electrophoresis. Electrophoresis is a technique where a electrical field is applied to a solution. The electrical field will influence the motion of any charged solute in the solution. Integrated with a miniaturized ATPS this will mean an increase or decrease in the biomolecules K_p . The electrodes are Aluminum (Al) electrodes etched into a glass substrate which are then used to seal the microfluidic device. The electrodes are initially etched without a gap between them which is etched by flowing Al etching solution in the microchannel. The biomolecules used for this study were Prot-A, IgG, BSA and insulin all marked with FITC so that their diffusion can be followed using fluorescent microscopy. The in situ etching of the electrode gap provided a fast and easy to replicate alignment. Furthermore, the integration of the electrophoresis proved successful by altering the K_p observed for the biomolecules when the electrical field was applied.

Key-words: Aqueous two phase systems, microfluidics, separation and purification of biomolécules, fluorescent microscopy, determination of partition coefficients

III Resumo alargado em português

O despertar do estilo de vida moderno nas últimas décadas aumentou enormemente a importância e necessidade de uma grande variedade de biomoléculas. Como tal, a sua produção foi, ao longo dos anos, muito melhorada para aumentar a disponibilidade de biomoléculas. Todavia, certos sectores, como o da medicina, requerem materiais com alto teor de pureza e, como tal, existe hoje em dia uma crescente demanda por técnicas de separação e purificação que sejam eficientes, escaláveis e económicas. Os sistemas aquáticos bifásicos (ATPS) em particular, têm mostrado um potencial interessante para o processamento de biomoléculas.

A primeira fase deste trabalho tem como objectivo o desenvolvimento de um dispositivo microfluidico integrado para a purificação de anticorpos a partir de um meio complexo, usando ATPS como instrumento para acelerar a etapa de concepção de forma económica. Imunoglobulina G (IgG) previamente purificada foi usada como sistema modelo. ATPS permite integração de processos e processamento em larga escala de grandes quantidades de substâncias biológicas ao mesmo tempo que estabelece um meio não-tóxico. Apesar de a conceptualização e optimização de processos envolvendo ATPS serem demorados e requererem grandes volumes de materiais, o desenvolvimento de dispositivos lab-on-a-chip eficientes pode superar estes problemas. Ademais, dispositivos microfluidicos aproximam processos em escala laboratorial a processos em larga escala. A partição de IgG marcada com isotiocianato de fluoresceína (FITC) num ATPS composto de polietilenoglicol(PEG)/tampão de fosfatos com cloreto de sódio(NaCl) foi testada em vários dispositivos microfluidicos. A estrutura final usada foi um microcanal com 16,8 cm de comprimento com três entradas e três saídas. Difusão completa foi atingida com velocidades menores que 1 $\mu\text{L}/\text{min}$, mas o fluxo dentro do microcanal era instável. Aumentar a velocidade para 2 $\mu\text{L}/\text{min}$ estabilizou o fluxo, mas a difusão não era completa. Obter o rendimento do processo não foi possível devido a um erro de quantificação, mas valores teóricos atingem os 90% e o coeficiente de partição (K_p), obtido a partir de valores de fluorescência dentro do microcanal, foi de 2,15. Adicionalmente, o sistema provou ser facilmente previsível usando simulações como Comsol e outros.

Durante o trabalho desta tese, também tentamos caracterizar o comportamento de ATPS dentro de um dispositivo microfluidico. Assim, microscopia confocal foi usada para determinar como a interface de um ATPS se comporta dentro de um canal microfluidico. Microscopia confocal é uma técnica de microscopia fluorescente que pode isolar planos horizontais de vista e, usando programas informáticos apropriados, reconstruir os planos obtidos num modelo 3D da amostra a ser estudada. Os ATPSs escolhidos para estudo foram ATPS compostos de PEG/tampão de fosfatos e PEG/dextranos. A composição do ATPS de PEG/tampão de fosfatos era de 14,5%/11,7%, respectivamente, e a composição do ATPS de PEG/dextrano era de 15,8%/9,5%, respectivamente. Microscopia confocal é uma técnica que

necessita fluorescência na amostra e, como tal, insulina marcada com FITC foi usada para este propósito. Devido ao K_p da insulina nos ATPS usados, à volta de 13 para o ATPS de PEG/tampão de fosfatos e à volta de 4 para o ATPS de PEG/dextrano, a adição de insulina-FITC ao ATPS cria um contraste agudo entre as duas fases quando usada em microscopia confocal. Microscopia confocal permitiu-nos ver a interface em condições microfluídicas e determinar que não se trata de uma barreira direita mas sim uma curva que favorece a interação entre a fase rica em PEG e a parede de polidimetilsiloxano(PDMS).

Devido ao aumento da importância de ATPSs em processos de separação e purificação, caracterização de ATPS também se tornou numa parte essencial do uso de ATPSs. Para facilitar o uso de ATPS, desenvolveu-se um dispositivo microfluidico com o objectivo de eficiente e rapidamente caracterizar a curva binodal de ATPSs. A curva binodal é uma linha expressa em gráficos de ATPSs que plotam a concentração de um dos componentes do ATPS contra a concentração do outro componente e representa o limiar a partir do qual a solução forma uma interface. Soluções padrão contendo PEG, tampão de fosfatos e dextrano foram usados para testar o dispositivo microfluidico. O dispositivo microfluidico era um canal com 20,5 cm de comprimento, 150 μm de largura e 20 μm de altura com três entradas. Para cada ATPS usados como teste, duas das soluções de padrão apropriadas foram inseridas junto com água milli-Q no dispositivo microfluidico. Devido ao fenómeno de difusão, as soluções padrão misturam-se dentro do microcanal, criando um solução cuja composição é dependente da velocidade volumétrica à qual as soluções padrão e a água milli-Q são inseridas no microcanal. Microscopia é usada no fim do microcanal para verificar se existe formação de uma interface. As imagens microscópicas obtidas mostram uma clara distinção entre as soluções que formam uma interface e as soluções que não formam interfaces. Adicionalmente, a curva binodal que foi determinada usando este método é semelhante à curva binodal determinada usando o método de titração turbidometrico, um método em macroescala para a caracterização de ATPS já estabelecido.

O passo seguinte na caracterização de ATPS foi desenvolver um método para rapidamente determinar K_p num dispositivo microfluidico. O método desenvolvido para este objectivo tem muitas similaridades com o método usado para a determinação de curvas binodais. O canal microfluidico usado para este propósito tem um comprimento de 20,5 cm, uma largura de 150 μm , uma altura de 20 μm e três entradas. Soluções padrão de PEG, tampão de fosfatos e dextrano foram inseridos juntamente com água milli-Q nas combinações necessárias para formar cada respectivo ATPS dentro do dispositivo microfluidico. Tal como com a determinação da curva binodal, a composição dos ATPSs dentro do microcanal é determinada pela velocidade volumétrica das soluções padrão e água milli-Q. Os ATPSs usados para teste foram o ATPS composto por PEG/tampão de fosfatos e o ATPS composto por PEG/dextrano. A determinação de K_p foi feita para insulina-FITC, IgG-FITC, Proteína A(Prot-A)-FITC, Albumina de Soro Bovino(BSA)-FITC e Proteína Fluorescente Verde(GFP).

Com a excepção da GFP, todas as biomoléculas usadas foram marcadas com FITC uma vez que a fluorescência produzida pela FITC é usada para determinar a concentração das biomoléculas nas fases para calcular o K_p . GFP não necessita de um marcador de FITC já que a GFP já é fluorescente por si mesma. Consequentemente, no fim do microcanal onde a difusão deverá estar completa, microscopia fluorescente é usada para determinar o K_p da biomolécula que está a ser testada. A natureza rápida do teste de fluorescência e a rápida mudança de concentrações dentro do microcanal em resposta à alteração das velocidade volumétricas, permitem um rápido rastreio de K_p em diferentes composições de ATPS. Este método provou ser capaz de facilmente determinar valores de K_p . Além disso, os valores de K_p obtidos usando este método são semelhantes aos valores de K_p obtidos usando métodos de determinação em macroescala.

O trabalho final desenvolvido no âmbito desta tese foi estudar a possibilidade de integração de outros métodos de separação e purificação de biomoléculas já estabelecidos com o uso de ATPS num dispositivo microfluidico. O método escolhido para ser integrado foi a electroforese. Electroforese é uma técnica que envolve o estabelecimento de um campo eléctrico que é aplicado a uma solução. O campo eléctrico irá influenciar o movimento de qualquer soluto com carga eléctrica, empurrando os solutos com carga negativa para o eléctrodo positivo e os solutos com carga positiva para o eléctrodo negativo. Integrado com o uso de ATPS em dispositivos microfluidicos, a electroforese irá aumentar ou diminuir os valores de K_p de biomoléculas dependendo da carga eléctrica da biomolécula e da direcção do campo eléctrico. Os dispositivos microfluidicos usados para os testes tinham um microcanal com o comprimento de 3 cm, a largura de 50 μm e a altura de 20 μm . Para o uso do ATPS composto de PEG/dextrano, o microcanal tem duas entradas e para o uso do ATPS composto de PEG/tampão de fosfatos, o microcanal tem três entradas. Esta diferença no número de entradas deve-se ao facto de que existe instabilidade no fluxo quando a fase rica em fosfatos é inserida no microcanal numa entrada junto à parede do microcanal. Com três entradas é possível ter a fase rica em fosfatos na entrada do meio com duas fases ricas em PEG a serem inseridas nas entradas laterais. Os eléctrodos são eléctrodos de Alumínio(Al) gravados num substrato de vidro que é então usado para selar o dispositivo microfluidico. Isto permite que os eléctrodos de Al estejam perto do microcanal. Os eléctrodos são inicialmente gravados sem uma lacuna entre os dois eléctrodos. Depois da selagem, a lacuna é então gravada inserindo liquido de gravação de Al, o que permite que os eléctrodos estejam automaticamente alinhados com o microcanal. As biomoléculas usadas para este estudo foram a Prot-A, IgG, BSA e insulina, todas marcadas com FITC, para que a sua difusão pudesse ser seguida usando microscopia de fluorescência. A gravação *in situ* da lacuna entre os eléctrodos é um método rápido e fiável para replicar o alinhamento entre o microcanal e os eléctrodos. Adicionalmente, a integração de electroforese provou ser efectiva, pois foram observadas alterações nos valores de K_p quando o campo eléctrico foi aplicado.

IV Acknowledgements

I would like to thank professor Raquel Aires Barros, professor João Pedro Conde and professor Virginia Chu for all the guidance and help that they offered me during the realization of this work. I would also like to thank Researcher Ana Azevedo and Dr. Pedro Fernandes for their suggestions and availability. A special thanks to Pedro Novo, Diogo Martins, Ruben Soares, Inês Pinto for all the help through this work. And to anyone that have, in one way or another, helped or assisted me during this work, especially the staff and researchers of inesc-mn and Institute for bioengineering and biosciences. Finally, I would like to thank all my family and friends for all the support given especially my parents, Dulce Silva and António Silva

V Contents

I	Resumo	i
II	Abstract	iii
III	Resumo alargado em português	v
IV	Acknowledgements	viii
V	Contents	ix
VI	List of Acronyms and abbreviations	xii
VII	List of Figures	xiv
VIII	List of tables	xxi
1	Introduction	1
2	State of the Art.....	4
2.1	ATPS: An overview.....	4
2.1.1	Diffusion in ATPS	7
2.2	Microfluidics Systems.....	8
2.2.1	ATPS in microfluidic devices.....	12
2.3	SWOT Analysis and Future Trends of ATPS.....	16
3	Methodology	18
3.1	Development of the solutions.....	18
3.2	Microfluidic devices design and fabrication.....	19
3.2.1	AI masks fabrication	19
3.2.2	SU-8 mold fabrication.....	20
3.2.3	PDMS structure fabrication and sealing.....	20
3.3	ATPS and microfluidic devices experiments.....	20

4	IgG separation using a phosphate/PEG ATPS	23
4.1	Study of the microfluidic ATPS interface using confocal microscopy	23
4.2	Simulations development	28
4.2.1	Comsol multiphysics simulations	28
4.2.2	Diffusion progression simulation	33
4.2.3	Yield and final concentration of IgG prediction	35
4.3	IgG separation and purification.....	38
4.3.1	Preliminary microfluidic structure design studies	38
4.3.2	IgG partitioning in ATPS microfluidic device	39
4.3.3	Effect of microchannel length.....	40
4.3.4	Effect of the flow rate of the two phases	42
4.3.5	Macro and microscale comparison	43
4.4	Conclusions	44
5	Aqueous Two Phase Systems characterization in microfluidic devices.....	46
5.1	ATPS formation in a microfluidic device.....	47
5.2	Determination of the binodal curve.....	51
5.3	Conclusions	54
6	Determination of partition coefficients of biomolecules in a microfluidic platform.....	55
6.1	K_p determination within the microfluidic platform using fluorescence	55
6.2	Comparison of the microfluidic and macroscale K_p determination.....	61
6.3	Conclusions	62
7	Electrical field assisted ATPS partition in a microfluidic platform.....	63
7.1	Electrode etching in the microfluidic platform.....	63
7.2	Effect of the electrical field on biomolecule partition.	68

7.3	Conclusions	72
8	Conclusions and future Perspectives	73
9	Bibliography	75

VI List of Acronyms and abbreviations

Monoclonal antibodies - mAbs

Aqueous Two Phase Systems - ATPS

Immunoglobulin G - IgG

Fluorescein isothiocyanate - FITC

Polyethylene glycol - PEG

Polydimethylsiloxane - PDMS

Molecular weight - MW

Isoelectrical point - pI

Aluminum - Al

Partition coefficient - K_p

Protein A - ProA

Bovine Serum Albumin - BSA

Green Fluorescent Protein - GFP

Polymerase Chain Reaction - PCR

Computer aided design - CAD

Propylene glycol methyl ether acetate - PGMEA

Reynolds number - Re

Capillary number - Ca

Water Fraction - wf

Strengths, Weaknesses, Opportunities and Threats - SWOT

isopropyl alcohol - IPA

silica - Si

Rotations per minute - rpm

ultraviolet - UV

Deionized - DI

Incompressible Navier Stokes - INS

finite element method - FEM

partial differential equations - PDE

Péclet number - Pe

VII List of Figures

Figure 2.1 - Aqueous polymer phase diagrams of an ATPS made of PEG 3400/Potassium Phosphate/Water at 4°C. The PEG 3400 is PEG with a molecular weight of 3400 Dalton (Adapted from Silva, et al., 2006).

Figure 2.2 - Diffusion across two different phases (Cussler, 2009).

Figure 2.3 – Scheme for the rapid prototyping of a master in a silicon wafer (Adapted from McDonald, et al., 2000).

Figure 2.4 – The fabrication of micropatterned slabs of PDMS by using replica molding. The master consists of a silicon wafer with features of photoresist in bas-pattern. The PDMS is poured on the master and then cured at 60 or 65 °C for about one hour. After peeling the PDMS, it has the microstructures embossed in its surface (Adapted from Weibel, et al., 2007).

Figure 2.5 – Liquid–liquid two-phase flow patterns: flows at different Capillary number (Ca) and water fraction (wf). The top is an example of segmented flow type, while the bottom is an example of parallel flow type (adapted from Shui, et al., 2007).

Figure 2.6 - Summary of the main strengths, weaknesses, opportunities and threats of ATPS extraction performed at the microscale (Soares, et al., 2015).

Figure 3.1 – Mask for the two inlets and two outlets device, and the three inlets and three outlets device.

Figure 3.2 - Set of 16 glass substrates for electric field aided ATPS extraction. The gap between the electrodes has not been etched yet.

Figure 3.3 - Example of final structure for the electrical field aided ATPS extraction. Picture taken after the gap between the electrodes was etched.

Figure 4.1 - Schematic model of the experimental setup used for measuring ATPSs interface in the confocal microscope. a) Model for the PEG/phosphate buffer ATPS. b) Model for the PEG/dextran ATPS.

Figure 4.2 - Series of micrographs obtained using a confocal microscope. Images a) through h) are all from the same x-y coordinates but the z coordinate changes 2 μm from each image. The images are a close-up of the interface area within a microfluidic channel using a phosphate buffer/PEG ATPS with insulin-FITC dissolved in it. The microchannel is a 3 inlet microchannel with phosphate-rich phase being inserted in the middle inlet at 1 $\mu\text{L}/\text{min}$ and PEG-rich phase being inserted in both side inlets at 0,3 $\mu\text{L}/\text{min}$. The middle black represents the phosphate rich phase that contains little insulin due to high k_p while the grey sides are the PEG-rich phases that are fluorescent due to the presence of Insulin-FITC.

Figure 4.3 - 3D model of the microfluidic channel with phosphate buffer/PEG ATPS being flown. Insulin-FITC was used to distinguish the phases using fluorescence. The middle dark area corresponds to the phosphate-rich phase, while the gray side areas correspond to the PEG-rich phase. This model was obtained by using software to assemble the series of images in figure 4.2.

Figure 4.4 - Image obtained from 3D model from Figure 4.3 Representation of a cross section of the microchannel with a phosphate buffer/PEG ATPS using insulin-FITC to distinguish the phases with fluorescence.

Figure 4.5 - Image obtained from 3D model from a source similar to figure 4.2 with different solution loading rates. Representation of a cross section of the microchannel with a phosphate buffer/PEG ATPS using insulin-FITC to distinguish the phases with fluorescence. The phosphate-rich phase was inserted at 1.2 $\mu\text{L}/\text{min}$ and the PEG-rich phase was inserted at 0,5 $\mu\text{L}/\text{min}$.

Figure 4.6 - Image obtained from 3D model from a source similar to figure 4.2 with different ATPS and different solution loading rates. This image is a representation of a cross section of the microchannel with a dextran/PEG ATPS using insulin-FITC to distinguish the phases with fluorescence. The PEG-rich phase was inserted at 0.3 $\mu\text{L}/\text{min}$ and the dextran-rich phase was inserted at 0.3 $\mu\text{L}/\text{min}$.

Figure 4.7 - Image obtained from 3D model from a source similar to figure 4.2 with different ATPS and different solution loading rates. This image is a representation of a cross section of the microchannel with a dextran/PEG ATPS using insulin-FITC to distinguish the phases with fluorescence. PEG-rich phase was inserted at 0.6 $\mu\text{L}/\text{min}$ and dextran-rich phase was inserted at 0.6 $\mu\text{L}/\text{min}$.

Figure 4.8 – Velocity field predicted by Comsol Multiphysics® for a single phase solution. The solution considered was water ($\rho=1000 \text{ kg}/\text{m}^3$, $\eta=1 \times 10^{-3} \text{ Pa}/\text{s}$) and the velocity in the inlets was 3,125 m/s. The mesh predefined size was extremely fine and was refined once. The final number of mesh elements was 6956.

Figure 4.9 – Salt phase ratio in the microchannel predicted by Comsol using the level set module, detail of the beginning of the microchannel. The mesh was refined several times to a final number of 111296 elements of mesh. The initial trepidation in the interface is a result of numerical instabilities. However, since the ϕ in that area is smooth and between 0 and 1 (see attachments) it does not invalidate the simulation.

Figure 4.10 – Detail of the IgG diffusion Comsol simulation in the microchannel at approximately 7 mm of the beginning. The initial concentration in the salt phase used was of $0,04 \text{ mol/m}^3$. The number of mesh elements was of 98560 and the tuning parameter used for the isotropic artificial diffusion was 0,005.

Figure 4.11 – Simulation of the final IgG concentration in the PEG phase with the variation of R_v , based on equation 4.10. The partition coefficient considered was 2,15 (Rosa, et al., 2007).

Figure 4.12 – Simulation of the yield of the system with the variation of R_v , based on equation 4.7. The partition coefficient considered was 2,15 (Rosa, et al., 2007).

Figure 4.13 - (a) Schematic of the microfluidic structure for the ATPS extraction of antibodies from a salt-rich to PEG-rich phases. The total microchannel length is 16.8 cm. The blue lines are the microchannel walls, the red dotted lines indicate the locations for the interfaces between the salt-rich (center) and PEG-rich (sides) phases, The red arrows indicate the expected direction of antibody diffusion. (b) Detail of the inlets. (c) Detail of the outlets.

Figure 4.14 - Optical (left) and fluorescence (right) micrographs taken at the beginning ($L=0$), at $L=3$ cm and at the end ($L=18.8$ cm) of the extraction microchannel. The salt-rich phase containing IgG with a concentration of 2 mg/mL was introduced through the middle inlet with a volumetric pumping rate of $1 \text{ } \mu\text{L/min}$ and the PEG-rich phases were introduced through the side inlets with a volumetric pumping rate of $0,2 \text{ } \mu\text{L/min}$. L is the distance from the beginning of the microchannel. In the fluorescence micrographs, the boundaries of the microchannel are indicated with a dashed white line.

Figure 4.15 - Fluorescence intensity profiles across the width of the microchannel structure at $L=0$, 2.2, and 14.8 cm from the inlet. The profiles show the evolution of the concentration of the FITC-tagged IgG from being exclusively in the salt-rich phase at the beginning of the microchannel (solid) to its partitioning to the PEG-rich phase along the channel (dashed) to its diffusion within the PEG-rich phase at the end (dotted).

Figure 4.16 - (a) Fluorescence intensity slope for the PEG-rich phase along the channel, with detail showing the tangent of the PEG-rich phase data, and (b) average IgG concentration for the PEG-rich phase for the serpentine like structures with extraction microchannels 10.45 cm and 16.8 cm of length. The ATPS used was made with 7.04% of PEG, 16.37% of phosphate salt and 10% of NaCl. The volumetric flow was 0.2 $\mu\text{L}/\text{min}$ for both PEG-rich phases and 1 $\mu\text{L}/\text{min}$ for the salt-rich phase. All data series were normalized.

Figure 4.17 - Fluorescence intensity slope for the PEG-rich phase along the channel. The ATPS used was made with 7.04% of PEG, 16.37% of phosphate salt and 10% of NaCl. The volumetric flow was from 0.2 to 0.8 $\mu\text{L}/\text{min}$ for both PEG-rich phases and 1 to 2 $\mu\text{L}/\text{min}$ for the salt-rich phase. All data series were normalized.

Figure 4.18 - Fluorescent average for both phases in the microfluidic channel. The ATPS used was made with 7.04% of PEG, 16.37% of phosphate salt and 10% of NaCl. The volumetric flow was from 0.2 to 0.8 $\mu\text{L}/\text{min}$ for both PEG-rich phases and 1 to 2 $\mu\text{L}/\text{min}$ for the salt-rich phase. All data series were normalized.

Figure 5.1- Schematic illustration of the system setup. The microfluidic channel has three inlets and two outlets. The main channel is 20 μm high and 150 μm wide and it is 52.2 cm of long.

Figure 5.2 - Graphical representation of the PEG 1000/phosphate buffer system binodal curve. The horizontal axis represents the percentage of phosphate buffer weight to total system weight and the vertical axis represents the percentage of PEG 1000 weight to total system weight. The black square points represent the data obtained through the turbidometric titration method and the black line is the binodal curve fitted to the black square points. Points A, B and C indicate the conditions chosen to be tested in the microfluidic approach.

Figure 5.3 - (a, c) Optical micrographs of the PEG 1000/phosphate buffer system taken at the end of the microchannel. The solution containing PEG and the solution containing phosphate buffer were inserted in the side inlets while milli-Q water was inserted in the middle inlet. The solutions loading rates have been set so that the concentration of PEG and phosphate in the microchannel were 7.8% (w/w) and 7.6% (w/w), respectively, for (a) and 18.8% (w/w) and 14.6% (w/w), respectively, for (c), corresponding to points A and B in Figure 5.2, respectively, while the total flow rate was 2 $\mu\text{L}/\text{min}$. (b, d) – Graphical representation of the Gray Value along the linear yellow mark in (a) and (c), respectively, obtained with ImageJ software. The vertical dashed lines represent the location of the PDMS walls.

Figure 5.4- Optical micrographs of the PEG 1000/phosphate buffer system taken at the end of the microchannel at different times. The solution containing PEG and the solution containing phosphate buffer were inserted in the side inlets while milli-Q Water was inserted in the middle inlet. The solutions loading rates have been set so that the concentration of PEG and phosphate in the microchannel were 15.9% (w/w) and 10.1% (w/w), respectively, corresponding to point C in Figure 5.2, while the total flow rate was 2 $\mu\text{L}/\text{min}$. The images were obtained about 10 s apart.

Figure 5.5 - Graphical representation of the PEG 1000/phosphate buffer system binodal curve. The horizontal axis represents the percentage of phosphate buffer weight to total system weight and the vertical axis represents the percentage of PEG 1000 weight to total system weight. The solid line represents the fitting of the results from the macroscale turbidometric titration method. The experimental coefficients of Eq. (1) are in this case $A= 123.2$, $B = -0.6$ and $C = -1.8 \times 10^{-4}$. The solid blue dots are the concentrations that formed an interface between the two aqueous phases (and hence an ATPS) in the microfluidic device, the open red dots correspond to the concentrations that did not form an interface, and the half-filled green dots correspond to the concentrations with an unstable interface. The red dotted line represents the binodal curve fitted to the unstable state system points. The experimental coefficients of Eq. (1) are in this case $A= 81.1$, $B = -0.4$ and $C = -2 \times 10^{-4}$.

Figure 5.6 - Graphical representation of the bimodal curves for the PEG1000/Dextran 20 system. The horizontal axis represents the percentage of Dextran weight to total system weight and the vertical axis represents the percentage of PEG weight to total system weight. The dotted lines represent the fitting of the results from the turbidometric titration method. The experimental coefficients in this case are $A= 34.1$, $B = -0.2$ and $C = 4.2 \times 10^{-6}$. The solid blue dots and squares are the concentrations that formed an interface in the microfluidic device, the open red dots and squares are the concentrations that did not form an interface and the crossed green dots and squares are the concentrations displaying an unstable interface. The red lines represent the binodal curve fitted to the unstable state system points. The experimental coefficients in this case are $A= 28.7$, $B = -0.1$ and $C = 3.1 \times 10^{-5}$.

Figure 5.7 - Graphical representation of the bimodal curves for the PEG 6000/Dextran 298 system. The horizontal axis represents the percentage of Dextran weight to total system weight and the vertical axis represents the percentage of PEG weight to total system weight. The dotted lines represent the fitting of the results from the turbidometric titration method. The experimental coefficients in this case are $A= 12.7$, $B = -0.5$ and $C = 2.9 \times 10^{-5}$. The solid blue dots and squares are the concentrations that formed an interface in the microfluidic device, the open red dots and squares are the concentrations that did not form an interface and the crossed green dots and squares are the concentrations displaying an unstable interface. The red lines represent the binodal curve fitted to the unstable state system points. The experimental coefficients in this case are $A= 10.9$, $B = -0.3$ and $C = 5.6 \times 10^{-6}$.

Figure 6.1 - (a) Schematic representation of the experiment for the determination of K_p . The microfluidic structure has a height of 20 μm , a width of 150 μm and a length of 20.5 cm. The solutions are inserted in the microfluidic structure using syringe pumps. (b) Schematic representation of the diffusion within the microfluidic structure and formation of the interface.

Figure 6.2- Graphical representation of the fluorescence for several FITC-tagged molecules in different ATPS component solutions. The concentration of FITC tagged molecules was of 150 mg/L in all solutions. The phosphate buffer solution contained 15% (w/w) of phosphate buffer, the PEG solution contained 20% (w/w) of PEG 1000 and the dextran solution contained 15% (w/w) of dextran 20.

Figure 6.3 - (a) Graphical representation of the microfluidic experimental points with the determined K_p for the PEG/salt system using protein-A labelled with FITC as a target. (b) Fluorescence micrograph of the ATPS system with 20.8 % (w/w) of PEG and 16.7 % (w/w) of salt. (c) Fluorescence micrograph of the ATPS system with 17.8 % (w/w) of PEG and 14.3 % (w/w) of salt. (d) Fluorescence micrograph of the ATPS system with 16.6 % (w/w) of PEG and 13.3 % (w/w) of salt.

Figure 6.4- Microfluidic-determined K_p for the PEG/salt system using several FITC tagged proteins as targets.

Figure 6.5 - Microfluidic-determined K_p for the PEG/dextran system using several FITC tagged proteins as targets.

Figure 7.1- (a) schematic representation of the electrode placement in the microfluidic platform. The light blue is the glass substrate while the gray is the aluminum electrodes. The location for the microchannel is highlighted by black lines. (b) Transversal schematic view of the microchannel at the site where the Al electrodes are present.

Figure 7.2 - Image obtained by microscopy of the microfluidic platform with aluminum electrodes. The micrograph was obtained where the microchannel meets the aluminum electrodes and after the etching of the gap. The microchannel has a width of 50 μm , a height of 20 μm and a length of 3 cm. The black portion is the opaque aluminum.

Figure 7.3 - Graphical representation of the measured resistance during the gap etching procedure. Time 0 corresponds to the moment where the Al etchant was inserted in the microfluidic channel.

Figure 7.4 - Image obtained by microscopy of the microfluidic platform with deteriorated aluminum electrodes. The micrograph was obtained in the area in the middle of the aluminum electrodes and after the application of an electrical field for about 1 minute. The black portion is the opaque aluminum.

Figure 7.5 - Image obtained by microscopy of the microfluidic platform with aluminum electrodes. The micrograph was obtained where the microchannel meets the aluminum electrodes and after the etching of the gap. The microchannel has a width of 50 μm , a height of 20 μm and a length of 3 cm. The black portion is the opaque aluminum. The etching process was allowed to continue for 30 seconds after the resistance increase.

Figure 7.6 - Graphical representation of the influence of time on the overetch distance. Time 0 corresponds to the time when the resistance increase occurs signifying that the gap between the electrodes has formed.

Figure 7.7 - Schematic of the setup used for testing the effect of the electrical field in biomolecule partition in the PEG/dextran ATPS. (a) fluorescent microscopy image of the end of the microchannel. The dashed white lines represent the position of the microchannel walls. The white solid line represents the position of the electrodes edge.

Figure 7.8 - Schematic of the setup used for testing the effect of the electrical field in biomolecule partition in the PEG/phosphate ATPS. (a) fluorescent microscopy image of the end of the microchannel. The dashed white lines represent the position of the microchannel walls. The white solid line represents the position of the electrodes edge.

Figure 7.9 - Graphic representation of the K_p shift of insulin-FITC when under the effects of a electrical field (E). The results correspond to the partition coefficient when the positive electrode is on the left side.

Figure 7.10 -Graphic representation of the K_p shift of insulin-FITC when under the effects of a electrical field (E). The results correspond to the partition coefficient when the positive electrode is on the right side.

VIII List of tables

Table 2.1 - Summary of response parameters for various types of ATPS extraction aimed at the purification of a wide range of biomolecules. The abbreviations P-S, P-P, A-S, IL-X and R refer to systems composed of polymers and salts, two polymers, alcohols and salts, ionic liquids and temperature-responsive polymers, respectively.

Table 2.2 - Summary of recent applications of ATPS in extraction at the microscale and obtained results.

Table 4.1 - Density and viscosity values for the PEG phase and the salt phase used on the microfluidic system. Values from Rosa et al., 2009.

Table 4.2 - Schematic of the method used for the simulation of the diffusion progression along the length of the microchannel (L). The time (t) is calculated based on the length (L) attributed to the row and the velocity of the fluids. D is the diffusion coefficient, c_{ji} is the concentration value of the cell at row number j and column number i . l_w represents the distance between two adjacent columns, equivalent to l in Equations 1.1 and 1.2. In this case l_w is always $5\ \mu\text{m}$, and t_d represents the time required for the fluid to move between two adjacent rows. The calculation of the equations used to calculate the antibody concentration for characteristic selected matrix positions highlighted with circles (circled in the table) is detailed at the bottom given below the table.

Table 6.1 - K_p for FITC-tagged proteins for different compositions of PEG/Phosphate buffer ATPS comparing the microfluidic approach and the standard macroscale approach.

Table 6.2 - K_p for FITC-tagged proteins for different compositions of PEG/Dextran ATPS comparing the microfluidic approach and the standard macroscale approach.

Table 7.1 - Variation of biomolecules K_p when subjected to an electrical field. The second row indicates the position of negative and positive electrodes.

1 Introduction

The great and fast advances in technology that have occurred in the past decades have changed several aspects of our society, which created a series of new challenges. One of those challenges is in the health area. Many disease related with advanced age have experienced a increased number of cases, such as Alzheimer or Parkinson, and the lifestyle now observed primarily in first world countries augmented the number of diseases related to that lifestyle, such as cancer or diabetes. Given these conditions, it is not surprising that the healthcare technologies suffered great changes and that the production of biopharmaceuticals needed to fight these diseases has increased greatly.

Due to the increasing demand of biopharmaceuticals, their production has suffered a great increase in the past decades. However, despite the fact that the production of pharmaceuticals has suffered great technological advances which has greatly increased the production of molecules such as mAbs (Murphy, et al., 2008) (Mark, et al., 1994) (Albertsson, 1995) (Bensch, et al., 2007), the downstream purification processes have been somewhat neglected. This is mainly due to the fact that the pharmaceutical companies are unwilling to replace well known processes which are responsible for cost increase in downstream processes (Azevedo, et al., 2009). A typical platform approach used in the downstream processing of mAbs includes clarification, concentration, selective purification steps and virus inactivation and removal. The most expensive step is the selective purification step, usually comprising the mAbs adsorption to a protein A (ProA) resin, that can account for more than 79% of the total downstream costs (Azevedo, et al., 2009) (Albertsson, 1995). Normally this step is performed by chromatography (Przybycien, et al., 2004), however, additionally to the fact that this is a costly operation, the increase in upstream production is pushing chromatography beyond its limit (Azevedo, et al., 2009). Therefore, in the present day, great amount of investigation is being done in the area of biomolecule separation and purification with hopes that a cheap and fast process may be used to replace the expensive processes that are widely used nowadays, such as the ProA chromatography (Azevedo, et al., 2009).

Among the different processes that may substitute these older and expensive processes, methods involving ATPS have been the focus of much attention (Przybycien, et al., 2004) (Merchuk, et al., 1998). The ATPS are normally constituted by 60 to 95% of water allowing dissolution of most biomolecules without loss of biological function (Silva, et al., 2006). Methods involving ATPS have been used to separate and partially purify several biomolecules:

proteins, nucleic acids, genetic material, low molecular weight products, cells and cell organelles (Benavides, et al., 2008).

The interest in microfluidics has also been increasing in the past decade. Microfluidics offers several advantages comparing to the manipulation of larger amounts of liquids, such as small requirements for solvents, reagents, and cells, short reaction times, portability, low cost among others (McDonald, et al., 2000). These advantages make microfluidics an area of interest and many bioassays and biological procedures have been miniaturized into a chip format (Sia, et al., 2003). The general goal of this thesis is to increase understanding of the use of ATPS within microfluidic devices with the purpose of separation and purification of biomolecules. Several types of studies have been conducted including the miniaturization of an already established ATPS-based separation method and the development of a novel method for the rapid determination of biomolecule partition in microATPS among others.

. The first part of this thesis was to study the possibility of miniaturization of an already established ATPS based separation of IgG (Azevedo, et al., 2007). For this purpose, simulations were created using the COMSOL Multiphysics® version 3.5 software and the results were used to design a microfluidic system for ATPS. The chip was fabricated using soft lithography techniques to create a PDMS microfluidic structure through a mold made of SU-8, an epoxy-based negative photoresist.

These microfluidic structures were then tested for the partition of IgG using ATPS of PEG/phosphate salt with NaCl. Both phases were simultaneously inserted in the channel concurrently and the phase containing the phosphate salt, henceforth called the salt phase, contained IgG conjugated with FITC. Due to the FITC it was possible to track and study the IgG diffusion from the salt phase to the PEG containing phase, henceforth called PEG phase, using fluorescence microscopy. This work is described in chapter 6 and was published in 2012 in the *Journal of Chromatography A* under the name "Design of a microfluidic platform for monoclonal antibody extraction using an aqueous two-phase system". DOI: 10.1016/j.chroma.2012.05.089 (Silva, et al., 2012).

After the possibility of such miniaturization was demonstrated, the microfluidic platforms were used to develop new methods for the characterization of ATPS using microfluidics. A method was developed to allow the use of a microfluidic platform to rapidly map out the ATPS bimodal curves, a laborious process at the macroscale. The mixing of the stock solutions (PEG, phosphate buffer, and milli-Q water, and of PEG, dextran and milli-Q water, depending on what ATPS was being characterized) within the microchannel created a solution that, depending on the concentrations, either separate into two phases or not. By varying the flows it was possible to vary the concentration of each molecule in the solution within the microchannel to test whether the two phases are formed, allowing for mapping of the binodal curve. This work is described in chapter 4 and was published in 2014 in the *Journal of Chromatography A* under

the name " Determination of aqueous two phase system binodal curves using a microfluidic device". DOI: 10.1016/j.chroma.2014.10.035 (Silva, et al., 2014).

Afterwards the previous method was expanded by adding a molecule tagged with FITC in order to study the partition of molecules in various conditions of an ATPS. As before, stock solutions of PEG, dextran and milli-Q water or PEG, phosphate buffer and milli-Q water were flown into the microchannel causing their mixing inside the microfluidic platform. The difference is that a biomolecule marked with FITC was added into the milli-Q water in each experiment to test the biomolecule partition. The biomolecules used for this study were Insulin-FITC, Bovine Serum Albumin(BSA)-FITC, IgG-FITC, proA-FITC and Green Fluorescent Protein(GFP). This work is described in chapter 5 and was published in 2017 in the Journal of Chromatography A under the name "Determination of partition coefficients of biomolecules in a microfluidic aqueous two phase system platform using fluorescence microscopy". DOI: 10.1016/j.chroma.2016.12.036 (Silva, et al., 2017).

To better understand the behavior of the ATPS in the microfluidic platform, a study of the ATPS interface within a microfluidic platform was performed. In this study, PEG/phosphate ATPS and PEG/dextran ATPS were inserted in a microchannel and then the microchannel was studied under a confocal microscope. Confocal microscopy has several advantages, although for this study the most interesting advantage of confocal microscopy is the ability to focus on different heights of the studied sample. Thus, using confocal microscopy, it was possible to visually study the ATPS interface in greater detail and to study the interface shape within the microchannel. This work is described in chapter 4.1.

The last study performed was to ascertain the effect that an electrical field can have on the ATPS and on the partition of biomolecules within a microfluidic platform. For this study, Al electrodes are etched directly on top of glass and afterwards said glass is used to seal the PDMS microstructure. This was a simple method to allow the fabrication of electrodes very close to the microchannel. Afterwards PEG/phosphate and PEG/dextran are inserted in the microchannel and, by applying a voltage differential in the electrodes, an electrical field is created between them. With this setup is possible to see what effects the electrical field has on the ATPS within the microfluidic platform. Afterwards, several biomolecules marked with FITC are added individually in each experiment to study the effect that electrical fields have on biomolecule partition in ATPS. This work is described in chapter 7.

2 State of the Art

2.1 ATPS: An overview

ATPS are solutions that contain two or more phases in equilibrium (Diamond, et al., 1992). The phases of an ATPS are mainly composed of water, typically 60 to 95 % of the phase (Silva, et al., 2006) (Soares, et al., 2015). The fact that all phases in an ATPS are aqueous solutions means that separation of proteins is possible without denaturation. An ATPS is naturally formed when certain solutes are in the same solution at a high enough concentration. In these conditions, the solution separates into phases. It is also possible to create an ATPS by preparing two solutions separately, with determined solutes and concentration so that the two solutions won't mix (Silva, et al., 2006) (Soares, et al., 2015).

The formation of ATPS is known since 1896, when Beijerinck first noticed that aqueous solutions of agar and gelatin or gelatin and soluble starch, when in certain concentrations and temperatures, would form a solution that would eventually separate spontaneously into two limpid aqueous phases (Diamond, et al., 1992). But it was only with the work developed by Per-Åke Albertsson in the 1950s that the scientific community was convinced of the great potentiality of ATPS for separation and purification of biological molecules (Tiselius, et al., 1963) (Silva, et al., 2006). Since water is the solvent in all phases, an ATPS is an acceptable environment for the biological molecules, preventing changes in their structures and loss of their biological activities. Additionally the interfacial region has a low interfacial tension, in the order of 10^{-7} N cm^{-1} (Diamond, et al., 1992) (Soares, et al., 2015), which means that when the biomolecules diffuse through the interface, they are exposed to less tension and therefore there is a smaller chance of changes in the molecules structures (Bensch, et al., 2007). Furthermore, it is possible to obtain good resolution and yields by altering the conditions of the system, such as pH, ionic strength and polymer molecular weight (Azevedo, et al., 2007). They can also be easily scaled-up, separation can be achieved with only diffusion, are less expensive than other separation methods and ATPS separation can be made selective, fast and can be carried out at room temperature (Soares, et al., 2015) (Diamond, et al., 1992).

From the previously presented advantages, it is possible to conclude that the ATPS based methods are good approaches to replace the traditional, more expensive, chromatography in the separation and purification of antibodies. However, there are still some problems to overcome. The mechanisms of ATPS partition are, to this date, still poorly understood and the method development is still entirely empirical (Huddleston, et al., 1991) (Soares, et al., 2015)

The formation of an ATPS from an aqueous solution of polymer/polymer or polymer/salt depends largely on the nature of the polymers and/or salt and on the percentages of weight

masses of these solutes. Even if a solution has solutes that have the potential to form an ATPS, the ATPS will not form unless these solutes have concentrations above a certain limit (Silva, et al., 2006) and that limit depends on the nature of the solutes (Diamond, et al., 1992). For well characterized ATPS, such as the PEG/Phosphate potassium system, those limits have been already defined and are represented through phase diagrams such as the one in Figure 2.1

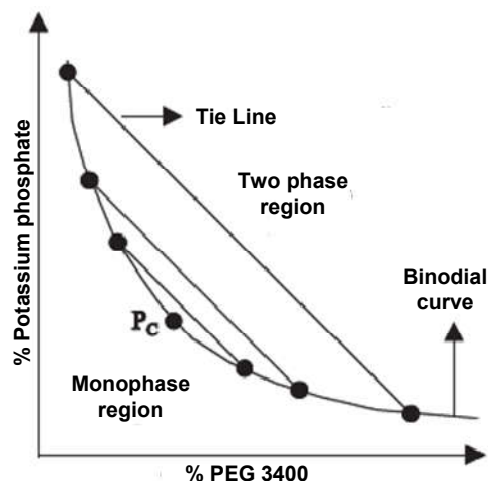


Figure 2.1 - Aqueous polymer phase diagrams of an ATPS made of PEG 3400/Potassium Phosphate/Water at 4°C. The PEG 3400 is PEG with a molecular weight of 3400 Dalton (Adapted from Silva, et al., 2006).

These diagrams have all the important information usually needed to characterize the ATPS formation. The binodal curve represents the minimal concentrations required for ATPS formation, which means that, for established systems, it is possible to know in advance if a solution separates into phases by knowing its composition (Silva, et al., 2006). The critical point, sometimes referred as the plait point, is the point at which the compositions and volumes of the two phases theoretically become equal (Diamond, et al., 1992). The tie lines are the connection of points in the diagram where the ATPSs will separate into phases with the same composition. However, proprieties such as mass, volume are different (Silva, et al., 2006).

Nowadays, there are already a large number of studies on the capacity of polymer-salt based ATPS to separate proteins in macroscale (Azevedo, et al., 2007), (Rämsch, et al., 2000) (Azevedo, et al., 2009) (Benavides, et al., 2008) (Rosa, et al., 2009) (Rosa, et al., 2012). The validity of the ATPS concept using microfluidics has already been exploited in the recovery of whole cells (Tsukamoto, et al., 2009) (Nam, et al., 2005) (Soohoo, et al., 2009) (Yamada, et al., 2004) (Sousa, et al., 2011) (Azevedo, et al., 2009), tagged proteins (Meagher, et al., 2008) and membrane proteins (Hu, et al., 2007) small organic compounds such as metabolites and antibiotics (Soares, et al., 2014) (Pereira, et al., 2013), plasmids (Kepka, et al., 2004), large macromolecular complexes such as virus-like particles (Jacinto, et al., 2015). More examples can be seen in table 2.1.

Table 2.1 - Summary of response parameters for various types of ATPS extraction aimed at the purification of a wide range of biomolecules. The abbreviations P-S, P-P, A-S, IL-X and R refer to systems composed of polymers and salts, two polymers, alcohols and salts, ionic liquids and temperature-responsive polymers, respectively.

	System (% w/w)	Additive	Target	Source matrix	K_p	Y (%)	Purity	Ref.
P-S	12% PEG 400, 18% phosphate pH 6	None	mAb	CHO Cell culture supernatant	Affinity to the PEG-rich phase	95	75% (73% HCP reduction)	(Eggersgluess, et al., 2014)
	17.2% PEG 2000, 6% phosphate pH 6	None	mAb	CHO Cell culture supernatant	0.009	95.5	Purification factor of 3.3	(Shu, et al., 2016)
	(i) 13.3% PEG 3000, 6.3% phosphate pH 7 (ii) 12.4 % PEG 3000, 6.3% phosphate pH 7	(i) None (ii) 1.3% NaCl	Laccase from <i>p. Sapidus</i>	Clarified <i>P. Sapidus</i> broth	(i) Affinity to top phase (ii) affinity to bottom phase	96	(i) Clearance of 6.45 relative to Laccase from <i>T. versicolor</i> (ii) Purification factor of 2.74	(Prinz, et al., 2014)
	10% PEG 6000, 20% phosphate pH 6	None	Retamycin	<i>S. Olandensis</i> broth	8.2	91.3	Full separation from whole cells	(Esmanhoto, et al., 2004)
	22.06% PEG 400, 6.8% phosphate pH 8.5	7.5% NaCl	VLP	Crude Sf9 cell lysate	Affinity to the PEG-rich phase	102	16.8% HPLC purity and 99.6 DNA depletion	(Ladd Effio, et al., 2015)
P-P	8% PEG 3350, 8% citrate pH 6	15% NaCl and 5% NaCl for back extraction	mAb	Hybridoma cell culture supernatant	>5 with 15% NaCl and <0.2 without NaCl	99	76% HPLC purity and an IgG/protein ratio of 0.96	(Azevedo, et al., 2009)
	17.7% PEG 8181 (avg.), 10.3% phosphate pH 7.5	None	Plasmid DNA	Mixture of pDNA from <i>E. Coli</i> with mRNA and tRNA	<0.01	97.4	13.6% RNA yield in bottom phase	(Wiendahl, et al., 2012)
	9.6% PEG 8000, 1.0% dextran 500 kDa	None	Extracellular lipase	<i>B. pseudomallei</i> fermentation broth	0.9	92.1	Cells contained in the bottom dextran-rich phase	(Ooi, et al., 2011)
	10% PEG 4000, 20% sodium polyacrylate 8000	6% Sodium sulfate pH 6.5	Clavulanic acid	<i>S. clavuligerus</i> culture supernatant	9.15	55	Contaminant proteins partition also to the top phase	(Pereira, et al., 2012)
A-S	22% phosphate, 21% ethanol	None	rHSA	<i>P. pastoris</i> fermentation broth	Affinity to the top ethanol-rich phase	95-100	99.9% removal of cells, 87.2% polysaccharide removal	(Dong, et al., 2012)
	18% 2-propanol, 22% ammonium sulfate	1% NaCl	Interferon alfa-2b	<i>E. coli</i> lysate supernatant	Affinity to the top alcohol-rich phase	74.6	Purification factor of 16.24	(Lin, et al., 2013)
IL-X	15% PEG 1500, 15% phosphate pH 7	5% [C6mim]Cl	Lipase	<i>Bacillus sp. ITP-001</i> cell culture supernatant	0.15	77.6	Purification factor of 103.5	(Souza, et al., 2015)
	53% PEG 2000, 27% [C2mim]Cl pH 6.15	None	(i) caffeine (ii) Nicotine	Purified molecules	(i) 0.24 (ii) 1.40	100	Maximum selectivity factor of 19	(Pereira, et al., 2013)
R	42.1 TLL EOPO 3900, phosphate pH7	None	CGTase	Crude <i>B. cereus</i> feedstock	>10	87	Purification factor of 13.1	(Ng, et al., 2012)
	10% EOPO 3900 pH 8.5	Heating above 50°C	Lipase	<i>Burkholderia cepacia</i> fermentation broth	22.3	99.3	Purification factor of 14, full separation of cells to bottom EOPO-rich phase	(Show, et al., 2012)

Since proteins are hydrophilic molecules, they will have a preference towards the salt phase instead of the polymer phase. This preference is used to increase the purification factor by directing the partition of proteins to the PEG phase, so that the majority of impurities are retained in the salt phase (Azevedo, et al., 2007). Unfortunately, this means that the antibody also has a preference for the salt phase which will decrease the global yield of the process (Azevedo, et al., 2007). Thus it is necessary to enhance the partition of the antibody to the PEG phase by using low molecular weight polymers, high ionic strengths and low pH values (Azevedo, et al., 2007) (Rosa, et al., 2007).

Low molecular weight polymers are used because, as the polymer molecular weight decreases, the exclusion effects on the polymer phase decrease as well, leading to an increase of partition. As for the ionic strength of the solution, using high ionic strengths means that salting out effects are responsible for the precipitation of proteins. The addition of neutral salts to the system increases the ionic strength of the salt-phase, leading to the partitioning of antibodies to the PEG-rich phase. Regarding the pH value, normally high values are used in ATPS based protein separation to enhance protein separation. However, in the case of antibodies, high pH values might denature the antibodies. Alternatively, the use of lower pH will increase intermolecular repulsion, stabilizing the antibody that, at high ionic strength, has tendency to aggregate and precipitate.

2.1.1 Diffusion in ATPS

The phenomenon of diffusion is one of the most important aspects of ATPS. The diffusion is basically a mixing process caused by random molecular motion (Cussler, 2009). The main characteristic that influences the speed of the molecular motion and, therefore, the time that is needed for complete mixing, is the nature of the material in which the diffusion process occurs, in cases where there is no artificial mixing. If it is a gaseous substance, than the average speed of molecular motion is 5 cm/min. In liquids, that average speed is 0,05 cm/min and in solids it is 0,00001 cm/min. The temperature does not affect much this speed, at least as much as it affects in other phenomena (Cussler, 2009).

One of the most used equations to describe diffusion in solutions is a equation based in Fick's first law.

$$N_i = D \left(\frac{\Delta c_i}{l} \right) \quad \text{Equation 2.1}$$

where N_i is the flux of the solution component i , the coefficient D is the diffusion coefficient, the Δc_i is the concentration difference of the component i and l is the distance of diffusion (Cussler, 2009).

Although the previous equation works well for most cases where there isn't a significant mechanical stir, for the diffusion in ATPS needs is somewhat different. In Equation 2.1, it is assumed that the diffusion occurs between two points in the solution with equal composition and, therefore, the solubility of component i is the same on both points (Cussler, 2009). However, in ATPS this is not the case, as can be seen in Figure 2.2. The different phases have different constitutions and, therefore, the solubility of the component is different. So, instead of using the difference between the concentrations on each phase, it can be used the concentration in benzene minus the product between the concentration of water and a partition coefficient, H . The partition coefficient, H , is the ratio of the concentration in benzene and the

concentration in water, when the system has reached equilibrium (Cussler, 2009). Consequently, the concentration of the component i will be different in each phase.

Bromine extraction

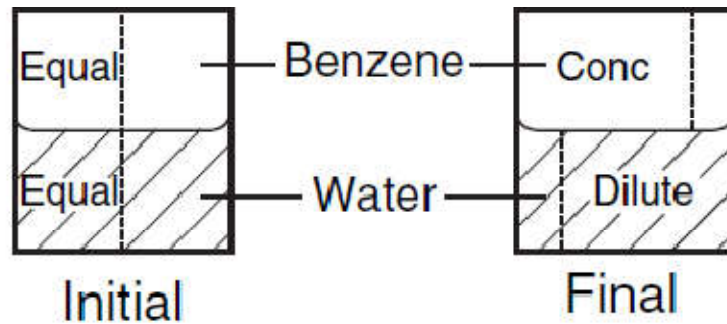


Figure 2.2 - Diffusion across two different phases (Cussler, 2009).

Mathematically, this is represented by:

$$N_i = D \left(\frac{c_{i1} - H \times c_{i2}}{l} \right) \quad \text{Equation 2.2}$$

where N_i is the flux of the solution component i , the coefficient D is the diffusion coefficient, the c_{i1} is the molar concentration in phase 1, the c_{i2} is the molar concentration in phase 2, H is the partition coefficient and l is the distance of diffusion (Cussler, 2009).

The time of diffusion can be calculated using the diffusion coefficient of the solute. However, since the diffusion on the interface is ruled by a different law, using this factor is not entirely correct. However it can be used as an approximation time (Shui, et al., 2007).

$$t = \frac{l^2}{D} \quad \text{Equation 2.3}$$

where t is time.

2.2 Microfluidics Systems

Microfluidics refers to processes and methods that manipulate fluids in channels with heights and widths in the tens to hundreds of micrometers (McDonald, et al., 2000). Microfluidics offers several advantages when compared to processes and methods that manipulate larger amounts of fluids, such as the lower volume of reagents necessary (critical for valuable samples and for high-throughput screening), short reaction times, portability, low cost, low consumption of power (Sia, et al., 2003) (Beebe, et al., 2002), increased separation efficiency and reduced production of potentially harmful by-products (McDonald, et al., 2000).

These advantages make microfluidics an area of interest and many bioassays and biological procedures have been miniaturized into a chip format. Examples of this are DNA sequencing (Paegel, et al., 2003), polymerase chain reaction (PCR) (Zhang, et al., 2006), electrophoresis (Theo, et al., 1995), DNA separation (Huang, et al., 2006), enzymatic assays (Boer, et al., 2005), immunoassays (Soares, et al., 2017), cell counting (Cheng, et al., 2007), cell sorting (Kruger, et al., 2002), cell culture (Mehling, et al., 2014), and protein purification (Silva, et al., 2012).

Nonetheless, microfluidics techniques have certain features, because of its small size, that can offer a challenge, such as the increased importance that surface forces have in these systems, the complexity of the device geometry at such small dimensions and the possibility that suspended particles may have sizes comparable to the cross-sectional dimensions of the channel (Stone, et al., 2001).

Nowadays, liquid polymers that solidify under certain conditions are extensively used as materials for fabrication of microchannels. They are inexpensive, the microchannels can be easily formed by embossing or molding and the devices can be sealed thermally or by using adhesives. The downsides of using polymers are that it is necessary to be careful to control their surface chemistry, incompatibility with organic solvents or low molecular weight organic solutes is often a problem and they are generally incompatible with high temperatures (McDonald, et al., 2000).

The material used in this work was the elastomeric polymer PDMS, because it is an excellent material to be used for the fabrication of microchannels since features on micron scale can be reproduced, it is transparent at the visible range and down to 280 nm, it works at low temperatures, it is nontoxic, unreactive and impermeable to water and its surface chemistry is easily altered, and it is permeable to certain gases including oxygen (McDonald, et al., 2000) (Sia, et al., 2003) (Weibel, et al., 2007) (Boxshall, et al., 2006).

The microfabrication approach used in this work was the soft lithography technique. Soft lithography refers to a collection of techniques for creating microstructures and nanostructures based on printing, molding and embossing. The name of this technique derives from the fact that is based on using a patterned elastomeric polymer as a mask, stamp or mold, to pattern 'soft materials' (for example, polymers, gels and organic monolayers) (Lei, 2014) (Weibel, et al., 2007). This technique is composed by three steps: rapid prototyping, mold replication and sealing (McDonald, et al., 2000).

The first step, is the creation of a master, using photolithographic techniques, that can be used to cast of PDMS devices (Figure 2.3). The master, a mold often made of SU-8 on a silicon wafer, is durable can be used indefinitely (McDonald, et al., 2000). This process starts by creating a pattern in a computer aided design (CAD) program. The CAD file is then used for the

fabrication of a mask that is a pattern in a transparent substrate using various types of patterning techniques depending on the dimensions desired. For micron range dimensions, these masks are usually made by photolithography. Next, by using UV light, the pattern is transferred from the mask to a photoresist layer (SU-8) that has been deposited in a silicon wafer. The photoresist is then developed by an organic solvent, which in the case of SU-8 is propylene glycol methyl ether acetate (PGMEA), causing the removal of the unexposed photoresist, leaving behind the bas-relief structure in the photoresist layer. The height of the microchannels is controlled by the thickness of the photoresist. This process can create structure with features as small as 30 nm (McDonald, et al., 2000) (Weibel, et al., 2007) (Xia, et al., 1998).

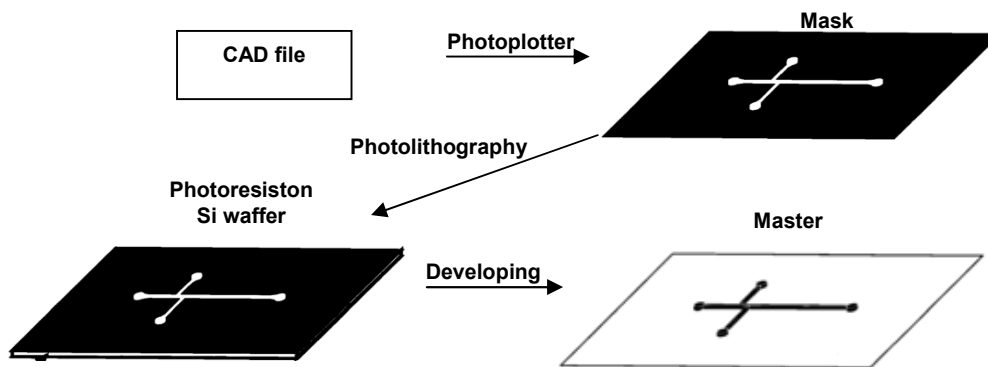


Figure 2.3– Scheme for the rapid prototyping of a master in a silicon wafer (Adapted from McDonald, et al., 2000).

The next step is the replica molding (Figure 2.4). Replica molding is simply the casting of a prepolymer against a master and generating a negative replica of the master. The advantage of this step is that many PDMS structures can be easily made using a single master (McDonald, et al., 2000) (Weibel, et al., 2007). The PDMS is poured on the master, cured at 60 or 65°C for about 1 hour, and then it is peeled from the master. Access holes or reservoirs can be easily done by placing posts in the master prior to the PDMS pouring or by punching holes in the PDMS after it is peeled (McDonald, et al., 2000).

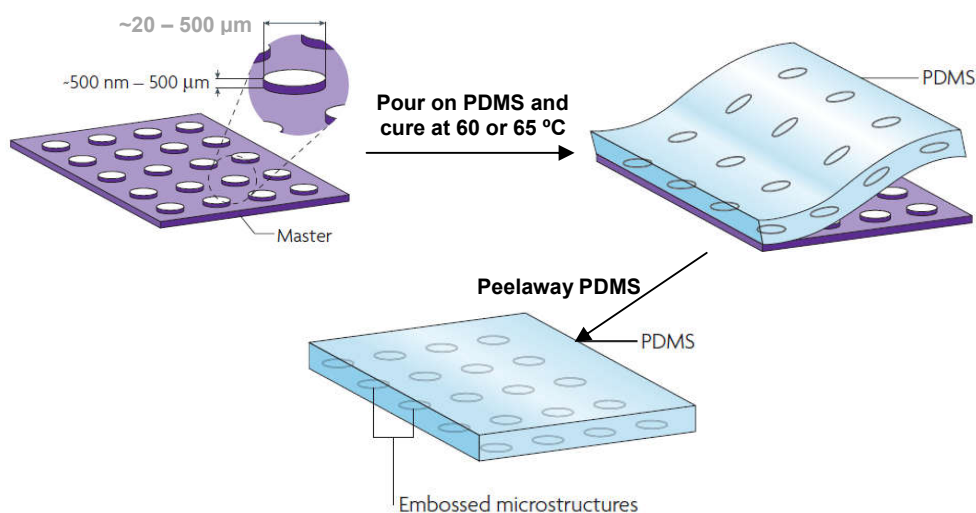


Figure 2.4 – The fabrication of micropatterned slabs of PDMS by using replica molding. The master consists of a silicon wafer with features of photoresist in bas-pattern. The PDMS is poured on the master and then cured at 60 or 65 °C for about one hour. After peeling the PDMS, it has the microstructures embossed in its surface (Adapted from Weibel, et al., 2007).

The final step is the sealing of the structure against a flat surface. The replica molding provides the structure with three of the four walls necessary for enclosure and the flat surface that the PDMS is sealed against makes the fourth wall (McDonald, et al., 2000). PDMS can be reversibly or irreversibly sealed against a variety of materials, including itself. Reversible sealing does not require treating PDMS, while irreversible sealing requires treatment of the PDMS surface. However, irreversible sealing produces a sealing that can withstand greater pressures than the sealing produced by reversible sealing. Furthermore, irreversible sealing alters the PDMS surface, making it hydrophilic, allowing easier passage of aqueous solutions (McDonald, et al., 2000). Additionally the formation of bubbles is less probable and the channel becomes less prone to non-specific protein adsorption, which prevents clogging of the microchannel and changes in the flow properties (Boxshall, et al., 2006).

As for the driving of the flows of fluids in microchannels, there are two methods that are the more commonly used: pressure driven and electrokinetic (Sia, et al., 2003). In this thesis, the method used was the pressure driven, so only this one will be explained. In the pressure driven flow (also called hydrodynamic flow) the flow is driven by either the use of a syringe pump in the inlet or by applying negative pressure with a syringe pump in the outlet, opening the unused outlets or inlets, respectively, to the atmospheric pressure. One interesting aspect of pressure driven methods is that the flow velocity assume a parabolic shape in the cross section of the microchannel, due to interactions between the fluid and the walls of the microchannel (Stone, et al., 2001) (Sia, et al., 2003).

One of the advantages of microfluidics is that it can explore a set of physical proprieties of fluids that occur at micro-meter scale. At this scale, one of the most important physical propriety of the fluids is the absence of turbulence in microfluidic flows, which means laminar flows (Sia, et al., 2003). The importance of this phenomenon is that, without turbulence, there is

no mixing of the solution and diffusion processes are, therefore, defined only by random molecular motions. The turbulence of a flow can be measured by a dimensionless parameter known as the Reynolds number (Re). This parameter is defined by:

$$Re = \frac{vLp}{\eta} \quad \text{Equation 2.4}$$

where v is the velocity of the fluids flow, L is the cross section dimension, p is the density of the fluid and η is the viscosity of the fluid (Sia, et al., 2003) (Stone, et al., 2001). For dimensions typical of microfluidic devices (100 μm) and with a low rate fluid flow (1 cm/s) the Reynolds number is almost always inferior to one which correspond to a laminar flow (typically flows are laminar with $Re < 2000$ and turbulent with $Re > 2000$). The existence of a laminar flow means that there is no turbulence to aid diffusion. Therefore, diffusion processes in a microfluidic device are often slow (Sia, et al., 2003).

2.2.1 ATPS in microfluidic devices

The use of ATPS in microfluidic devices has several advantages over the use of macroscale ATPS. The specific interfacial area, also known as the surface area-to-volume ratio, can be very large. The specific interfacial area is the ratio between the interface area and the system's volume. For example, in a normal reactor used for chemical processing the specific interfacial area is normally around the 100 m^2/m^3 . However, in a $250\mu\text{m} \times 20\mu\text{m} \times 3\text{cm}$ microchannel, the value of specific interfacial area is of 4000 m^2/m^3 . Furthermore, due to the high specific interfacial area and the low diffusion distances, the mass transfer coefficient is higher than in macroscale. Simulations have shown that typical widths for the interfaces are lesser than 1 nm, though that width can be manipulated by adding surfactants. One other advantages is that, unlike what happens in the macroscale use of ATPS, the only contact between reactants is exclusively in the interface, making it very appropriate for the study of interfacial phenomena, diffusion-controlled interfacial reactions and extraction (Shui, et al., 2007) (Huh, et al., 2011) (Reddy, et al., 2005). Lastly, the processing in microATPS can be continuous, a difficult feat for traditional ATPS (Huh, et al., 2011).

When ATPS are driven by pressure in a microfluidic device, the resulting flow can be of two different types: when the flow is based on droplets or bubbles, the system is categorized as segmented; when the flow is a stratified flow, where the interface is elongated across the microchannel, then it is categorized as parallel. These two flow regimes are caused by the relation between interfacial and viscous forces and that relation can be expressed by the dimensionless capillary number (Ca) (Shui, et al., 2007).

$$Ca = \frac{\eta v}{g_c \sigma} \quad \text{Equation 2.5}$$

where η is the fluid viscosity, v is the flow velocity, g_c is a geometrical constant and σ represents the interfacial forces. In systems with high Capillary number, the viscous forces are dominant and the system will have the tendency to assume the parallel type flow. Conversely, in systems with low Capillary number, the interfacial forces are dominant and the system will have the tendency to assume the segmented type flow (Figure 2.5).

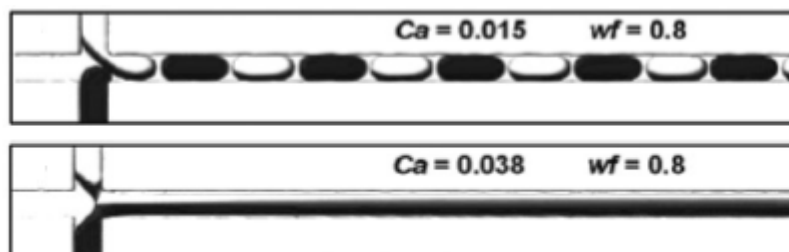


Figure 2.5 – Liquid–liquid two-phase flow patterns: flows at different Capillary number (Ca) and water fraction (wf). The top is an example of segmented flow type, while the bottom is an example of parallel flow type (adapted from Shui, et al., 2007).

Of the two types of ATPS flow in microfluidics, the parallel type flow is the most commonly used (Soares, et al., 2016). This is due mainly due to the greater ease of separation that the parallel type flow offers when compared to the segmented type flow. However, there is not much information on the behavior of the interface of ATPS in microfluidic conditions.

Although the use of microfluidic ATPS in biotechnology is still very limited, research is rapidly increasing and there are already several examples of its use as can be seen in table 2.2.

Table 2.2 - Summary of recent applications of ATPS in extraction at the microscale and obtained results.

ATPS forming solutions	Channel dimensions	Application	Achievements	Ref.
24% w/w PEG 4000 solution 20% w/w ammonium sulfate	Round 1 mm outer tube and 50–100 μ m inner tube	Extraction and purification of bovine serum albumin (BSA)	71.1% of extraction yield in 3.6 s	(Huang, et al., 2013)
7.04% w/w PEG 3350 14.37% w/w phosphate buffer, pH 7 10% w/w NaCl	Rectangular 20 by 150 μ m	Extraction and purification of FITC labeled IgG	54% of recovery yield in a 16.8 cm microchannel in 19 s	(Silva, et al., 2012)
20% w/w PEG 3350 9–29% w/w PEG 1500 15% w/w dextran 100 000 14% w/w potassium phosphate 14.5% w/w ammonium sulfate 15% w/w trisodium citrate	Rectangular 20 by 100 μ m	Extraction of virus like particles	A K of up to 3.9 within a microchannel	(Jacinto, et al., 2015)
10% w/w caseinate solution 6% w/w PEG 6000 solution	Square 70 by 70 μ m	Extraction of lysine aided by an electric field	100% extraction of lysine	(Campos, et al., 2014)
1–10% w/w PEG 3350, 4000 and 8000 1–10% w/w dextran 40 000 and 500 000	Rectangular 100 by 500 μ m	Cell separation in blood samples	99% of the erythrocytes in the dextran rich phase and 96% of the leukocytes in the PEG rich phase	(Tsukamoto, et al., 2009)
N, N, N-trioctyl ammonium propionate Water	Rectangular 50 by 240 μ m	Extraction of Bisphenol A for detection in HPLC	95% of extraction yield in 2 s	(Qi, et al., 2015)
14–18.5% w/w PEG 8000 and 20 000 4.5–18.5% w/w phosphate buffer	Rectangular 20 by 100 μ m	Polyphenol and OTA extraction for OTA immunodetection in wine	LoD of 0.26 ng mL ⁻¹ for raw red wine using a competitive immunoassay in-line with ATPS extraction-based sample preparation	(Soares, et al., 2014)
50% w/w PEG 1000 and 6000 30% w/w dextran 20 000 and 300 000 40% w/w phosphate buffer	Rectangular 20 by 150 μ m	Determination of phase diagrams binodal curves	Ability to measure an ATPS binodal curve with sub-mL volumes	(Silva, et al., 2014)
2.5% w/w PEG 35 000 3.2% w/w dextran 500 000	Rectangular 100 by 1500 μ m	Micropatterning of cells in a microfluidic channel	Micropatterning of cells with minimal cross-contamination and selective harvesting	(Frampton, et al., 2011)

Bacteriorhodopsin, a light sensitive protein found in the purple membrane of *Halobacterium Salinarium*, has already been successfully purified by combining a two phase system of PEG and potassium phosphate extraction and the rapid separation of three phase desalting system (Huh, et al., 2010). In 2007 Hu et al. separated membrane proteins using a detergent/polymer ATPS in a microfluidic device (Hu, et al., 2007). Nam et al., (2005) used a PEG/dextran system to extract live and dead CHO K-1 cells from a culture medium (Nam, et al., 2005) and, using the same polymers, Soohoo et al., (2009) were able to extract leukocytes from whole blood samples (Soohoo, et al., 2009). Huang et al. used a coaxial capillary microfluidic device to create a co-laminar flow to extract bovine serum albumin (BSA). On the other hand, using a different microchannel setup, Silva et al., in a work from this thesis research to be discussed in Chapter 6 (Silva, et al., 2012), successfully demonstrated extraction of a FITC labeled IgG from a salt rich flow to a PEG rich flow. IgG diffusion to the PEG-rich phase was complete after 16 cm of channel. Besides proteins and cells, ATPS have also been used to separate other biomolecules in microfluidics such as virus-like-particles. Jacinto et al. optimized an ATPS for the purification of human immunodeficiency virus-like particles at small scale and successfully achieved similar results in a microfluidic platform (Jacinto, et al., 2015).

The potential of miniaturization as a high-throughput screening tool has also been explored. Silva et al. successfully used microfluidics for the rapid determination of ATPS binodal curves in a work from this thesis and discussed in Chapter 4 (Silva, et al., 2014). Using a three inlet microchannel, two solutions containing separate ATPS solution precursors were loaded into the side inlets, while milli-Q water was loaded into the middle inlet. This setup allowed the screening of a wide range of concentrations inside the microchannel by varying the flow rates of the solutions while using sub-mL volumes for each ATPS-forming system. Finally, ATPSs have also been used for the micropatterning of surfaces. Frampton et al. performed the micropatterning of different cell populations within a microfluidic channel using an ATPS composed of dextran and PEG. This approach enabled good cellular viability and adhesion with minimal cross-contamination between cell populations (Frampton, et al., 2011).

2.2.1.1 Application of electrical fields to microATPS

An electric field is produced by charges attracting or repelling other electric charges by exerting force (Purcell, et al., 2013). Mathematically the electric field is a vector field that associates to each point in space the force, called the Coulomb force, that would be experienced per unit of charge, by an infinitesimal test charge at that point (Purcell, et al., 2013) (Munchow, et al., 2006). The units of the electric field in the SI system are newtons per coulomb (N/C), or volts per meter (V/m). The augmentation of ATPS separation potential by applying an electric field is a technique that has been applied for more than 20 years (Theo, et al., 1995) (Stichlmair, et al., 1992) (Lindblad, 2009). In these macroscale applications, the electrical field

was the primary principle behind the extraction, while the ATPS purpose was to prevent the formation of convection flows that would disrupt the extraction, resulting in a process that is called electroextraction. A microfluidic approach to this has already been performed (Schoonen, et al., 2014), however, as with the macroscale example, the primary extraction principle is the electric field.

In this work the electrical field is created by placing two electrodes parallel to each other and maintaining a potential difference between them. This creates an electric field that is an approximation to an uniform field. The reason why it is only an approximation is that the two electrodes cannot be infinite planes and near the edge of the electrodes the electrical field is distorted. In uniform fields the magnitude of the electric field E is:

$$E = \frac{\Delta V}{d} \quad \text{Equation 2.6}$$

where ΔV is the potential difference between the plates and d is the distance separating the plates. In micro-applications, for instance, in relation to semiconductors, a typical magnitude of an electric field is in the order of 10^6 V/m, achieved by applying a voltage of the order of 1 volt between conductors spaced 1 μm apart.

Furthermore, a uniform electric field will also have an influence on the motion of dispersed particles relative to a fluid under the influence of the electric field (Lyklema, 2000) (Stichlmair, et al., 1992) (Hahn, et al., 2011) (Munchow, et al., 2006). This electrokinetic phenomenon, referred to as electrophoresis, was observed for the first time in 1807 by Russian professors Peter Ivanovich Strakhov and Ferdinand Frederic Reuss, who noticed that the application of a constant electric field caused clay particles dispersed in water to migrate. It is ultimately caused by the presence of a charged interface between the particle surface and the surrounding fluid. It is the basis for a number of analytical techniques used in chemistry for separating molecules by size, charge, or binding affinity (Lyklema, 2000).

Unlike with the work of stichlmair et al or schoonen et al (Stichlmair, et al., 1992) (Schoonen, et al., 2014), the purpose of this work is to use the full separation potential of ATPS and aid the separation using the electrokinetic properties of the electrical field. One of the advantages of ATPS is the adaptability of the ATPS to each process of separation allowing greater specificity and yields in the extraction processes (Soares, et al., 2015). The addition of the electric field adds a new dimension in the extraction process allowing even greater specificity and yields by either increasing the extraction of the molecule of interest or by decreasing the extraction of impurities. The multi-phase nature of ATPS can reduce the convection problems of electrophoresis in solution, as Stichlmair et al discovered (Stichlmair, et al., 1992) and the laminar flowing nature of microfluidics can further reduce any convection problems that electroextraction can experience. Furthermore, in the small distances in

microfluidics, electrokinetic phenomena can be completed in a small amount of time, similar to diffusion processes, allowing for a fast separation.

2.3 SWOT Analysis and Future Trends of ATPS

Considering the current and emerging applications of ATPS extraction performed at the microscale versus their mL-scale counterparts, a strengths, weaknesses, opportunities and threats (SWOT)-type of analysis is fitting in order to summarize the previously discussed information and to put the two approaches in perspective (Figure 2.6).

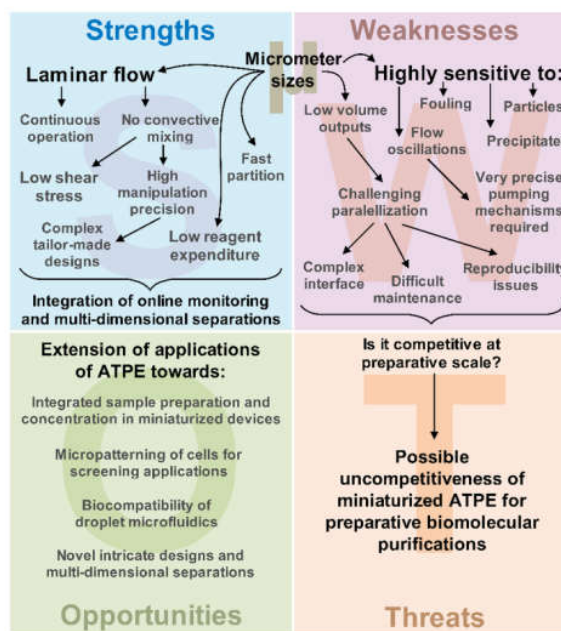


Figure 2.6 - Summary of the main strengths, weaknesses, opportunities and threats of ATPS extraction performed at the microscale (Soares, et al., 2015).

Among the strengths (S) of ATPS extraction performed at the microscale, laminar flow conditions are critical in allowing a continuous operation without convective mixing, while still providing a very fast rate of molecular partition (typically <1 min) by diffusion, with negligible mixing of the phases. Simultaneously, this results in a very low shear stress and a high precision in liquid flow manipulation. Owing to the small dimensions of the system, the lower usable volumes of reagents in the nL range are useful for applications in which the sample is valuable or available only in small amounts. Another important characteristic of the microfluidic platform is that it can be integrated with in-line monitoring via optical measurements or with integration of multi-dimensional separations via the precise manipulation of electric or magnetic fields, for example. On the other hand, among the weaknesses (W) of microfluidics is the intrinsic property of providing very low volume outputs, of the order of a few tens of μL per hour. This characteristic may not be a limitation when the aim is screening or analytical applications, on the other hand, it is strongly limiting at the preparative scale. It is hard to predict at this time whether or not the theoretically feasible massive parallelization (scale-out) of these systems would be economically advantageous, considering the complexity of engineering and integrating

an efficient and reliable flow splitting mechanism that can simultaneously guarantee the quality and reproducibility of several thousands of structures. Furthermore, the small dimensions also require very precise pumping mechanisms and render the system very sensitive to potential aggregates present in solution and to the accumulation of fouling on the surface of the microchannels. Considering the high sensitivity to small particulates, this also renders solid matrix extraction applications unpractical. Nevertheless, analyzing the extrinsic properties when compared to the “macrofluidic approach”, the opportunities (O) of the microscale relate to the extension of applications of ATPS extraction beyond the traditional biomolecular purification towards simpler screening approaches, towards (i) the integration of sample preparation and/or molecular concentration modules in analytical point of care devices, (ii) molecular and cellular patterning at the microscale for high density applications, (iii) the extension of the biocompatibility and possibilities conferred by droplet microfluidics and (iv) the extension of the versatility in engineering novel designs for precise phase manipulation and integration of multi-dimensional types of separation. The main threats (T) to this approach are derived directly from its weaknesses and mainly related to the increased complexity and possible economic constrains related to scale-out applications. Overall, considering the large and rapidly expanding interest in developing portable analytical tools for several fields of application, ranging from environmental to medical analysis and the emerging features of ATPS extraction within the analytical field, microfluidic applications using ATPS extraction are expected to be a trending field of research in the years to come.

3 Methodology

3.1 Development of the solutions

PEG with different molecular weight (MW) (PEG1000 with MW 1000 Da, PEG 3350 with MW of 3350 Da and PEG 6000 with MW 6000 Da) and dextran (dextran 20 with MW 19,800 and dextran 298 with a MW 298,000 Da) were purchased from Sigma–Aldrich (St. Louis, MO, USA), while potassium phosphate dibasic anhydrous (K_2HPO_4) and potassium phosphate monobasic anhydrous (NaH_2PO_4) were purchased from Panreac (Barcelona, Spain). PDMS was obtained from Dow Corning (Midland, MI, USA), under the trade name of Sylgard® 184.. Rabbit anti-goat IgG, BSA, protein A and insulin (all fluorescently labeled with FITC) were purchased from Sigma. Green fluorescent protein (GFP) was produced in house using a standard cultivation procedure for *E. coli* (Campos-Pinto, et al., 2017).

Stock solutions of 50% (w/w) PEG 1000, PEG 3350 and 25% (w/w) PEG 6000 were prepared in deionized (DI) water. Stock solutions of 30% of Dextran 20 and Dextran 298 were prepared in DI water and stock solutions of 40% (w/w) phosphate buffer were prepared in DI water. Phosphate buffer at pH 7 was prepared by mixing 40% (w/w) K_2HPO_4 solution and 40% (w/w) NaH_2PO_4 solution with volume ratio of 2,13 (K_2HPO_4/NaH_2PO_4). The correct pH value was achieved with the addition of 40% (w/w) K_2HPO_4 .

For the experiment that required the ATPS phases separately, ATPS consisting of the proper amounts of PEG, phosphate buffer at pH 7 and NaCl were prepared by weighting the appropriate amounts of the stock solutions of 50% (w/w) PEG, 40% (w/w) phosphate buffer and 99% (w/w) NaCl. The total system weight always corresponded to 10 g. After stirring and settling overnight, the interface separating the two phases became completely formed and clear. The two phases were separated using a 2 ml syringe and stored in different vessels.

Syringe pumps (New Era Pump Systems, Inc., NE-300 model) were used to load the required solutions into the microchannels. For the determination of the binodal curve, stock solutions of PEG, dextran and phosphate buffer were inserted in the appropriate inlets along with milli-Q water. For the determination of the partition coefficient, stock solutions of PEG, dextran and phosphate buffer were inserted in the appropriate inlets along with milli-Q water. The concentration of the target biomolecules in the milli-Q water was 170 mg/L for all the FITC tagged biomolecules and 50 mg/L for the GFP. For the microATPS extraction of mAbs experiment, mAbs-FITC were added to the salt-rich phase to a concentration of 170 mg/L. The salt-rich phase was inserted in the middle inlet while the PEG-rich phase was added to the side inlets. For the experiment involving electrophoresis, the target biomolecules tagged with FITC

were added to the salt-rich phase to a concentration of 170 mg/L. The salt-rich phase and the PEG-rich phase were then inserted in the microchannel.

3.2 Microfluidic devices design and fabrication

3.2.1 Al masks fabrication

The devices were designed using AutoCAD 2011 – STUDENT VERSION software. The designs were used to develop non-inverted Al/glass masks using a photolithography process. For the fabrication of the Al masks, glass substrate (50 mm per 50 mm per 2 mm of thickness) was cleaned with isopropyl alcohol (IPA) (purchased from José M. Vaz Pereira S.A.) and DI water. After being blown dry with a compressed air stream, aluminum with 300 nm thickness was deposited on top of it using Nordiko 7000 Magnetron Sputtering System. Afterwards, the aluminum was coated with the positive photoresist PFR 7790G 27cP (from ©JSR) by the SVG 88 series track system. The photolithography process occurred on Lasarray, DWL 2.0 (Direct Writer Laser) lithography from ©Heidelberg instruments.

The use of glass substrate allowed the passage of ultraviolet (UV) light during the exposure. Since the photoresist used was a positive photoresist, the areas that were exposed to the UV light became soluble to the photoresist developer and were removed. The photoresist was developed on SVG 88 series track system. Afterwards, the sample was immersed in Al etchant from ©Microchemicals. The etching was performed on the exposed Al regions, corresponding to the areas where the photoresist had been removed. The remaining photoresist was striped with acetone (purchased from José M. Vaz Pereira S. A.) The sample was then cleaned with IPA and DI water. An example of one of the masks made can be seen in Figure 3.1.

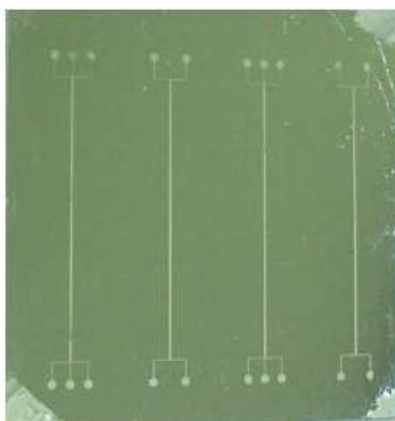


Figure 3.1 – Mask for the two inlets and two outlets device, and the three inlets and three outlets device.

3.2.2 SU-8 mold fabrication

A silica (Si) piece was cleaned with Piranha solution 4:1 (H₂SO₄:H₂O₂) (sulfuric acid at 97% from MERCK and hydrogen peroxide at 30%) for 10 minutes. The negative photoresist SU-8 2005 from MicroChem was poured on the Si substrate and spin-coated to a final thickness of the SU-8 was of 200 μm (1st step of spin coating: 500 rotations per minute (rpm) for 5 seconds; 2nd step: 2000 rpm for 30 seconds), followed by a soft baking on a hot plate at 95°C for 4 min. After a 5 min cooldown at room temperature, the SU-8 was exposed. To expose the SU-8, the Al/glass mask was put on contact with the photoresist (the contact face of the mask was the face containing the Al). The whole structure was put into the UV chamber and was exposed to UV radiation during 25 seconds from a 250 W lamp from UV Light Technology Limited. Since the SU-8 is a negative photoresist, the parts of the photoresist exposed to the UV light got harder and weren't removed during development of the photoresist. After the exposure, a bake of 5 minutes at 95°C was performed. After a 5 minutes cool down, the SU-8 was developed by immersing the sample during approximately 3 minutes in PGMEA from ©Sigma Aldrich. Finally, the sample was cleaned with IPA and dried with compressed air. A final hard bake was made at 150°C for 15 minutes.

3.2.3 PDMS structure fabrication and sealing

PDMS (SYLGARD® 184 silicone elastomer from Dow Corning) was prepared by mixing a base (liquid silicon rubber) and a curing agent in a 10:1 ratio of weight. The mixture was stirred for 5 minutes and de-gassed in a vacuum desiccator (Ted Pella, Inc.) Afterwards, the PDMS was placed on top of the SU-8 mold and cured at 70°C in an oven for 2 hours. After being peeled from the master molds, the access holes were punched with the help of a blunt syringe tip. In order to close the microchannels, glass substrates or PDMS slabs were used. These glass substrates or PDMS slabs were cleaned with water and IPA, and dried with compressed air. The PDMS structures were irreversibly sealed to the glass substrates or PDMS slabs through the use of the Plasma Cleaner (EXPANDED PLASMA CLEANER Model PDC-002 from Harrick Plasma.) The up-sided samples were deposited inside the plasma cleaner chamber which was then sealed, and vacuum was used to deplete the atmosphere in the chamber. Afterwards the chamber was flowed with oxygen gas, and the UV lamp turned to medium for 1 minute. The flow oxygen gas is stopped and vacuum is used to remove the gases inside the chamber. The vacuum is then turned off and the chamber is unsealed. The structures were then withdrawn from the plasma cleaner and bonded to one another. This process also turned the surface of the PDMS structure hydrophilic.

3.3 ATPS and microfluidic devices experiments

Both the salt phase and the PEG phase obtained in section 3.1 were filtered before use. Anti-goat IgG (whole molecule) – FITC antibody, produced in rabbit with a concentration of 3.6

mg/ml was purchased from SIGMA and was mixed with the salt phase to achieve the necessary IgG concentration.

The sealed PDMS structure was placed on a glass cover slip with 50 mm x 50 mm. and placed on the stage of a DMLM model fluorescence microscope from Leica Microsystems Ltd. The salt phase and the PEG phase were inserted in syringes (U-100 insulin) that were connected to the PDMS structure by capillaries (Instech Solomon). The syringes were placed on syringe pumps (NE-300, SyringePump.com). In the experiments with 3 inlet and 3 outlets structures, the configuration of the flow was always PEG phase – salt phase – PEG phase.

The structures were analyzed with the 20X objective. The visible and the fluorescence images were obtained with a digital color camera Leica DFC300 FX. The visible images were obtained with a exposure rate of 1,13 ms. For the observation of the fluoresce images several different exposure rates were used. The analysis of the images taken was made with the image analysis software Image J (Schneider, et al., 2012).

For the experiments involving an electrical field, a glass substrate as described in section 3.2.1 was procured sliced to the appropriated size and cleaned. Using the process described for the Al deposition, etching and development described in section 3.2.1, Al electrodes were added to the glass substrates. An example of these glass substrates with the Al electrodes can be seen in figure 3.2.

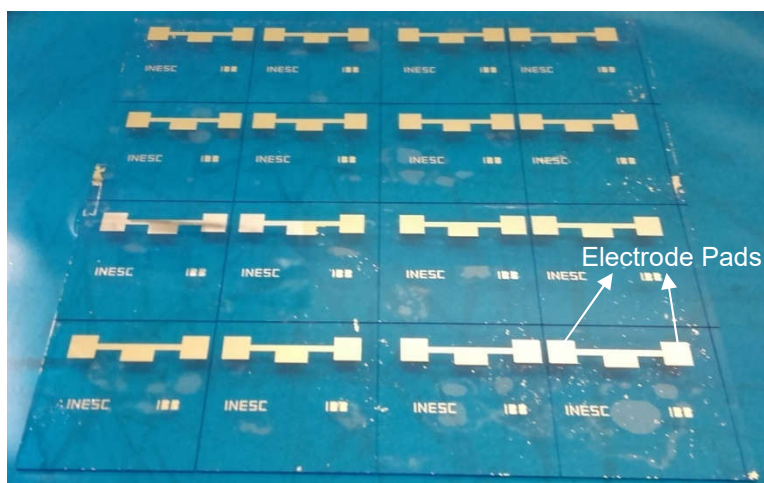


Figure 3.2 - Set of 16 glass substrates for electric field aided ATPS extraction. The gap between the electrodes has not been etched yet.

The glass with the electrodes was then used as substrate for the sealing process of the microfluidic channel. After sealing the tips of two thin gold wires were placed in top of point A of the electrodes pads and contact is ensured by using cadmium to adhere to the pad while enveloping the gold wires. An example of the final structure can be seen in figure 3.3.

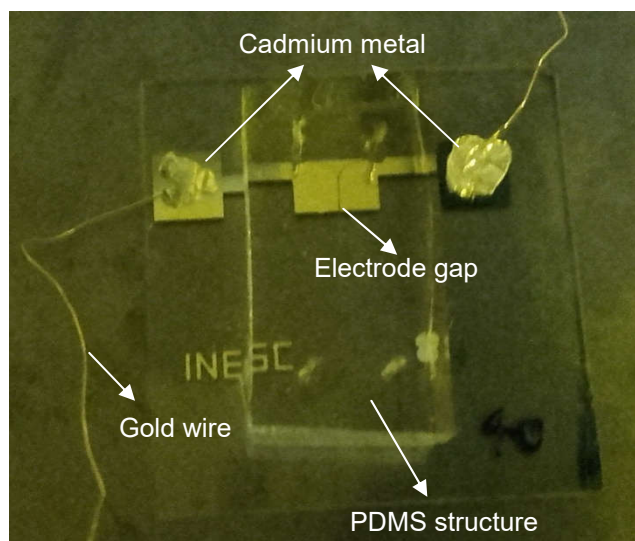


Figure 3.3 - Example of final structure for the electrical field aided ATPS extraction. Picture taken after the gap between the electrodes was etched.

Al etchant was then flowed at $3 \mu\text{L}/\text{min}$ in the microchannel to etch the gap between the electrodes. The etch was monitored by measuring the resistance between the two electrode pads. Once the etch was completed, the microchannel was cleaned by flowing DI water at $5 \mu\text{L}/\text{min}$, followed by an air stream to remove the DI water from the microchannel. Afterwards the microfluidic device is placed on a hot-plate at 110°C for 5 minutes to completely dry the microchannel and then placed in the plasma cleaner and the PDMS structure is resealed against the glass substrate to seal the PDMS around the electrode gap and the microchannel.

The experiments are performed with the syringes pumps and configurations described previously and the micrographs, both normal and fluorescent, were obtained using the microscope described previously. For the establishment of the electrical field, a voltage differential was applied to the electrical fields.

4 IgG separation using a phosphate/PEG ATPS

The miniaturization of a process, such as the separation and purification of biomolecules using ATPS, presents with unique challenges and opportunities that must be taken in consideration when planning possible experiments. As such, in order to simplify the miniaturization of a process, it is best to use an already known process and study what kind of obstacles the miniaturization can face and the methods to surpass said obstacles.

Therefore, in order to develop miniaturized ATPS, a system used to separate IgG was chosen based in an already established and optimized process. In the work of Azevedo et al.,2007, the researchers studied the separation and purification of IgG using an ATPS composed of PEG and Phosphate with NaCl as an additive. Based on this paper, we started our work by attempting to successfully partition the IgG using a PEG/phosphate ATPS within a microfluidic platform. The objective of this work was to be able to use the ATPS extraction within the microfluidic platform with an equal or better efficiency than when the ATPS extraction was used in macroscale setting.

Furthermore, to better understand the conditions in which the ATPS partition occurs in a microfluidic setting, a simulation of the diffusion of molecules in a microchannel and across the interface was developed and compared to the data recovered from the microfluidic ATPS extraction experiments. Additionally, confocal microscopy was also used in order to better understand the behavior of ATPS in microfluidic setting by allowing us to obtain a profile of the shape that a interface assumes while in a microfluidic platform.

Section 4.3 of this work contains information that has been in published in 2012 in the Journal of Chromatography A under the name " Design of a microfluidic platform for monoclonal antibody extraction using an aqueous two-phase system". DOI: [10.1016/j.chroma.2012.06.089](https://doi.org/10.1016/j.chroma.2012.06.089) (Silva, et al., 2012)

4.1 Study of the microfluidic ATPS interface using confocal microscopy

In order for the phases to be distinguishable by the Laser scanning confocal microscopy (LSCM) used, Insulin marked with FITC was added to both ATPS. Insulin-FITC has a partition coefficient of 6.4 and 17.1 for the PEG/dextran ATPS and the PEG/phosphate buffer ATPS, respectively. This means that in both systems the majority of insulin-FITC will be in the PEG phase. This permits the distinction of the phases by the confocal microscope.

With the PEG/phosphate buffer system, the PEG-rich phase was inserted in the two side inlets while the phosphate-rich phase was inserted in the middle inlet (Figure 4.1).

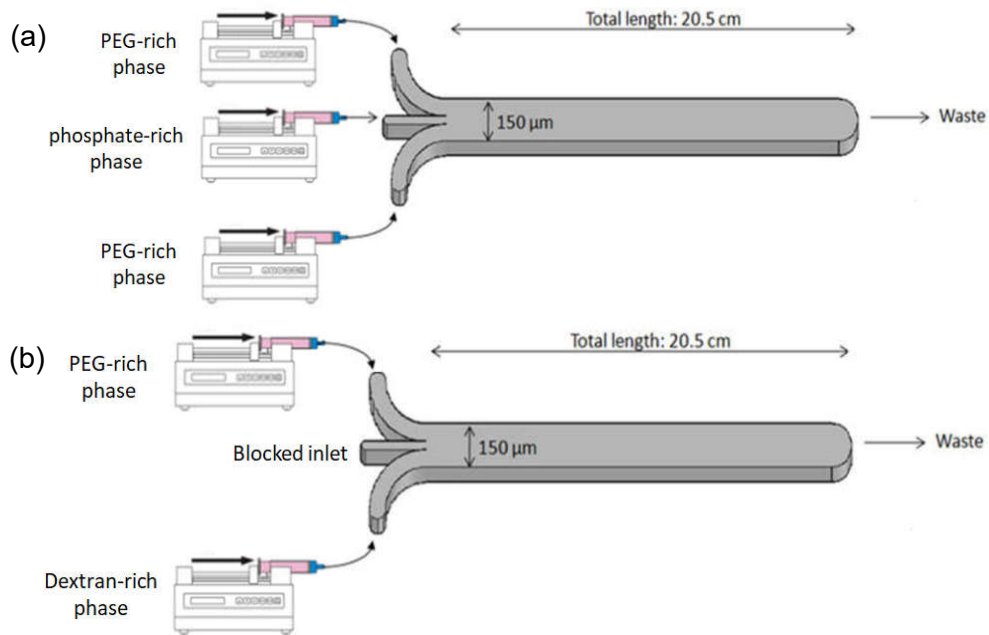


Figure 4.1 - Schematic model of the experimental setup used for measuring ATPSs interface in the confocal microscope. a) Model for the PEG/phosphate buffer ATPS. b) Model for the PEG/dextran ATPS

With this setup, the interface is more stable than attempting only one interface with PEG-rich phase in one side and Phosphate-rich phase in the other. With the PEG/dextran ATPS, the middle inlet is blocked while the dextran-rich phase is inserted in one of the remaining inlets and the PEG-rich phase is inserted in the other remaining inlet (Figure 4.1b). With the higher viscosities associated with the PEG/dextran ATPS, the interface is naturally more stable and, therefore, does not need two interfaces to increase its stability. Furthermore, the higher viscosity nature also means that there is more pressure within the microfluidic channel and it is, therefore, more difficult to insert more than 2 fluids in the microfluidic channel without the microfluidic channel experiencing leaks.

The microfluidic device, once the ATPS phases are being pumped, is then inserted in the confocal microscope. The area of interest for image acquisition is near the outlet of the microchannel.

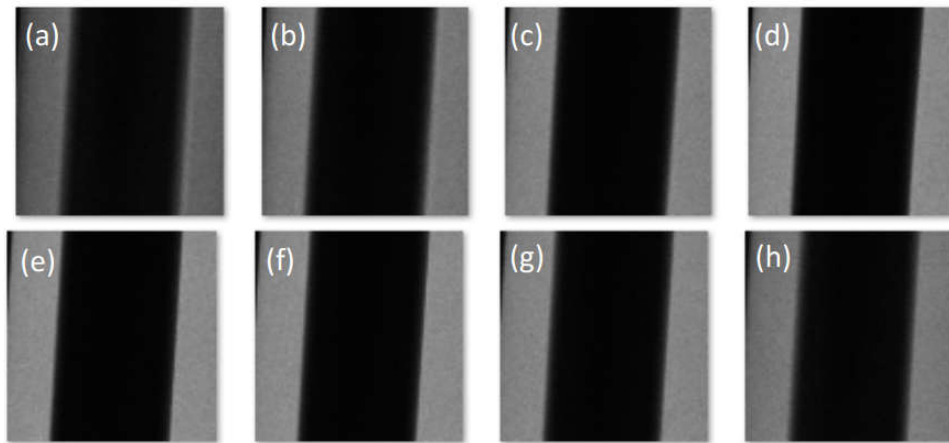


Figure 4.2 - Series of micrographs obtained using a confocal microscope. Images a) through h) are all from the same x-y coordinates but the z coordinate changes $2\ \mu\text{m}$ from each image. The images are a close-up of the interface area within a microfluidic channel using a phosphate buffer/PEG ATPS with insulin-FITC dissolved in it. The microchannel is a 3 inlet microchannel with phosphate-rich phase being inserted in the middle inlet at $1\ \mu\text{L}/\text{min}$ and PEG-rich phase being inserted in both side inlets at $0,3\ \mu\text{L}/\text{min}$. The middle black represents the phosphate rich phase that contains little insulin due to high k_p , while the grey sides are the PEG-rich phases that are fluorescent due to the presence of Insulin-FITC

Figure 4.2 shows multiple images obtained from the confocal microscope. This series of images is then processed by software to create a 3D model shown in figure 4.3.

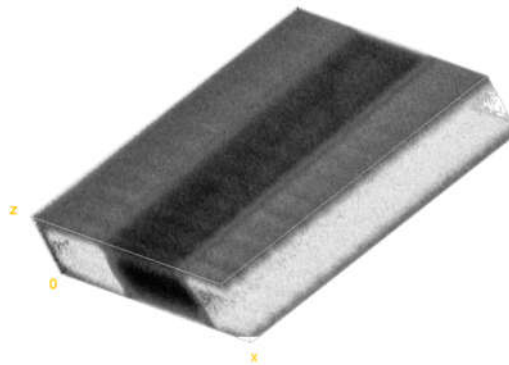


Figure 4.3 - 3D model of the microfluidic channel with phosphate buffer/PEG ATPS being flown. Insulin-FITC was used to distinguish the phases using fluorescence. The middle dark area corresponds to the phosphate-rich phase, while the gray side areas correspond to the PEG-rich phase. This model was obtained by using software to assemble the series of images in figure 4.2

In Figure 4.3, the top visible plane corresponds to figure 4.2h. The objective of this work is to analyze the interface. The best plane to achieve this objective is the cross-sectional x-z plane, the bottom-left plane in Figure 4.3.

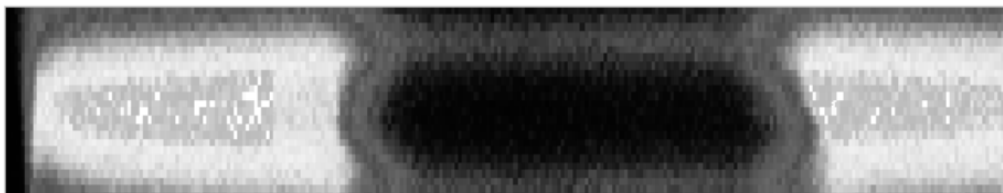


Figure 4.4 - Image obtained from 3D model from Figure 4. Representation of a cross section of the microchannel with a phosphate buffer/PEG ATPS using insulin-FITC to distinguish the phases with fluorescence.

In Figure 4.4, the ATPS used was the PEG/phosphate buffer ATPS. The side bright areas represent the PEG-rich phase while the middle dark area is the phosphate-rich phase. The phases of the ATPS were being pumped at 0.3 $\mu\text{L}/\text{min}$ for the two PEG-rich phases and 1.0 $\mu\text{L}/\text{min}$ for the phosphate-rich phase. As can be seen the interface presents a rather marked curvature. This is most likely caused by the fact that the PEG-rich phase, being more hydrophobic than the phosphate-rich phase, has a greater affinity for the PDMS walls of the microfluidic channel and, as such, the interface buckles to increase the contact of the PEG-rich phase to the microchannel walls. Also of note, there is some brightness in the top and bottom of the middle darker phosphate-rich phase. This suggests that there exists a thin layer of the PEG-rich phase between the microchannel walls and the phosphate-rich phase. Again, this is most likely due to the higher affinity that the PEG-rich phase has for PDMS.

The next step was to see if the increase in speed of the phases within the microchannel has any effect in the interface.



Figure 4.5 - Image obtained from 3D model from a source similar to figure 4.2 with different solution loading rates. Representation of a cross section of the microchannel with a phosphate buffer/PEG ATPS using insulin-FITC to distinguish the phases with fluorescence. The phosphate-rich phase was inserted at 1.2 $\mu\text{L}/\text{min}$ and the PEG-rich phase was inserted at 0,5 $\mu\text{L}/\text{min}$.

In Figure 4.5, the ATPS used was the PEG/phosphate buffer ATPS. The side bright areas represent the PEG-rich phase while the middle dark area is the phosphate-rich phase. The phases of the ATPS were being pumped at 0.5 $\mu\text{L}/\text{min}$ for the two PEG-rich phases and 1.2 $\mu\text{L}/\text{min}$ for the phosphate-rich phase. As seen before, the interface shows a curvature that is increasing the contact of the PEG-rich phase with the microchannel wall, for the same reasons stated previously. However, Figure 4.5 lacks the small amounts of brightness in the top and bottom of the middle darker phosphate-rich phase, which suggests that the thin layer of PEG-rich phase present in Figure 4.4 has disappeared in Figure 4.5. This is possibly due to the increase in pressure that is a result of the increase in speed of the phases. This increase in pressure within the microchannel creates difficulties in the appearance of such a thin layer such as the one present in Figure 4.4.

The next system to be tested was a polymer/polymer system, dextran/PEG ATPS. Since the experimental setup for the PEG/dextran system is different from the PEG/phosphate ATPS (Figure 4.4), the 3D models obtained for this system will be different from the ones obtained for the PEG/phosphate buffer ATPS.

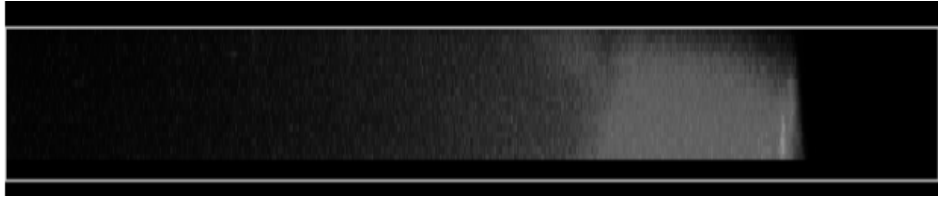


Figure 4.6 - Image obtained from 3D model from a source similar to figure 3.2 with different ATPS and different solution loading rates. This image is a representation of a cross section of the microchannel with a dextran/PEG ATPS using insulin-FITC to distinguish the phases with fluorescence. The PEG-rich phase was inserted at 0.3 $\mu\text{L}/\text{min}$ and the dextran-rich phase was inserted at 0.3 $\mu\text{L}/\text{min}$.

As can be seen in Figure 4.6, there is only one interface, with the bright PEG-rich phase in one side and the dark dextran-rich phase on the other, as expected. The curvature in the interface is again visible, with a similar explanation as before and there is no layer of brightness around the dark dextran-rich phase. This is due to the fact that the PEG/dextran ATPS is much more viscous than the PEG/phosphate-buffer ATPS, which means that, even at low fluid speed, the PEG/dextran ATPS has a greater pressure within the microchannel.



Figure 4.7 - Image obtained from 3D model from a source similar to figure 3.2 with different ATPS and different solution loading rates. This image is a representation of a cross section of the microchannel with a dextran/PEG ATPS using insulin-FITC to distinguish the phases with fluorescence. PEG-rich phase was inserted at 0.6 $\mu\text{L}/\text{min}$ and dextran-rich phase was inserted at 0.6 $\mu\text{L}/\text{min}$.

The increase in fluid velocity does not seem to have an impact on the interface in the PEG/dextran ATPS. Figure 4.7 does not show any significant difference from Figure 4.6. The explanation and conclusions drawn from Figure 4.6 also apply to Figure 4.7.

The curvature of the interface can also offer additional information by measuring the contact angle between the interface and the PDMS walls represented by the bottom and top of Figure 4.4 to Figure 4.7. Unfortunately, it was not possible to accurately measure this contact angle in the models that were obtained. The contact angles obtained varied from 35° to 53° for the PEG/phosphate buffer system with PEG-rich phase was inserted at 0.5 $\mu\text{L}/\text{min}$ and phosphate-rich phase was inserted at 1.2 $\mu\text{L}/\text{min}$, and from 29° to 45° for the PEG/dextran system with PEG-rich phase was inserted at 0.6 $\mu\text{L}/\text{min}$ and dextran-rich phase was inserted at 0.6 $\mu\text{L}/\text{min}$. This is presumably caused by the fact that the interface is in fact a small area, so there is always a small blurriness which makes measuring the angle exactly a difficult operation. Furthermore, since the ATPSs are in constant motion within the microfluidic channel, the interface is also in constant movement and small motions of the interface can easily interfere with the acquisition of images from the confocal microscope.

4.2 Simulations development

4.2.1 Comsol multiphysics simulations

The emulation of real-life situations is the objective of any simulation. In our case the situation to be emulated is the behavior of two phase systems in a microchannel with diffusion occurring from one phase to the other. To achieve this, the first step in the comsol multiphysics simulation was to emulate the behavior of single phased fluids in the microchannel. Following that, the behavior of the interface in two phased fluids in the microchannel was emulated. Lastly using the velocity fields obtained in the previous simulations and coupling them with the equations that define the IgG diffusion in the system, a simulation of our system was obtained. To simplify the simulation, it was developed only in two dimensions (2-D) using several geometries created in AutoCAD. In all simulations the length of the microchannel was much shorter than that of the real-life system. Except for the diffusion of the IgG, the factors involved in our real-life systems and simulations, like the interface position, the velocity field and others, become fully developed very quickly. As for IgG diffusion, it is necessary that it is accelerated in the simulation, for reasons explained further ahead. Consequently, the microchannel in the simulation only needs a fraction of the length that the microchannels in the real-life systems possess, thus simplifying the simulation.

For the simulation of the velocity field with single phased fluids, the Incompressible Navier Stokes (INS) module was used, since the PEG and salt phases are considered to be Newtonian. As per the name of the module, the fluid is considered to be incompressible. The equation used by Comsol Multiphysics to determine the velocity field is, as expected, based on the INS equation.

$$\rho \frac{\partial v}{\partial t} - \nabla \cdot \left[-pI + \eta \left(\nabla \mu + (\nabla \mu)^T \right) \right] + \rho v \cdot \nabla v = F \quad \text{Equation 4.1}$$

$$\nabla v = 0 \quad \text{Equation 4.2}$$

where ρ is the fluids density, v is the flow velocity, η is the fluid density, p is the pressure, I is the identity matrix, which is a matrix that when multiplied with any other matrix will result in that other matrix, and F is the external forces acting on the fluids. The external forces are the gravitational force, the surface tension and additional body forces. Since the gravitational forces scale linearly with the dimensions of the channel, it can be neglected in microfluidic channels. Since the fluids are pressure driven in all cases, the body forces are null. As for the surface tension, this is neglected in order to simplify the simulation. Thus, F is null. As for the viscosity and density of the fluids, the values in Rosa et al. (2009) were used (Table 4.1). For the single phased simulations, only the values of the salt phase were considered.

Table 4.1 - Density and viscosity values for the PEG phase and the salt phase used on the microfluidic system. Values from Rosa et al., 2009.

	PEG phase	Salt phase
ρ (kg/m ³)	1161	1236
η (Pa/s)	27×10^{-3}	$2,8 \times 10^{-3}$

In order to solve the partial differential equations (PDE), Comsol Multiphysics require the definition of boundary conditions. On the device walls, the no-slip condition is applied, which means that at the solid-liquid interface, the liquid velocity will be equal to the solid velocity, which is 0 m/s. The boundary condition in the inlets was defined with the velocity condition, meaning that the velocity at which the fluids are driven into the channel is a defined value. And for the outlets the boundary condition defined was pressure and no viscous stress, meaning that the boundary is entirely controlled by pressure. Thus, the fluids velocity at the outlets is a ratio of the pressure drop along the channel and the resistance of the channel, according to

$$Q = \frac{\Delta p}{R} \quad \text{Equation 4.3}$$

where Q is the flow rate, Δp corresponds to the pressure difference along the channel and R corresponds to the channels resistance.

Lastly Comsol requires the establishment of a mesh, since it uses a finite element method (FEM) to solve the PDE. Comsol divides the original system into smaller subdomains called mesh elements, using then a linear function to approximate the mesh elements to the original system. The solution accuracy is determined by the individual mesh element size and Comsol automatically creates smaller sized mesh elements in areas with greater geometrical complexity. With decreasing size of individual mesh elements, the accuracy of the solution increases. In all simulations the mesh used had triangular geometry. In the INS module the type of solver used had the steady state condition. The use of the steady-state condition reflected a continuously running ATPS system with fully developed fluid flow shown in figure 4.8 (Lindblad, 2009).

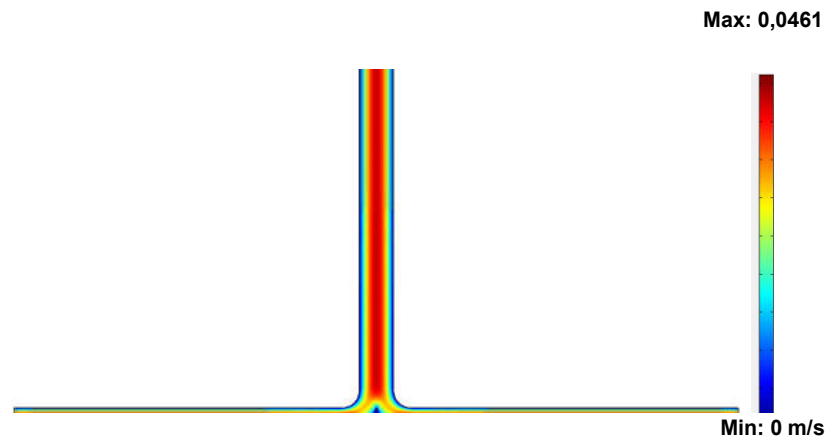


Figure 4.8 – Velocity field predicted by Comsol Multiphysics® for a single phase solution. The solution considered was water ($\rho=1000 \text{ kg/m}^3$, $\eta=1 \times 10^{-3} \text{ Pa/s}$) and the velocity in the inlets was 3,125 m/s. The mesh predefined size was extremely fine and was refined once. The final number of mesh elements was 6956

The simulation of the two phased flow is more complex than of the single phased flow. Instead of one, there are two sets of viscosity and density parameters that needs to be used in the simulation and the modeling of the interface is very complex. Comsol offers two modules capable of modeling the behavior of ATPS interface flow in a microfluidic device, the level set module and the phase field module. Both modules use a phase field variable (ϕ) to express the ratio between fluids in a certain location. This variable is important to account for the differences in the density and viscosity in a certain location. The difference between the modules is that the level set module uses the differences in the two fluids densities and viscosities to directly track the interface and includes the effect of surface tension and gravity, while the phase field defines the interfacial layer using the calculated ϕ value. The consequences are that the level set module offers a better mass conservation while the phase field module ensures that the total energy of the system decreases correctly. Thus, the phase field includes more parameters in its calculation, which means that it performs more complex operations. The selected module is the level set, because the mass conservation is, in this case, more important that the accuracy calculating the system's energy. Additionally, since the interface is in a straight line, there is no need for the greater complexity of the phase field module.

The level set module requires the definition of several new conditions. First the solver used is for transient instead of steady state. The equations form must be defined between conservative and non-conservative, the difference being that the conservative ensures absolute numerical conservation. When performing the calculations needed, there are small numerical fluctuations in the velocities and positions of the phases that can cause a small increase or decrease in factors such as the total mass within the system, which does not corresponds to reality that is being simulated, since this is necessarily a simulation of steady state microfluidics. The conservative form corrects the values mid simulation to ensure that factors such as mass, total velocity among others will be constant within the simulation. Even though the conservative form ensures correction, it has a greater tendency to fail due to numerical error, so the selected form was the non-conservative to ease the modeling. The conditions of the wall, inlets and outlets are equal to the conditions of the one phased fluid simulation in the INS module, with the

exception that there is a need to define the ϕ for each inlet (equal to 1 in one of the inlets and to 0 in the other) and it is necessary to define two sets of densities and viscosities. The densities and viscosities used are the ones of PEG and salt phase in Table 4.. The level-set module also requires two new parameters which are the reinitialization parameter (γ) and a parameter to control the interface thickness (ϵ). The parameter γ determines the amount of reinitialization or stabilization of the level set function. γ is an imposed limit in the simulation that tracks the amount of distortion of the interface that is the result of an accumulation of numerical errors. If γ is too small, then the simulation will have a higher likelihood of failing due to the corrections of the distortions causing failure, but if γ is too high then the simulation will have a higher degree of error. Both parameters were tuned by trial and error method to 0,0464 m/s for γ and $1,5 \times 10^{-5}$ m for ϵ .

Since the level set module tracks the interface directly, it is necessary to have a initialization of the interface to ensure a smooth progression of ϕ across the interface without exceeding 1 or dropping below 0. The interface initialization is calculated in a defined boundary and then the simulation tracks the interface development originated from that defined boundary during a set time. The time was defined as 2 seconds with a step time of 0.1 seconds. The chosen time did not permitted complete development of the system in the end of the channel (see attachments) but, since figure 4.9 shows that the system is well developed in the beginning of the microchannel it was not necessary to restart the simulation with more time.

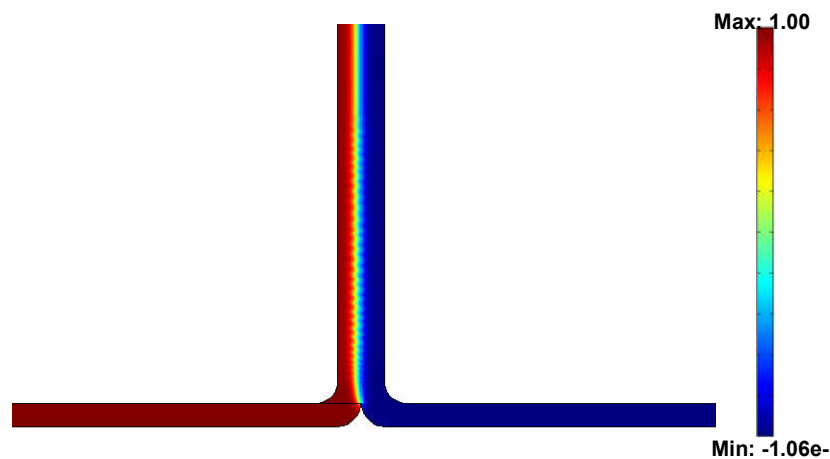


Figure 4.9 – Salt phase ratio in the microchannel predicted by Comsol using the level set module, detail of the beginning of the microchannel. The mesh was refined several times to a final number of 111296 elements of mesh. The initial trepidation in the interface is a result of numerical instabilities. However, since the ϕ in that area is smooth and between 0 and 1 (see attachments) it is does not invalidate the simulation.

The final stage of Comsol simulations is to model the IgG diffusion from the salt phase to the PEG phase with the convection and diffusion module. Comsol does not offer the possibility to link the level set module with the convection and diffusion module, which explains the option of leaving the level set simulation unfinished in the end of the channel. Instead a boundary was defined in the middle of the channel and the INS module was used to determine fluid behavior in those two domains. The boundary conditions are the same used previously.

Since there are two domains it is possible to define two fluids in the INS module and by establishing the imposed boundary with the condition continuity, the fluid behavior in this simulation is quite similar to the one in the level set modules.

As for the convection and diffusion module, it is necessary to define a diffusion coefficient, D , which will be $4,4 \times 10^{-11} \text{ m}^2/\text{s}$, the diffusion coefficient for the IgG (Mark, Radomsky, Whaley, & Cone, 1994) and an initial concentration in the salt phase. The velocities used are the ones obtained in the simulation with the INS module and the internal boundary. Finally the imposed internal boundary is once again used as the interface with the condition Flux, which allows the definition of a flux of the solute from one domain to the other. Equation 1. 2 was used to define the flux with a partition coefficient of 2,15 (Rosa, et al., 2007). The diffusion coefficient in the interface was defined as 10^4 m/s . This clearly exaggerated value is used to stabilize the simulation without meaningful consequences, since the diffusion speed will be controlled by the diffusion coefficient of the general system. Additionally, since the partition coefficient is bigger than one, diffusion would be faster in the interfacial area even with the correct diffusion coefficient, which means that the diffusion velocity would be controlled by the general diffusion regardless. One other condition imposed for the stabilization of the system is the conservative condition. This condition can only be used for systems that contain incompressible fluids and it helps to stabilize the system simply because the Comsol does not have to calculate the mass variation, decreasing the work load.

Even with all the stabilization methods used, Comsol cannot solve the simulation of the referenced system. The main problem lies with the mesh of the system and the Péclet number (Pe). The Pe is a measure of the relative importance of the convective effects compared to the diffusive effects; a large Pe indicates that the convective effects dominate over the diffusive effects. When the Pe is large, the formation of steep gradients often results in disturbances in the system if the size of the mesh elements is not small enough to reproduce the steep. In theory, it is possible to refine the mesh to a level where no disturbances originate, but in reality the refining of the mesh increases the work load of Comsol and a limit of mesh size exists that depends of the parameters of the computer used to solve the Comsol simulations. Thus it is common to use stabilization techniques incorporated in Comsol to fix this problem. Comsol offers several stabilization techniques for the convection and diffusion module, but the only one used is the simpler one, the addition of isotropic diffusion. In this technique, a tuning parameter is added to the diffusion coefficient. It does not entirely resolves the problem but with this parameter the Pe decreases and the disturbance introduced in the system is dampened. Logically, this tuning parameter should be as small as possible to increase the accuracy of the solution, since it increases the diffusion coefficient, accelerating the diffusion speed across the channel.

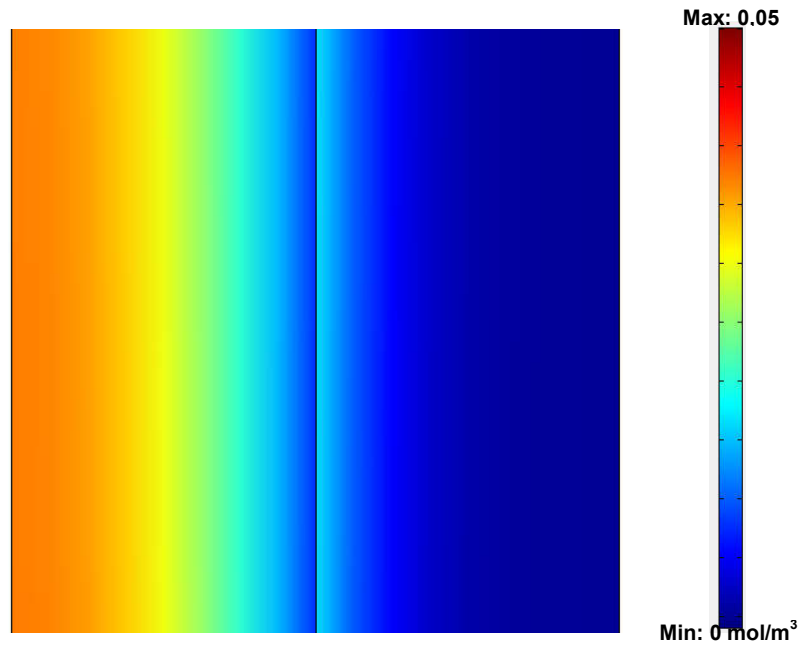


Figure 4.10 – Detail of the IgG diffusion Comsol simulation in the microchannel at approximately 7 mm of the beginning. The initial concentration in the salt phase used was of $0,04 \text{ mol/m}^3$. The number of mesh elements was of 98560 and the tuning parameter used for the isotropic artificial diffusion was 0,005.

4.2.2 Diffusion progression simulation

The Comsol simulation, although good to see the concentrations profiles at determined points, is unsuited to track the diffusion across the interface, due to the artificial diffusion that was necessary to add. Hence, another simulation was done without using Comsol. The simulation of the effect of the partition and diffusion of the antibody was made by constructing a two dimensional matrix that represented the position along the length and across the width of the microchannel. In this matrix, each row, j , corresponds to a given distance along the length of the microchannel and each column, i , to a given distance across the microchannel cross section. Each row represented a section $70 \mu\text{m}$ long along the microchannel and each column a section $5 \mu\text{m}$ wide across the microchannel. Therefore, each node in this simulation represented an area of $350 \mu\text{m}^2$ of the microchannel. The width of each phase was chosen based on experimental observations, i.e., $30 \mu\text{m}$ for the middle salt-rich phase and $60 \mu\text{m}$ for each of the side walls PEG-rich phases. It was assumed that, at the beginning of the microchannel, the concentration of the antibody was 0.2 mg/mL in the salt-rich phase and zero in the PEG-rich phases. The flux of antibody from the salt-rich phase to the PEG-rich phases was calculated according to Fick's first law. Equation 2.1 was used to describe the antibody diffusion in the bulk phases and Equation 2.2 to describe the antibody partition at the interface.

The partition coefficient is a measure of the distribution of a solute between two immiscible phases and it is given by the quotient between the concentration of the solute in the top phase (PEG-rich phase) and in the bottom phase (salt-rich phase). For this reason in the

model the concentration in the top phase was always expressed as the concentration in the bottom phase times the partition coefficient. The molecular diffusion in the j axis is negligible compared to the movement of particles caused by the convection of solutions. Therefore, molecular diffusion in the j axis was not considered in the simulation. At the beginning of the microchannel, row number $j=1$, there is 0.2 g/L of antibody in the salt-rich phase and no antibody in the PEG-rich phases. The flux of antibody to the adjacent cells is calculated using Equations 2.1 and 2.2. Since the solutions are flowing, the distance along the channel also corresponds to the time available for diffusion between each rows. Therefore the antibody concentration in each cell is affected by the cells in the row before and not by cells in the same row. Table 4.2 represents a small part of the simulation with the equation used to calculate the antibody concentration of a few cells.

Table 4.2 - Schematic of the method used for the simulation of the diffusion progression along the length of the microchannel (L). The time (t) is calculated based on the length (L) attributed to the row and the velocity of the fluids. D is the diffusion coefficient, $c_{j,i}$ is the concentration value of the cell at row number j and column number i . l_w represents the distance between two adjacent columns, equivalent to l in Equations 1.1 and 1.2. In this case l_w is always 5 μm , and t_d represents the time required for the fluid to move between two adjacent rows. The calculation of the equations used to calculate the antibody concentration for characteristic selected matrix positions highlighted with circles (circled in the table) is detailed at the bottom given below the table.

Row number, j	Column number, i					
	...	PEG-rich phase		Salt-rich phase		...
j	...	11	12	13	14	...
1	0	0	0	2.00×10^{-1} ^A	2.00×10^{-1}	2.00×10^{-1}
2	0	0	1.91×10^{-2}	1.81×10^{-1} ^B	2.00×10^{-1}	2.00×10^{-1}
3	0	8.46×10^{-4}	3.51×10^{-2}	1.65×10^{-1}	1.99×10^{-1} ^B	2.00×10^{-1}
4	3.75×10^{-5}	2.33×10^{-3} ^C	4.86×10^{-2} ^D	1.51×10^{-1}	1.98×10^{-1}	2.00×10^{-1}
5	1.37×10^{-4}	4.28×10^{-3}	6.00×10^{-2}	1.40×10^{-1}	1.96×10^{-1}	2.00×10^{-1}
...	3.15×10^{-4}	6.56×10^{-3}	6.96×10^{-2}	1.30×10^{-1}	1.93×10^{-1}	2.00×10^{-1}

$$\text{A: } c_{2;13} = c_{1;13} + (c_{1;12} - K_p c_{1;13}) \frac{Dt_d}{l_w} + (c_{1;14} - c_{1;13}) \frac{Dt_d}{l_w}$$

$$\text{B: } c_{4;14} = c_{3;14} + (c_{3;13} - c_{3;14}) \frac{Dt_d}{l_w} + (c_{3;15} - c_{3;14}) \frac{Dt_d}{l_w}$$

$$\text{C: } c_{5;12} = c_{4;12} + (c_{4;11} - c_{4;12}) \frac{Dt_d}{l_w} + (c_{4;12} - c_{4;11}) \frac{Dt_d}{l_w}$$

$$\text{D: } c_{5;12} = c_{4;12} + (c_{4;11} - c_{4;12}) \frac{Dt_d}{l_w} + (K_p c_{4;13} - c_{4;12}) \frac{Dt_d}{l_w}$$

The IgG diffusion coefficient in the salt-rich phase was determined by performing an experiment in which a solution identical to the salt-rich phase of the ATPS was pumped into all three inlets at 0.2 $\mu\text{L}/\text{min}$. In one of the side inlets, IgG was mixed in the solution. Fluorescence images from several points of the microchannels were obtained. The flux of antibody in the salt-rich phase along the microchannel from one side of the microchannel to the other was calculated from the variation in fluorescence and was used to calculate the diffusion coefficient. The IgG diffusion coefficient in the PEG-rich phase was calculated from the fluorescent

micrographs from the experiments. The flux of IgG in the PEG-rich phase was calculated from the variance in fluorescence in the PEG-rich phase only. Using the IgG flux in the PEG phase it was possible to calculate the diffusion coefficient. The diffusion coefficients of IgG thus determined were $20 \times 10^{-11} \text{ m}^2/\text{s}$ in the salt-rich phase and $6.8 \times 10^{-11} \text{ m}^2/\text{s}$ in the PEG-rich phase; the partition coefficient was 2.15 (Rosa, et al., 2007). The linear velocity of each of the two phases was determined by dividing the volumetric flow rate by the cross section that each phase occupied in the microchannel.

4.2.3 Yield and final concentration of IgG prediction

The determination of the IgG concentration in the PEG phase and of the yield uses the partition coefficient, H . Therefore both methods are only correct in cases where the separation of IgG between salt and PEG phase has been completed. To determine the theoretical yield, it is needed the definition of yield:

$$\gamma = \frac{m}{m_{total}} \quad \text{Equation 4.4}$$

where γ is the theoretical yield of the system, m is the IgG mass that is recovered at the end of the microchannel and the m_{total} is the total mass of IgG of the system. Equation 4.4 can be rewritten by considering that the total mass of IgG in the system equals the sum of IgG mass in the salt and PEG phase at the end of the microchannel. Since the mass is the product between the concentration and volume it becomes:

$$\gamma = \frac{c_{PEG} \times V_{Pr}}{c_{PEG} \times V_{PEG} + c_{salt} \times V_{salt}} \quad \text{Equation 4.5}$$

where c_{PEG} and c_{salt} are the concentrations of IgG in the PEG and salt phase respectively at the end of the microchannel, V_{PEG} and V_{salt} are the volumes of PEG and salt phases respectively and V_{Pr} is the volume of recovered PEG phase. A volume ratio between the salt and PEG phase will equal the ratio between the volumetric rates of salt and PEG phase. Using that ratio will allow to use the volumetric rates of the experiences directly in the equation and will allow the removal of all the volumes in equation 4.5, resulting in

$$\frac{V_{PEG}}{V_{salt}} = R_v = \frac{\vartheta_{PEG}}{\vartheta_{salt}} \quad \text{Equation 4.6}$$

where R_v is the volume ratio between the PEG phase and the salt phase and ϑ_{PEG} and ϑ_{salt} are the volumetric pumping rates of the PEG phase and the salt phase respectively. Considering the partition coefficient and that V_{Pr} is the product between V_{PEG} and a waste ratio, which is the ratio between the volume of recovered PEG phase and the total volume of PEG phase, equation 4.5 can be rewritten as:

$$\begin{aligned}
\gamma_{teorico} &= \frac{c_{PEG} \times V_{Pr}}{c_{PEG} \times V_{PEG} + c_{salt} \times V_{salt}} = \frac{c_{PEG} \times V_{PEG} \times R_{Pr}}{c_{PEG} \times V_{PEG} + \frac{c_{PEG} \times V_{PEG}}{R_v \times H}} \\
&= \frac{c_{PEG} \times V_{PEG} \times R_{Pr}}{\left(1 + \frac{1}{R_v \times H}\right) \times (c_{PEG} \times V_{PEG})} = \frac{R_{Pr}}{1 + R_v^{-1} \times H^{-1}}
\end{aligned}
\tag{Equation 4.7}$$

where R_{Pr} is the waste ratio. Calculating a ratio of recovered volume PEG phase is not easy, since the real value can vary. However, since the objective is to obtain the greatest yield possible, the system is engineered to have the smallest amount of loss possible. As such, a minimum of 5% and a maximum of 30% of the recovered PEG ratio will be considered. Losing more than 30% of PEG phase is not acceptable and the system will have to be modified to reduce the amount of PEG lost, so this interval is acceptable.

To determine the theoretical final concentration of IgG in the PEG phase, we start from the definition of the partition coefficient.

$$H = \frac{c_{PEG}}{c_{salt}} (=) c_{PEG} = c_{salt} \times H = H \times \frac{m_{salt}}{V_{salt}}
\tag{Equation 4.8}$$

where m_{salt} is the mass of IgG in the salt phase at the end of the channel. Due to the nature of the ATPS separation, the separation of any molecule in an ATPS will be more efficient if the accepting phase has none of that molecule initially. While there might be cases where that might not be possible, in our system, the accepting PEG phase, does not have any IgG initially. Thus, for our system, the m_{salt} can be expressed by the difference between the mass of IgG in the salt phase at the beginning of the channel and the mass of IgG in the PEG phase at the end of the channel,

$$\begin{aligned}
c_{PEG} &= \frac{m_{sb} - m_{PEG}}{V_{salt}} \times H = \frac{c_{sb} \times V_{salt} - c_{PEG} \times V_{PEG}}{V_{salt}} \times H = \\
&= c_{sb} \times H - c_{PEG} \times R_v \times H
\end{aligned}
\tag{Equation 4.9}$$

where m_{sb} is the mass of IgG in the salt phase at the beginning of the channel, m_{PEG} the mass of IgG in the PEG phase at the end of the channel and c_{sb} is the concentration of IgG in the salt phase at the beginning of the channel. By placing all terms with c_{PEG} in the same side of the equation becomes:

$$c_{PEG} \times (1 + R_v \times H) = c_{sb} \times H (=) c_{PEG} = \frac{c_{sb} \times H}{1 + R_v \times H} = \frac{c_{sb}}{H^{-1} + R_v}
\tag{Equation 4.10}$$

According to equations 4.7 and 4.10, Both the yield and the final concentration of IgG increase with the increase of the partition coefficient, which is logical, since the increase of the partition coefficient signifies an increase in the mass of IgG that goes from the salt phase to the PEG phase. In a microfluidic setup, it is possible to actively manipulate the R_v value during the experiment due to the use of syringe pumps. So simulations of the effects that R_v can have to the yield and the final IgG concentration were performed (Figure 4.11 and 4.12).

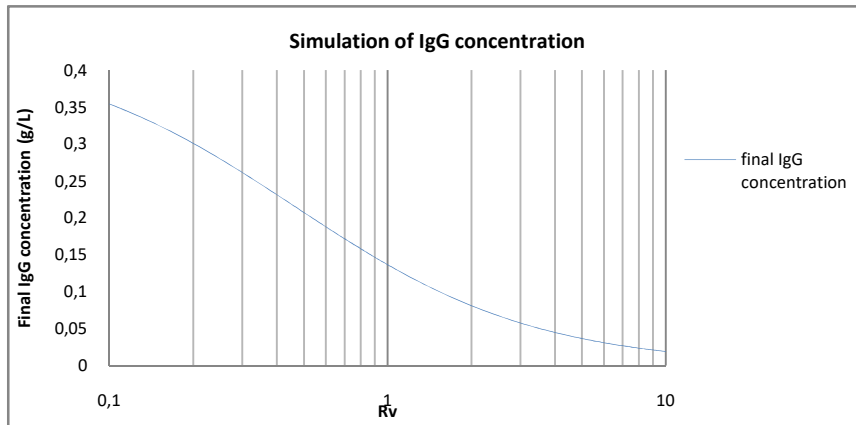


Figure 4.11 – Simulation of the final IgG concentration in the PEG phase with the variation of R_v , based on equation 4.10. The partition coefficient considered was 2,15 (Rosa, et al., 2007).

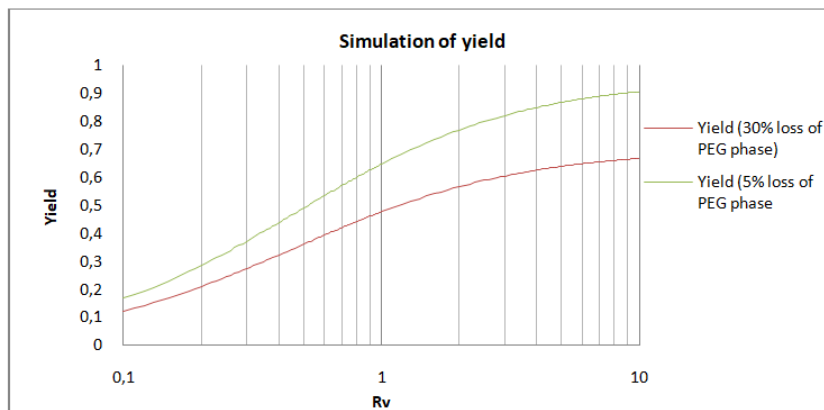


Figure 4.12 – Simulation of the yield of the system with the variation of R_v , based on equation 4.7. The partition coefficient considered was 2,15 (Rosa, et al., 2007).

It is interesting to note that the increase of the R_v , meaning the increase of volume of PEG phase relative to the salt phase, increases the yield but diminishes the final concentration of IgG in the PEG phase. The increase of volume of the PEG phase relative to the salt phase means that there is a greater amount of PEG phase to receive the IgG, so it is logical that the yield increases. The reason why the final concentration drops with the increase of R_v is due to the fact that, with greater amounts of PEG phase, the IgG will logically become more diluted.

4.3 IgG separation and purification

4.3.1 Preliminary microfluidic structure design studies

The first structure fabricated was a two inlets and two outlets straight microchannel with 200 μm of width, 20 μm of height and 3.14 cm of length.

Experiments performed with this first microchannel device showed that the two phases could coexist in a laminar flow, forming a stratified type flow. It was however observed that there was almost no variation in fluorescence of either phase indicating that partition was negligible probably due to the low residence time. The microchannel was then redesigned to enhance partition. The microchannel extraction structure was designed as a serpentine (Figure 4.13a) to increase the microchannel length while keeping a small footprint. The width of the microchannel was reduced to 150 μm to decrease the diffusion distance and a three inlets/three outlets structure were selected (Figure 4.13b and 4.13c). By feeding the salt-rich phase through the middle inlet, the average diffusion distance can be further reduced by half. This three inlets/three outlets design decreased, however, the stability of the stratified type flow and, except in specific flow rates, the flow degenerated into droplets, forming a segmented type flow. In addition, the three outlets design led to the loss of the PEG phase through the center channel. This was due to the constriction of the salt-rich phase caused by the curvature of the side outlets. To cope with this the structure was redesigned to include a narrower central outlet and smoother side outlets (see Figure 4.13c).

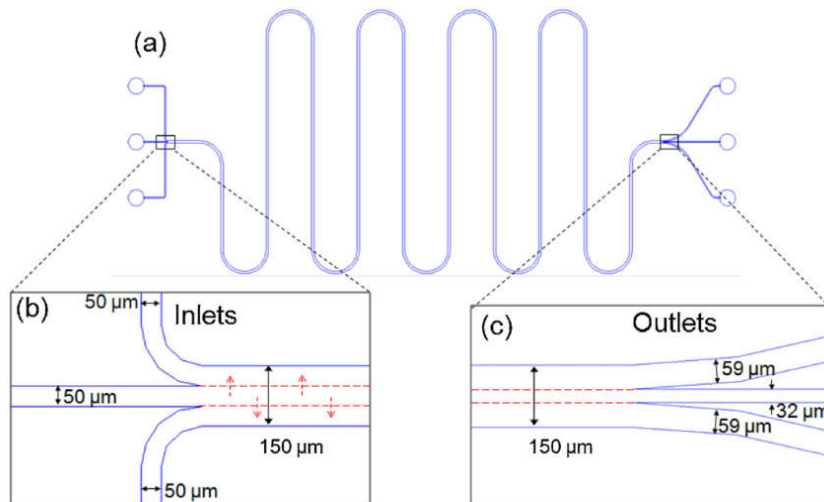


Figure 4.13 - (a) Schematic of the microfluidic structure for the ATPS extraction of antibodies from a salt-rich to PEG-rich phases. The total microchannel length is 16.8 cm. The blue lines are the microchannel walls, the red dotted lines indicate the locations for the interfaces between the salt-rich (center) and PEG-rich (sides) phases, The red arrows indicate the expected direction of antibody diffusion. (b) Detail of the inlets. (c) Detail of the outlets.

4.3.2 IgG partitioning in ATPS microfluidic device

The optimal ATPS composition obtained at the macroscale (5 g) for IgG purification in 15 mL test tubes (Azevedo, et al., 2007), was used as the starting condition for the microfluidic design and operating parameters. The system has an overall composition of 7.04% PEG, 16.37% phosphate buffer at pH 7.0, and 10% NaCl. A pure FITC-labeled IgG is used as the model antibody for separation. As the solutions progress along the extraction microchannel, the fluorescence resulting from the tag antibody is expected to move from the salt-rich phase to the PEG-rich phase.

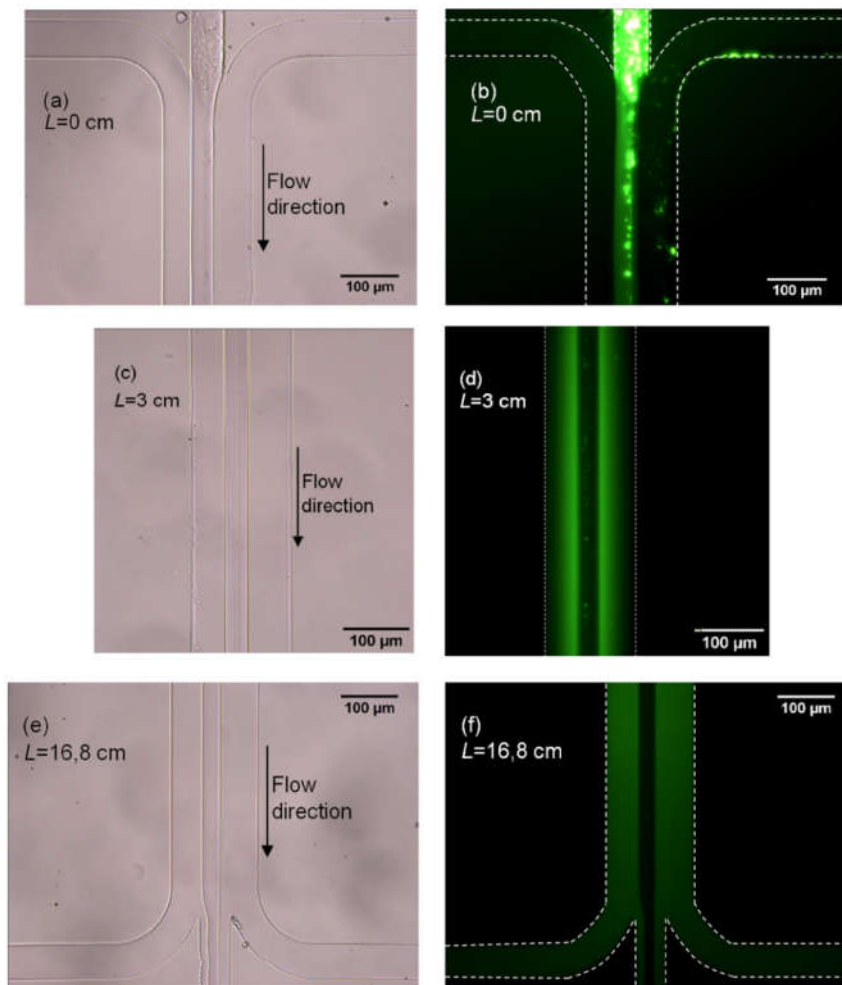


Figure 4.14 - Optical (left) and fluorescence (right) micrographs taken at the beginning ($L=0$), at $L=3$ cm and at the end ($L=16.8$ cm) of the extraction microchannel. The salt-rich phase containing IgG with a concentration of 2 mg/mL was introduced through the middle inlet with a volumetric pumping rate of 1 $\mu\text{L}/\text{min}$ and the PEG-rich phases were introduced through the side inlets with a volumetric pumping rate of 0.2 $\mu\text{L}/\text{min}$. L is the distance from the beginning of the microchannel. In the fluorescence micrographs, the boundaries of the microchannel are indicated with a dashed white line.

Partition of the FITC-labeled IgG from the salt- to the PEG-rich phases and diffusion in the PEG-rich phase along the microchannel is illustrated by the fluorescence micrographs in Figure 4.16. The micrographs were obtained at the entrance ($L=0$ cm), at $L=3$ cm from the entrance, and at the end of the main separation microchannel ($L=16.8$ cm). The images show

the diffusion of the FITC-labeled antibody from the middle, salt-rich, phase to the outer, PEG-rich, phases. In Figure 4.15, the fluorescence intensity profiles across the width of the channel are quantified at different distances from the inlets. As observed qualitatively in Figure 4.14, the fluorescence intensity decreases in the salt-rich phase and increases in the PEG-rich phase along the length of the extraction microchannel, highlighting the partitioning of IgG from the central salt-rich phase to the lateral PEG-rich phases. The diffusion of the IgG progresses along the channel in the PEG-rich phase until the concentration of FITC labeled antibody in the PEG-rich phase reaches a plateau and the ratio of IgG concentration in the two phases is given by the value of the partition coefficient.

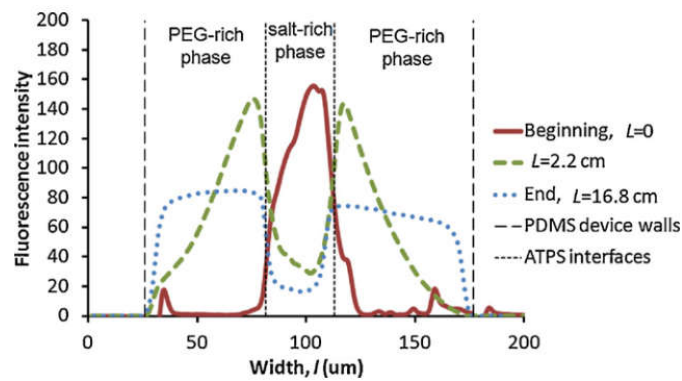


Figure 4.15 - Fluorescence intensity profiles across the width of the microchannel structure at $L=0$, 2.2, and 14.8 cm from the inlet. The profiles show the evolution of the concentration of the FITC-tagged IgG from being exclusively in the salt-rich phase at the beginning of the microchannel (solid) to its partitioning to the PEG-rich phase along the channel (dashed) to its diffusion within the PEG-rich phase at the end (dotted).

4.3.3 Effect of microchannel length

In order to allow for complete diffusion, the residence time of the diffusing species in a microfluidic device must be sufficiently long. There are two ways to change the residence time of IgG in the extraction microchannel: either by changing the length of the microchannel, or by changing the flow rates of the solutions. Two extraction channels with different lengths were studied: one with 10.45 cm and the other with 16.8 cm. Fig. 4.16 shows the effect of microchannel length on the diffusion and partition of IgG from the salt- to the PEG-rich phase, using flow rates of 1.0 and 0.2 $\mu\text{L}/\text{min}$, respectively, and the corresponding simulation as described in Section 4.2.2.

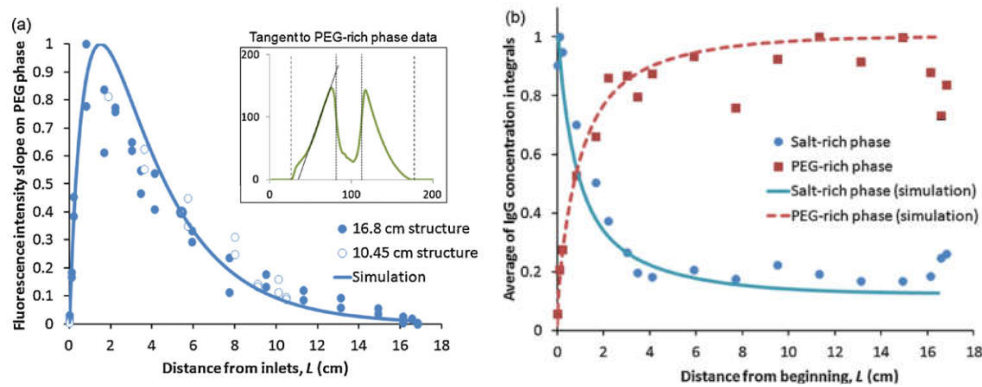


Figure 4.16 - (a) Fluorescence intensity slope for the PEG-rich phase along the channel, with detail showing the tangent of the PEG-rich phase data, and (b) average fluorescence for both phases for the serpentine like structures with extraction microchannels 10.45 cm and 16.8 cm of length. The ATPS used was made with 7.04% of PEG, 16.37% of phosphate salt and 10% of NaCl. The volumetric flow was 0.2 $\mu\text{L}/\text{min}$ for both PEG-rich phases and 1 $\mu\text{L}/\text{min}$ for the salt-rich phase. All data series were normalized

Figure 4.16a shows the slopes of the tangents to the corresponding PEG-rich phase fluorescence intensity profile at different distances, L , from the inlets. These slopes can be used as indication of the driving force for mass transfer. Initially, this slope increases rapidly because the IgG concentrates at the PEG-rich phase near the interface, causing a strong IgG concentration gradient in the PEG phases. This suggests that at the beginning of the extraction microchannel, the diffusion across the interface occurs faster than the regular diffusion in a single phase. After reaching a peak, the slope of the tangent decreases gradually to zero as the IgG diffuses in the PEG-rich phase, until the IgG concentration is constant along the PEG-rich phases. The experimental results agree closely with the simulation and show that the diffusion across the PEG-rich phase is complete at a distance of $L \approx 16.5$ cm. Figure 4.16b shows the values of the average fluorescence intensity across a phase, in both PEG-rich and salt-rich phases, for different locations L along the length of the extraction microchannel. It can be observed in Fig. 4.16b that the concentration of IgG in the salt-rich phase and in the PEG-rich phases reach stable values at $L \sim 10$ cm from the inlets, indicating that the partition of the IgG between salt-rich phase and PEG-rich phase is essentially complete before the end of the microchannel, in agreement with the simulation. Nevertheless, the extraction microchannel length must be longer to allow for the diffusion of IgG from the interface to the bulk PEG-rich phase and for the complete recovery of IgG in the PEG-rich phase at the end of the channel. If the diffusion in the PEG-rich phase is not complete, IgG will be concentrated near the interface on the PEG-rich side leading to lower recovery due to PEG-rich phase losses to the central exiting channel.

4.3.4 Effect of the flow rate of the two phases

The effect of changing the flow rates of the different phases was evaluated in a range where segmented flow is avoided. It was observed that, although a defined interface was maintained for the different flow rates tested, mass transfer of IgG from the salt- to the PEG-rich phase was incomplete when PEG-rich phase flow rate was increased from 0.2 up to 0.8 $\mu\text{L}/\text{min}$ and salt-rich flow rate was increased from 1.0 up to 2.0 $\mu\text{L}/\text{min}$, as evidenced in Figure 4.17.

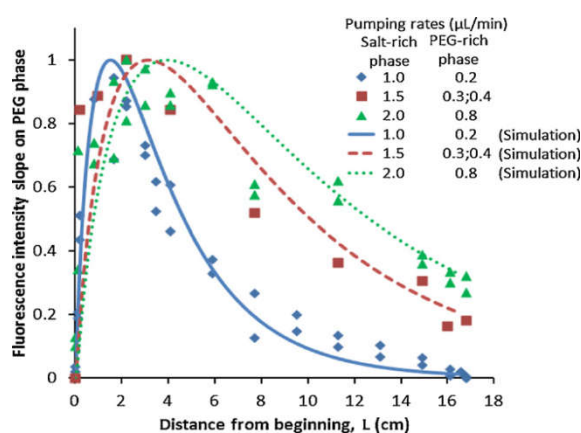


Figure 4.17 - Fluorescence intensity slope for the PEG-rich phase along the channel. The ATPS used was made with 7.04% of PEG, 16.37% of phosphate salt and 10% of NaCl. The volumetric flow was from 0.2 to 0.8 $\mu\text{L}/\text{min}$ for both PEG-rich phases and 1 to 2 $\mu\text{L}/\text{min}$ for the salt-rich phase. All data series were normalized.

These flow rates were chosen to maintain the interface stable and to minimize PEG losses in the outlet. Contrary to the lower flow rates, as the flow rates of both phases are increased, a driving force for mass transfer from the salt-rich phase, albeit decreasing after the initial peak, still persists at the end of the extraction microchannel (Figure 4.17), indicating that the diffusion of the IgG within the PEG-rich phase was not complete at the exit of the microchannel. As for the average concentration of IgG in the PEG- and salt-rich phases, the experimental values seem to have reached a steady value but the simulation suggest that, with higher flow rates, the steady value is not reached, despite being very close. This suggests that the partition of IgG to the PEG-rich phase (Figure 4.18) is not yet completed, despite being very close to completion.

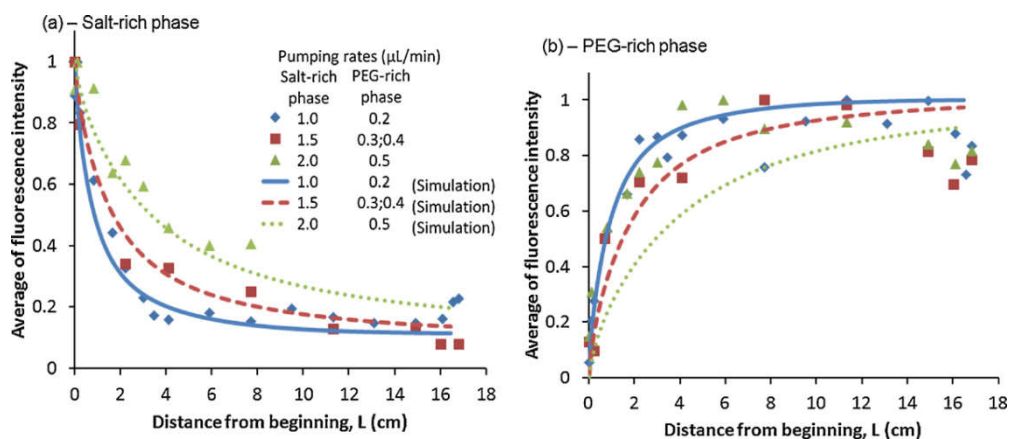


Figure 4.18 - Fluorescent average for the (a) salt-rich phase and the (b) PEG-rich phase in the microfluidic channel. The ATPS used was made with 7.04% of PEG, 16.37% of phosphate salt and 10% of NaCl. The volumetric flow was from 0.2 to 0.8 $\mu\text{L}/\text{min}$ for both PEG-rich phases and 1 to 2 $\mu\text{L}/\text{min}$ for the salt-rich phase. All data series were normalized.

Similar results are observed as the flow rates are further increased for the PEG- and salt-rich phases to 0.8 and 2.0 $\mu\text{L}/\text{min}$, respectively. These results suggest that, as expected, for the same microchannel length, a decreased residence time resulting from higher flow rates does not allow for full diffusion of the IgG within the PEG-rich bulk phase, and for complete partition of the IgG from the salt to the PEG-rich phase, though it is very close to completion, because of the shorter average distance for diffusion in the salt phase and the partition coefficient.

However, the incomplete diffusion of IgG within the PEG-rich bulk phase will mean that there will be a greater concentration of IgG in the area near the salt-rich phase. Since the loss of PEG-rich phase in the microchannel occurs next to the interface, this means that a drop of the recovery yield will inevitably occur. For these experiments, the recovery yields calculated were of 54% using flow rates of 1.0 $\mu\text{L}/\text{min}$ and 0.2 $\mu\text{L}/\text{min}$ for the salt-rich and PEG-rich phases, respectively; 41% using flow rates of 2.0 $\mu\text{L}/\text{min}$ and 0.8 $\mu\text{L}/\text{min}$ for the salt-rich and PEG-rich phases, respectively; and 46% using flow rates of 1.5 $\mu\text{L}/\text{min}$ and 0.4 $\mu\text{L}/\text{min}$ for the salt-rich and PEG-rich phases respectively.

4.3.5 Macro and microscale comparison

Extraction of IgG in ATPS at macroscale was already optimized and reported by the authors in previous studies (Rosa, et al., 2009). The authors showed that the driving force for IgG partition was the ionic strength. By increasing the NaCl concentration from 0 to 15%, the partition of IgG shifted from the bottom to the top phase. Macroscale partition assays were performed in 15 mL graduated centrifuge tubes. All system components were thoroughly mixed and phases were left to separate at 25 °C. To ensure complete phase separation the systems were further centrifuged; phase volumes were determined and samples from the top and bottom were analyzed by HPLC. The recovery yields obtained at the macroscale with 10% of NaCl in the ATPS ranged from 25% to 60% for pH between 6 and 8, respectively (Rosa, et al., 2009).

However, if the molecular weight of PEG was increased from 3350 to 6000 Da, a decrease in the recovery yield to 11.3% was observed at pH 7, showing that the PEG molecular weight has an important influence in the partition of the antibody in ATPS (Azevedo, et al., 2007). The change from macro to microscale does not appear to have a significant influence in the extraction yield as concluded from the results of the previous section. This is an expected result since the composition of the ATPS has not been greatly varied. However the use of microscale devices has greatly reduced the diffusion time by increasing the interface surface area to phase volume ratio and decreasing the diffusion distance.

4.4 Conclusions

This study showed that was possible to establish a stable, laminar flow of the two aqueous phases in the microfluidic network. The study performed with confocal microscopy shows that the interface within the microchannel takes a curved shape. Presumably this happens due to the different affinity of each phase to the PDMS wall. This is supported by the fact that the curvature that was observed was formed in a way that favored contact between the wall and the PEG-rich phase, which is the one with the greater affinity to PDMS.

A microfluidic device with a three inlets/three outlets design was fabricated using soft-lithography techniques based on PDMS and successfully demonstrated for the extraction of IgG with ATPS. It was possible to establish a stable, laminar flow of the two aqueous phases in the microfluidic network. Partition studies with FITC labeled IgG performed in PEG/phosphate ATPS showed a decrease of the fluorescence of the salt-rich phase, indicating partitioning of the IgG-PEG-rich phase, as observed in macro-scale experiments. Microchannel length and flow rates for efficient diffusion of IgG in PEG/phosphate ATPS were identified. The diffusion into PEG-rich phase was complete for a length of 16.8 cm with flow rates of 0.2 $\mu\text{L}/\text{min}$ and 1.0 $\mu\text{L}/\text{min}$, respectively in the PEG-rich phase and salt-rich phase. Furthermore, it was demonstrated that the reduction to the microscale does not greatly affect the antibody extraction yield when compared with macroscale results, but it does reduces the operation time. A mathematical model was developed to simulate the partition behavior of the FITC-labeled antibody, showing good agreement with experimental results.

The application of ATPS to the recovery of biomolecules still requires a somewhat trial-and-error approach since the behavior of a given biomolecule in the partition environment is unique. This is due to the chemical and physical interactions related to surface hydrophobicity, charge, and size that are involved in the partitioning process and that gain particular importance in a microfluidic environment. Thus, the use ATPS in an integrated microfluidic system for microscale protein purification using an automated high-throughput platform for cell separation, biopharmaceuticals purification and analysis could potentially provide a means to speed up the process optimization of ATPS in downstream processing.

The ATPS chip developed for IgG extraction has great potential in biotechnology as an example of an application of microscale lab-on-a-chip devices as a generic technological platform capable of monitoring and optimizing the pharmaceutical production process, and, in particular, provides a demonstration of miniaturized downstream processing in the case of protein drugs such as therapeutic antibodies.

5 Aqueous Two Phase Systems characterization in microfluidic devices.

One of the advantages of ATPS as a separation technique is the ability to be highly customizable to have better yield and resolution. This customization is due to the fact that ATPS can be composed of a wide variety of polymers and/or salts and that the concentrations of said polymers and/or salts can be adjusted, within reason, to better fit the requirements of the separation. However, this also means that extensive testing is required in order to find the most adequate conditions for every situation. The first step for that purpose is the characterization of the ATPS that are to be used.

Characterization of an ATPS normally entails the determination of the binodal curve. The binodal curve is the boundary conditions in which a solution with the adequate salt and/or polymers dissolved can form an ATPS. If the concentrations of the salt and/or polymers are below the binodal curve then the solution will not form phases and if the concentrations are higher than the binodal curve then the solution will form phases. When working with ATPS, it is necessary to know the binodal curve of the system that is being used to better plan the testing that will be done. Typically, this is done using one of two different techniques, the turbidometric titration method and the cloud point method. These two methods are done in a macroscale setting, usually in testing tubes, and they can require several hours of work and up to 100 mL of stock solutions of the salt and/or polymers.

Therefore, the work presented in this chapter represents an effort to create a microfluidic technique capable of characterizing ATPS quickly while expending less reagent. Due to their common use, ATPS composed of PEG/phosphate buffer and PEG/dextran were chosen as model systems for testing. Stock solutions of PEG, dextran and phosphates were inserted in a microfluidic platform along with milli-Q water. By controlling the flow of the stock solutions and of the milli-Q water, it is possible to change the concentration of these solutes within the microchannel. With a sufficiently long microchannel, diffusion will be enough for the solutions to combine within the microchannel and it is possible to use a microscope at the end of the microchannel to verify whether or not there is formation of interface.

This section of this work contains information that has been published in 2014 in the Journal of Chromatography A under the name "Determination of aqueous two phase system binodal curves using a microfluidic device". DOI: [10.1016/j.chroma.2014.10.035](https://doi.org/10.1016/j.chroma.2014.10.035)

5.1 ATPS formation in a microfluidic device

The formation of an ATPS in a microfluidic channel relies on the diffusion of the solutions in the microchannel perpendicular to the flow. Fluid flowing in a microchannel will always be in the laminar regime, so two different streams flowing in contact will not mix. The assumption is that the diffusion perpendicular to the flow is complete, so that the conditions necessary for the formation of the two phases in microfluidics under flow conditions are the same as those at the macroscale using the turbidometric titration method. Therefore, as long as the concentration of polymers or polymer and salt meet the criteria to form an ATPS in the macroscale, the system in the microchannel will also form an ATPS. Because the method being developed in this work requires the use of different solutions and changing their relative flow rates, the time for diffusion to be complete depends on the condition being used. Therefore, the microchannel was designed with a length of 52.2 cm to be long enough to guarantee that diffusion is complete in all cases (Figure 5.1).

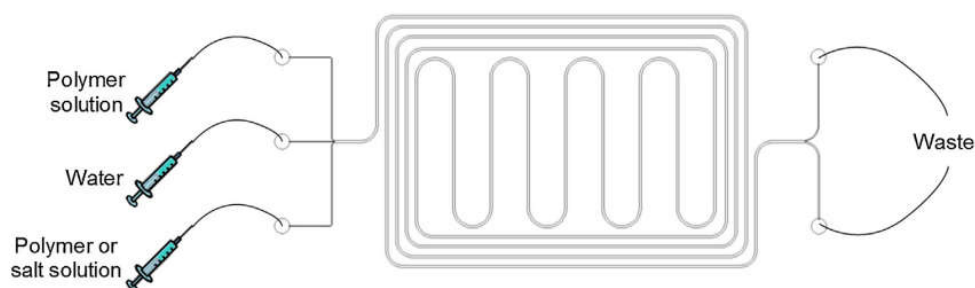


Figure 5.1- Schematic illustration of the system setup. The microfluidic channel has three inlets and two outlets. The main channel is 20 m high and 150 m wide and it is 52.2 cm of long.

The first ATPS studied was the PEG 1000 and phosphate buffer system, which is a system commonly used in ATPS separation (Soares, et al., 2016), and the low viscosity of solutions containing PEG 1000 or potassium phosphate facilitates the fluid handling in a microfluidic device. The sum of all solutions loading rate was always maintained at 1 to have a constant total solution volume in the microchannel. The macroscale phase diagram of this system was determined by the turbidometric titration method and is shown in Figure 5.1 (black squares and continuous line). This macroscale phase diagram was used to select three points, one below the binodal curve, one above the binodal curve and one in the vicinity of the binodal curve.

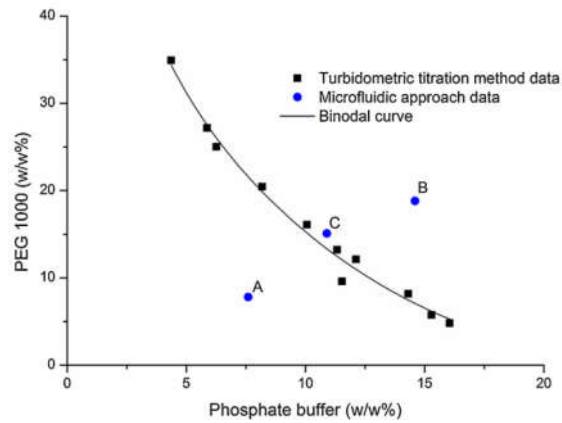


Figure 5.2 - Graphical representation of the PEG 1000/phosphate buffer system binodal curve. The horizontal axis represents the percentage of phosphate buffer weight to total system weight and the vertical axis represents the percentage of PEG 1000 weight to total system weight. The black square points represent the data obtained through the turbidometric titration method and the black line is the binodal curve fitted to the black square points. Points A, B and C indicate the conditions chosen to be tested in the microfluidic approach.

Figure 5.3 illustrates the difference between the systems that either do or do not form two phases in a microfluidic device. Figure 5.3a is an optical microscopy image of the end of the microchannel with the solution loading rates chosen so that the predicted concentration of PEG 1000 and phosphate buffer in solution is 7.8 and 7.6% (w/w), respectively, and Figure 5.3b is a graphical representation of the gray scale across a perpendicular cross-section of the microchannel obtained using ImageJ software (Schneider, et al., 2012), an image processing software. The edges of the microchannel are indicated by the two peaks in the gray scale values. In the macroscale phase diagram, this system is located below the binodal curve (point A of Figure 5.2) and, in the microfluidic device, only one phase is visible, in agreement with the macroscopic prediction. Thus, in Figure 5.3b, the gray scale value within the boundaries of the microchannel maintains a stable value across a width of the microchannel. Similarly, Figure 5.3c shows the end of the microchannel with solution flow rates set so that the target concentration of PEG 1000 and phosphate buffer in solution is 18.8 and 14.6% (w/w), respectively, and Figure 5.2d is a graphical representation of the gray scale across a perpendicular cross-section of the microchannel. In the macroscale phase diagram, this system is located above the binodal curve (point B in Figure 5.2) and, in the microfluidic device, the system is in a state where it has separated into two phases with a clear interface present. In Figure 5.3d, the gray value within the boundaries of the microchannel shows a pulse in the gray scale value at the location of the interface in the microchannel. However, although the examples presented in Figure 5.3 are easily distinguishable by the presence or absence of the interface, when the concentrations of PEG and phosphate are close to the binodal curve, such as point C in Figure 5.2, the interface in the microfluidic channel is unstable. In these cases the interface continuously forms and disappears with time.

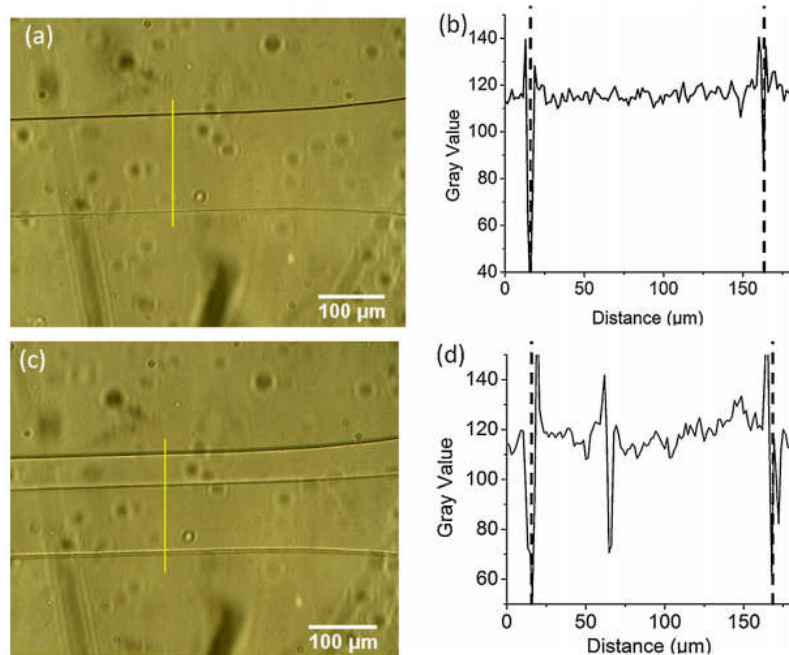


Figure 5.3- (a, c) Optical micrographs of the PEG 1000/phosphate buffer system taken at the end of the microchannel. The solution containing PEG and the solution containing phosphate buffer were inserted in the side inlets while milli-Q water was inserted in the middle inlet. The solutions loading rates have been set so that the concentration of PEG and phosphate in the microchannel were 7.8% (w/w) and 7.6% (w/w), respectively, for (a) and 18.8% (w/w) and 14.6% (w/w), respectively, for (c), corresponding to points A and B in Figure 5.2, respectively, while the total flow rate was 2 $\mu\text{L}/\text{min}$. (b, d) – Graphical representation of the Gray Value along the linear yellow mark in (a) and (c), respectively, obtained with ImageJ software. The vertical dashed lines represent the location of the PDMS walls.

Figure 5.4 is a sequence of microscopy images taken at the end of the microchannel at different times in a system with a target concentration of PEG 1000 and phosphate buffer of 15.9 and 10.1% (w/w) respectively. This point is extremely close to the binodal curve constructed using the turbidometric titration method (point C in Figure 5.2) and, in this situation, the system becomes unstable and changes continuously given enough time.

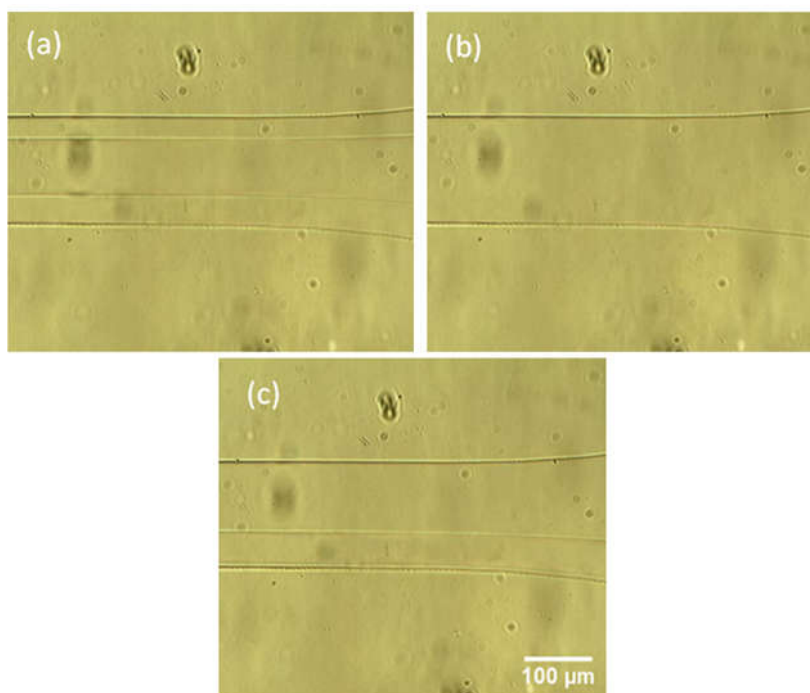


Figure 5.4- Optical micrographs of the PEG 1000/phosphate buffer system taken at the end of the microchannel at different times. The solution containing PEG and the solution containing phosphate buffer were inserted in the side inlets while milli-Q Water was inserted in the middle inlet. The solutions loading rates have been set so that the concentration of PEG and phosphate in the microchannel were 15.9% (w/w) and 10.1% (w/w), respectively, corresponding to point C in Figure 5.2, while the total flow rate was 2 $\mu\text{L}/\text{min}$. The images were obtained about 10 s apart.

The system represented in Figure 5.4 has an interface (Figure 5.4a), which then disappears (Figure 5.4b) only to reappear again (Figure 5.4c), and this fluctuation continues over time. This phenomenon, where the solution in the microchannel oscillates between either a defined interface or not, occurs possibly due to the fact that the syringe pumps have stepper motors, so that the syringe pump plunger moves in small discrete steps, rather than in a continuous motion. These steps create small variations of the volumes of the solutions being inserted in the microchannel (Silva, et al., 2014). Although these volume fluctuations are small, nevertheless they create small variations in the concentrations of PEG and phosphate in the microchannel and, when the system is very close to the binodal curve, they can cause the system to oscillate between the states in which the system can either separate or not in two phases. The time needed for the appearance or disappearance of the interface after altering the flow rate of the solutions depends on the diffusion of the solution components in the microchannel. As previously noted, the microchannel has sufficient length to allow for complete diffusion. Calculating the exact time necessary for the solutions to go through the microchannel is difficult, considering that it is possible to have two phases, each with different velocities. Assuming that all phases have the same viscosity and density, the solutions require less than 1 minute to go through the microchannel. However, some time is required to ascertain whether or not a certain set of polymers or polymer and salt concentrations forms an unstable interface in the microchannel. Therefore, whenever the solution pumping rates were changed, the state of

the interface for that particular set of concentrations of polymers or polymer and salt would be registered after an average of 4 minutes.

5.2 Determination of the binodal curve

Since the concentration of PEG and phosphate in the microchannel is dependent on the solution flow rates, changing these rates allows a quick testing of a wide range of total concentrations for ATPS formation. Figure 5.5 represents the results of the turbidometric titration method plotted in a phase diagram form. The equation used for the fitting of the binodal curves was the following (Merchuk, et al., 1998):

$$y = A \times e^{(B \times x^{0.5} + C \times x^3)} \quad \text{Equation 5.1}$$

In Equation 5.1, y represents the concentration of salt and x the concentration of PEG in weight to weight ratio. A , B and C are experimental coefficients. The experimental points were fit to Equation 5.1 using OriginPro, a graphing and data analysis software, to produce the binodal curves. For the results obtained using the microscale approach, the points used for the fits were the points for which the system was in the unstable state in the microfluidic device (the green dots in Figure 5.5). Since the unstable state occurs in points near the binodal curve, it is expected that fitting Equation 5.1 to these points will yield similar results as those obtained from the macroscale turbidometric titration method.

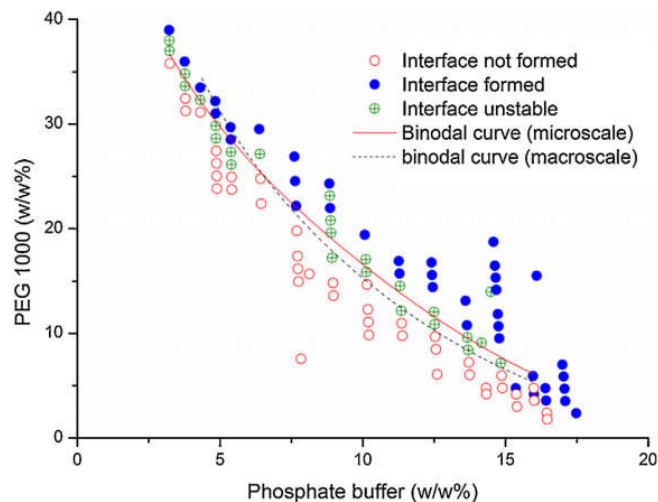


Figure 5.5 - Graphical representation of the PEG 1000/phosphate buffer system binodal curve. The horizontal axis represents the percentage of phosphate buffer weight to total system weight and the vertical axis represents the percentage of PEG 1000 weight to total system weight. The solid line represents the fitting of the results from the macroscale turbidometric titration method. The experimental coefficients of Equation 5.1 are in this case $A = 123.2$, $B = -0.6$ and $C = -1.8 \times 10^{-4}$. The solid blue dots are the concentrations that formed an interface between the two aqueous phases (and hence an ATPS) in the microfluidic device, the open red dots correspond to the concentrations that did not form an interface, and the half-filled green dots correspond to the concentrations with an unstable interface. The red dotted line represents the binodal curve fitted to the unstable state system points. The experimental coefficients of Equation 5.1 are in this case $A = 81.1$, $B = -0.4$ and $C = -2 \times 10^{-4}$.

The results in Figure 5.5 show a clear and continuous division between the compositions that separate in two phases, those that do not, and those that originate unstable systems. In general, the binodal curves obtained through the macroscale turbidometric technique and the microscale approach are similar and points towards the opportunity of using a microfluidic device as an automated platform for binodal curves determination, with the advantages of a more rapid processing and less volume consumption. The major difference between the microfluidic and macroscale bimodal curve results occurs when the system contains a large amount of salt and a small amount of PEG. In the microfluidic channels, when the concentration of salt is high, the system forms a stable interface even when the composition of the system is below the binodal curve and was not expected to form an interface. It is possible that this is caused by the greater affinity of PDMS toward hydrophobic molecules (Boxshall, et al., 2006). Since PEG is more hydrophobic than a salt, it will have a higher affinity to the PDMS walls of the microfluidic device than the salt. This affinity would preferentially attract the PEG to the wall and lead to an increase in the PEG concentration along the wall. Thus, in the low PEG, high salt region of the binodal curve, the concentration of the PEG on the walls is enough provide the system with the conditions to separate into two phases. Since the salt has a much lower affinity to the PDMS walls, the same phenomenon does not occur when the concentration of PEG is high and the concentration of salt is low. To evaluate the generality of the method, two other systems were tested, the PEG 1000/Dextran 20 and the PEG 6000/Dextran 298 systems, two polymer/polymer systems chosen due to their widespread use (Soares, et al., 2016). As before, the binodal curves for the macro and microscale approach were calculated using the data from the macroscale turbidometric titration method and with the points where the system is in the unstable state, respectively (Figure 5.6 and figure 5.7).

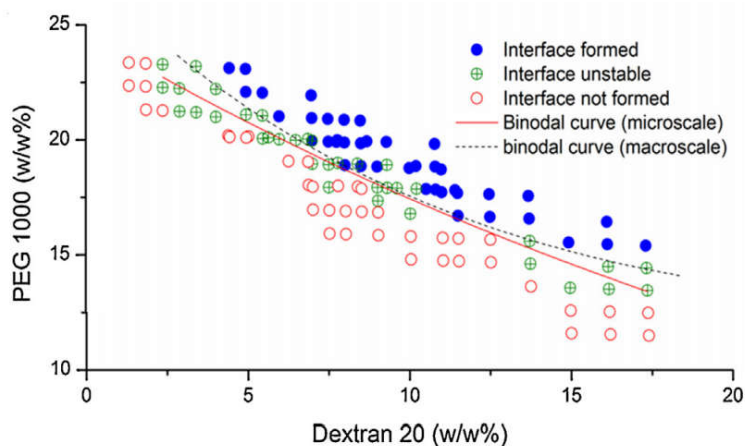


Figure 5.6 - Graphical representation of the bimodal curves for the PEG1000/Dextran 20 system. The horizontal axis represents the percentage of Dextran weight to total system weight and the vertical axis represents the percentage of PEG weight to total system weight. The dotted lines represent the fitting of the results from the turbidometric titration method. The experimental coefficients in this case are $A= 34.1$, $B = -0.2$ and $C = 4.2 \times 10^{-6}$. The solid blue dots and squares are the concentrations that formed an interface in the microfluidic device, the open red dots and squares are the concentrations that did not formed an interface and the crossed green dots and squares are the concentrations displaying an unstable interface. The red lines represent the binodal curve fitted to the unstable state system points. The experimental coefficients in this case are $A= 28.7$, $B = -0.1$ and $C = 3.1 \times 10^{-5}$.

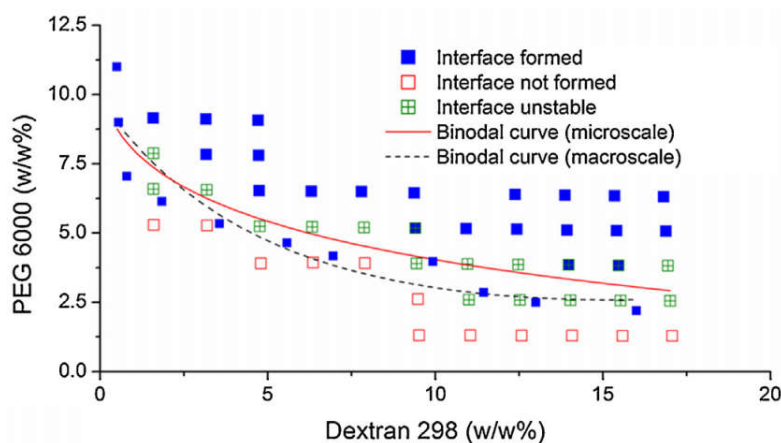


Figure 5.7 - Graphical representation of the binodal curves for the PEG 6000/Dextran 298 system. The horizontal axis represents the percentage of Dextran weight to total system weight and the vertical axis represents the percentage of PEG weight to total system weight. The dotted lines represent the fitting of the results from the turbidometric titration method. The experimental coefficients in this case $A = 12.7$, $B = -0.5$ and $C = 2.9 \times 10^{-5}$. The solid blue dots and squares are the concentrations that formed an interface in the microfluidic device, the open red dots and squares are the concentrations that did not form an interface and the crossed green dots and squares are the concentrations displaying an unstable interface. The red lines represent the binodal curve fitted to the unstable state system points. The experimental coefficients in this case are $A = 10.9$, $B = -0.3$ and $C = 5.6 \times 10^{-6}$.

For the PEG 1000/Dextran 20 system, the binodal curve predicted in the microfluidic device is very similar to the binodal curve determined by the turbidometric titration method. For the PEG 6000/Dextran 298 system, the binodal curves determined by the microfluidic approach and the turbidometric titration method also shows similarities, although to a lesser extent than the other two systems. This deviation is possibly due to the higher viscosity of the solutions. The higher viscosity hampers the pushing action of the syringe pumps, possibly increasing fluctuations of the volumes and destabilizing the system. The time needed for the determination of the binodal curve using a microfluidic approach is dependent on the number of points that each system requires to characterize the binodal curve. As stated before, each point requires 4 minutes before an assessment of whether that point represents a system with a formed interface, a system with no interface or a system with an unstable interface. The number of points assessed for the systems studied in this paper varied, but, for example, the PEG 6000/Dextran 280 required 48 points, which appears to be an appropriate number of points to just in other systems. Disregarding the time needed to initiate the process until the first point is taken, a system with around 50 experimental points would require between 3 h and 3½ h to complete. Furthermore, Figure 5.3b and d shows that the presence or absence of an interface within the microchannel can also be tracked by image processing software, which suggests that this microfluidic approach could be automated. Furthermore, the solution volumes required for the microfluidic approach are very small. To characterize an ATPS less than a milliliter of each of the three solutions is required. The turbidometric titration method requires a smaller number of points to determine the binodal curve, but each point has to be mixed individually and then diluted with water, drop by drop with mixing, until the interface disappears. This process can be time consuming, while, for the less viscous materials, the ATPS can be fully formed in one or

two hours, after mixture, for some of the more viscous materials, the process of ATPS phase separation can last more than 6 hours. Only after the phase separation can macroscale techniques be done to determine the binodal curve. Furthermore, a macroscale approach requires a minimum of 5 mL of solutions, often more and automation is not easy. In the macroscopic determination, it is rather difficult to decrease the sample size below 1 ml in total volume since water is added in steps until the interface disappears, and diminishing the volume used in this method leads to an increase in the error of the assay.

5.3 Conclusions

The method used allowed a rapid determination of the conditions that are necessary for the system to separate into two phases. Moreover the data gathered was used to plot binodal curves which were consistent with binodal curves determined using the turbidometric titration technique. The only significant deviation between the microfluidic approach and macroscale method for the determination of ATPS formation occurred in the PEG 1000/phosphate system where the microfluidic approach data showed formation of interface below the macroscale determined binodal curve conditions in conditions of high salt concentration and low PEG concentration. This situation represents a set of potential ATPS conditions that can only be used within a microfluidic platform. Furthermore, the microfluidic platform showed that it can handle viscous solutions, an important factor when working with ATPS due to the possible presence of polymers with high viscosities.

This method provides an easy, fast, inexpensive and continuous approach for the determination of the binodal curve, providing an alternative to the time-consuming traditional methods. It also uses smaller amounts of reagents and produces smaller amounts of waste. The formation of the ATPS is clearly distinguishable by the appearance of the interface and, thus, it is possible to use image processing software to automate the determination process eliminating human error and further reducing the time required. The manipulation of conditions can also be automated since the change of the concentration of the system's components is made by simply manipulating the solution pumping rates, further reducing the time that calculating an ATPS binodal curve usually requires.

6 Determination of partition coefficients of biomolecules in a microfluidic platform

Besides the characterization of the ATPS and determination of the binodal curve, the use of ATPS for separation and purification of biomolecules also requires the determination of the partition coefficient of these biomolecules in the ATPS. For that purpose, testing is usually needed to determine which ATPS and under which conditions the extraction process is more efficient. However this presents the same problems that the characterization of ATPS presents relating to the time required for the testing and also the amount of reagents spent in such testing.

Therefore, the work presented in this chapter is an attempt to use a microfluidic platform for a quick and inexpensive way to determine partition coefficients of biomolecules in ATPS with varying compositions. The method used for this is similar to the method used in Chapter 5. The ATPSs used as models for this work are PEG/phosphate and PEG/dextran ATPS and the biomolecules used as models are IgG-FITC, insulin-FITC, protein A-FITC and BSA-FITC.

Stock solutions of PEG and phosphate, or PEG and dextran, are inserted into a microfluidic platform along with milli-Q water. Prior to this the target biomolecule is dissolved in the milli-Q water. Similar with the work of Chapter 5, the composition of the ATPS within the microchannel can be manipulated by varying the volumetric flow of each solution. The solutions mix within the microchannel and, as long as the conditions are sufficient to form an interface, the target biomolecule will partition in the ATPS formed within the microchannel. At the end of the microchannel, fluorescent microscopy is applied so that the concentration of the target biomolecule can be known for each phase and, thus, we can calculate the target biomolecule partition coefficient.

This chapter contains work that has been published in 2017 in the Journal of Chromatography A under the name "Determination of partition coefficients of biomolecules in a microfluidic aqueous two phase system platform using fluorescence microscopy". DOI: [10.1016/j.chroma.2016.12.036](https://doi.org/10.1016/j.chroma.2016.12.036)

6.1 K_p determination within the microfluidic platform using fluorescence

The chosen ATPS systems were based on PEG/dextran and PEG/salt systems, which are the most frequently investigated and utilized systems and the ATPS compositions were selected to ensure the formation of the ATPS based on binodal curves determined in previous

experiments. These ATPS systems were used to test the partition coefficient of different biomolecules: IgG, BSA, Insulin and ProA, all labeled with FITC, and GFP (Figure 6.1).

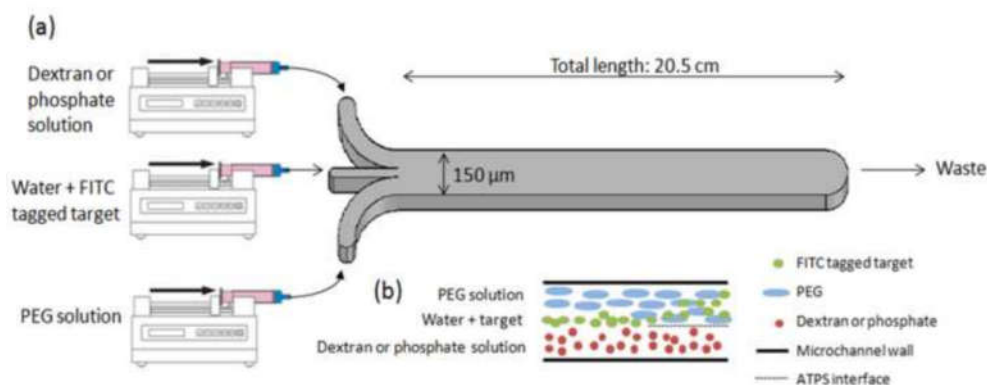


Figure 6.1 - (a) Schematic representation of the experiment for the determination of K_p . The microfluidic structure has a height of 20 μm , a width of 150 μm and a length of 20.5 cm. The solutions are inserted in the microfluidic structure using syringe pumps. (b) Schematic representation of the diffusion within the microfluidic structure and formation of the interface.

Fluorescence micrographs were used at the end of the microchannel to determine the partition coefficient K_p , defined as the ratio of the target concentration in the top phase to the target concentration in the bottom phase, for each ATPS composition. In a microfluidic setting, due to the negligible influence of gravity (Beebe, et al., 2002), the two phases do not order themselves as top and bottom due to the differences in density. Nevertheless, the formal designation of bottom phase and top phase are still used in analogy to the macroscale assays. In this case, the PEG phase is defined as the top phase for the PEG/Dextran and PEG/salt systems. Since the target biomolecules were tagged with FITC, the fluorescence values were used to quantify the concentration of these biomolecules (Silva, et al., 2012). To ensure proportionality between the fluorescence measured and the concentration of the labeled biomolecules, it is necessary to compare the values of fluorescence for known concentrations in the PEG, dextran and phosphate buffer solutions so that effects of the phase composition on the fluorescence can be corrected if necessary. Individual solutions containing 15% w/w of phosphate buffer, 20% w/w of PEG 1000 and 15% w/w of Dextran 20 were prepared, each containing 150 mg/L of a target biomolecule. These were introduced into a single inlet microchannel and their fluorescent values were taken at the end of the microchannel. The results shown in Figure 6.2 demonstrate that, for equal concentrations of FITC-tagged molecules, those in saline solutions show slightly higher fluorescence than in PEG and dextran solutions.

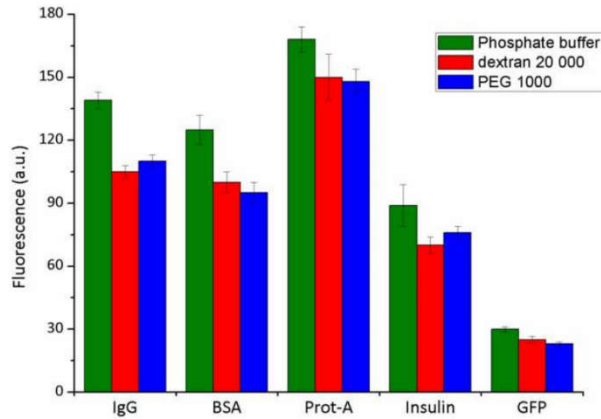


Figure 6.2- Graphical representation of the fluorescence for several FITC-tagged molecules in different ATPS component solutions. The concentration of FITC tagged molecules was of 150 mg/L in all solutions. The phosphate buffer solution contained 15% (w/w) of phosphate buffer, the PEG solution contained 20% (w/w) of PEG 1000 and the dextran solution contained 15% (w/w) of dextran 20.

FITC-tagged molecules in PEG and dextran solutions appear to have similar fluorescence levels. Hence the fluorescence values obtained for the salt-rich phase must be corrected accordingly before being used for the calculations of the K_p . A correction factor can be derived by averaging the ratio between the values of fluorescence of the salt rich phase and the polymer rich phase. This factor would be used to correct the fluorescence data obtained in the salt rich phase to be used in the partition coefficient calculation. In this particular case, the fluorescence data obtained for the salt-rich phase must be divided by a factor of 1.23. As an example, Figure 6.3 shows the partition of FITC-tagged ProA in a PEG/phosphate system as well as the binodal curve determined in a previous work in a microfluidic structure for this ATPS system (Silva, et al., 2014).

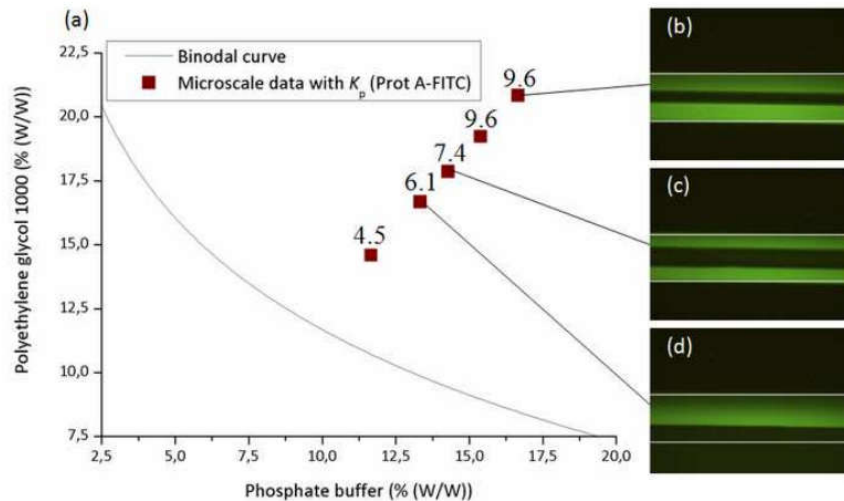


Figure 6.3 - (a) Graphical representation of the microfluidic experimental points with the determined K_p for the PEG/salt system using protein-A labeled with FITC as a target. (b) Fluorescence micrograph of the ATPS system with 20.8 % (w/w) of PEG and 16.7 % (w/w) of salt. (c) Fluorescence micrograph of the ATPS system with 17.8 % (w/w) of PEG and 14.3 % (w/w) of salt. (d) Fluorescence micrograph of the ATPS system with 16.6 % (w/w) of PEG and 13.3 % (w/w) of salt.

The composition of the ATPS in the microfluidic channel were selected taking in account the binodal curve, in order to ensure that two-phases were formed and that the systems were not on the same tie-line. Since two systems on the same tie-line will separate in phases with the same concentrations, these two systems will have the same partition coefficient, excluding other effects, such as limits to the solubility of the target biomolecule. Therefore the ATPS compositions should be chosen so that no two compositions were in the same tie-line, to ensure that ATPS compositions represent the different conditions in an ATPS while minimizing the number of experimental points. Figure 6.3b, c and d are fluorescence micrographs at the end of the microchannel with different compositions of the ATPS. The target biomolecule partitions mainly to the PEG-rich phase, making this phase appear green in the fluorescence micrograph, while the phosphate-rich phase (middle dark area) becomes dark showing little of the target.

The reason why there are two PEG (green) phases on either side of the middle dark phosphate phase in Figure 6.3b and c is that since the ATPS is formed within the microchannel, the position of the phases within the microchannel depends on the differential affinity that these immiscible phases have for the channel walls. Since the PEG-rich phase has higher affinity to the PDMS channel walls when compared to the phosphate-rich phase, the PEG-rich phase divides in two streams, each touching one of the side walls of the PDMS microchannel. As the diffusion in the microfluidic channel is complete, this phenomena will not affect the partition coefficient measured. Moreover, this phenomena only occurs in systems where the phases have significantly different affinities to the PDMS and even in systems where such a difference exists this effect is not always visible.

The partition of ProA to the PEG phase most likely occurs due to the low molecular weight of PEG, which makes the PEG-rich phase more amenable (Albertsson, 1995) to the target biomolecule. The preferential partitioning for the PEG-rich phase, is also promoted by the high salt concentration in the salt-rich phase which can induce salting out effects. Figure 6.3a also shows that the K_p values of the target biomolecule increase as the composition of the ATPS moves further away from the binodal curve, as expected. Increasing the concentration of the ATPS components will create ATPS systems with greater physical and chemical differences between the two immiscible phases. Since the partition of molecules in an ATPS occurs due to the difference in affinity that the molecules have for one phase over another, increasing the difference in composition between each phase will also increase the difference in the affinity that a molecule has for each phase. Therefore, increasing the distance of the ATPS to the binodal curve will increase the partition of a molecule in that ATPS (Diamond, et al., 1992).

The time needed for the microfluidic determination of the partition coefficient of a particular molecule at a specific composition depends on the width and length of the microchannel and on the loading rates of the solutions. The total loading rate of the solutions into the microchannel was 1 $\mu\text{L}/\text{min}$, as stated in section 5.1. Considering the width, the height

and the length of the microchannel (150 μm , 20 μm and 20.5 cm, respectively), any change in the loading rates will affect the composition of the ATPS at the end of the microchannel within 37 seconds, according to equation 2.2. However this value is only correct if it is assumed that there is only one fluid flowing in the microchannel. The formation of the two phases within the microchannel, causes a randomness in the interface position which was constantly moving within the microchannel. Additionally each phase has different characteristics such as viscosity and affinity to the PDMS wall. These two factors combined mean that knowing the velocity of each phase within the microchannel is likely constantly changing. Also, due to the randomness in the interface position, recovering the phases separately is impossible.. Therefore the time required for ATPS stabilization in the microfluidic system was higher than 37 seconds. The time that was used to ensure stabilization was 4 minutes.

In this work, for each target biomolecule and each ATPS system studied, five different sets of solution loading rates, which correspond to five different ATPS compositions within the microchannel, were used. To determine the partition coefficients of a biomolecule corresponding to 5 different ATPS compositions requires approximately 30 minutes when using a single microfluidic device. In comparison, in the standard macroscale procedure, each of these compositions would have to be prepared in a test tube and then allowed to settle for up to several hours depending on the ATPS. Afterwards, the immiscible phases would need to be separated and the target molecule concentration in each phase would have to be determined, in a process that can take up to a full day and require solution volumes at the very least of the order of several milliliter and a quantity of target molecule of several tens of micrograms to characterize an ATPS. The volumes required for the microfluidic assay are considerably smaller than those required in the standard macroscale approach. To study the partition of one molecule in one ATPS system, which in our experiment corresponds to determining the K_p of that molecule at five different ATPS compositions, the experiments require approximately 30 minutes, a maximum of 30 μL of each of the solutions needed for the ATPS formation and only a few micrograms of the target molecules. To obtain the same information through macroscale methods would require to create the ATPS in a test tube, allow it to settle and separate the molecule of interest, separate the phases and measure the fluorescence of both phases. This would require a minimum of 2 hours for the ATPS formation (if the ATPS is such that the phases separate fast), a minimum of several mL of all solutions and several mg of the target molecule, depending of the fluorescence.

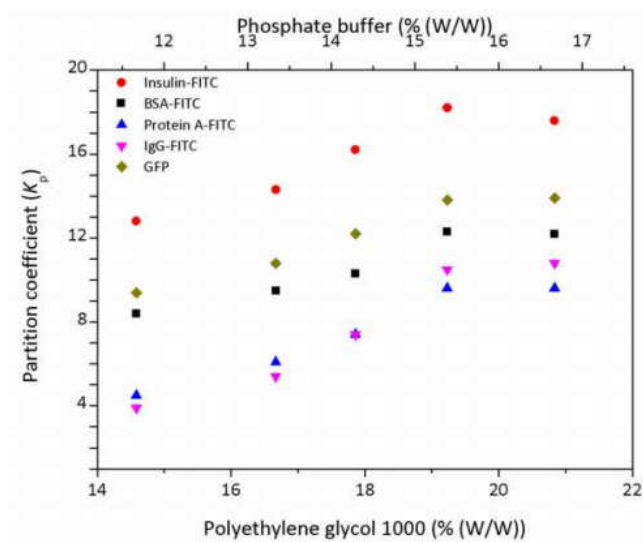


Figure 6.4- Microfluidic-determined K_p for the PEG/salt system using several FITC tagged proteins as targets.

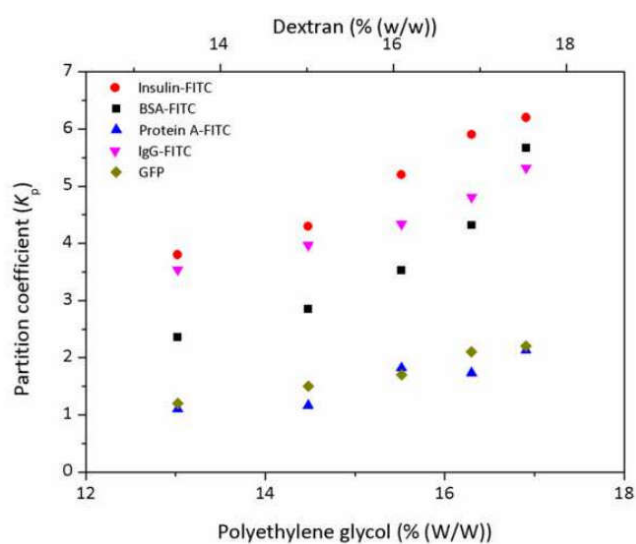


Figure 6.5 - Microfluidic-determined K_p for the PEG/dextran system using several FITC tagged proteins as targets.

K_p determined with a microfluidic device using the methodology described was extended to other biomolecules to demonstrate the generality of the developed ATPS-microfluidic platform. The partition coefficients of a set of different FITC-tagged biomolecules were determined for different PEG/Dextran and PEG/phosphate system compositions. In addition, different PEG polymer molecular weights were tested.

Figure 6.4 shows the values of K_p obtained for BSA, protein A and insulin(FITC-tagged) biomolecules in a PEG/phosphate buffer ATPS. Since the K_p is being measured for specific compositions of the ATPS system, Figure 6.4 has two X axes representing the composition of

the ATPS and the Y axis representing the partition coefficient. All the FITC-labeled target biomolecules studied, namely insulin, BSA and ProA, partition preferentially to the PEG-rich phase.

The partition of insulin, BSA, ProA and IgG was also tested in PEG/dextran ATPS and the K_p obtained are shown in Figure 6.5. As observed for the PEG/phosphate ATPS, $K_p > 1$, showing that the target biomolecules have a higher affinity towards the PEG rich-phase with increasing concentrations of PEG and dextran (higher tie-line lengths).

6.2 Comparison of the microfluidic and macroscale K_p determination

For the two ATPS tested in the microfluidic system, corresponding tests at the macroscale were also carried out and the results are summarized in Tables 6.1 and 6.2.

Table 6.1- K_p for FITC-tagged proteins for different compositions of PEG/Phosphate buffer ATPS comparing the microfluidic approach and the standard macroscale approach.

PEG/phosphate concentrations (%w/w)	Insulin		ProA		BSA		IgG		GFP	
	K_p micro	K_p macro	K_p micro	K_p macro	K_p micro	K_p macro	K_p micro	K_p macro	K_p micro	K_p macro
20.8%/16.7%	17.6 (±1.5)	16.8 (±1.7)	9.6 (±1.0)	9.2 (±1.1)	12.2 (±2.1)	13.3 (±1.8)	10.8 (±1.1)	10.0 (±1.3)	13.9 (±1.5)	14.1 (±1.6)
17.9%/14.3%	16.2 (±1.3)	15.6 (±1.2)	7.4 (±0.7)	7.6 (±0.5)	10.2 (±1.6)	11.1 (±1.4)	7.4 (±0.6)	7.3 (±0.5)	12.2 (±1.3)	11.3 (±1.2)
14.5%/11.7%	12.8 (±1.7)	13.4 (±1.1)	4.5 (±0.7)	4.2 (±0.6)	8.4 (±1.1)	8.9 (±1.3)	3.9 (±0.5)	4.2 (±0.6)	9.4 (±1.1)	8.4 (±1.2)

Table 6.2- K_p for FITC-tagged proteins for different compositions of PEG/Dextran ATPS comparing the microfluidic approach and the standard macroscale approach.

PEG/dextran concentrations (%w/w)	Insulin		ProA		BSA		IgG		GFP	
	K_p micro	K_p macro								
20% / 12%	6.2 (±0.7)	6.1 (±0.6)	2.1 (±0.4)	1.9 (±0.3)	5.6 (±0.7)	5.9 (±0.6)	5.3 (±0.5)	5.5 (±0.4)	2.2 (±0.5)	2.5 (±0.4)
17.6% / 10.6%	5.6 (±0.7)	5.2 (±0.5)	1.8 (±0.3)	1.7 (±0.3)	3.5 (±0.5)	3.6 (±0.4)	3.5 (±0.3)	3.4 (±0.4)	1.7 (±0.3)	1.5 (±0.4)
15.8% / 9.5%	3.8 (±0.5)	4.1 (±0.4)	1.1 (±0.2)	1.0 (±0.1)	2.3 (±0.6)	2.7 (±0.5)	2.3 (±0.3)	2.1 (±0.2)	1.2 (±0.2)	1.1 (±0.2)

For the macroscale approach, a smaller number of compositions of each ATPS were tested. As can be seen in Tables 6.1 and 6.2, K_p values obtained at both the macro- and macroscale are in close agreement with the percentage difference between the micro and macroscale data sets always below 10%.

6.3 Conclusions

The proposed microfluidic platform was successful in the determination of partition coefficients of biomolecules in different ATPS with high speed and low material consumption. Furthermore, the data gathered during experimentation is similar with the data that was gathered using a macroscale approach. This method has proved to be an easy, fast, inexpensive and continuous approach for the determination of partition coefficients, providing an alternative to the time-consuming and more expensive traditional methods.

The microfluidic approach developed relies in simply altering the loading rates of the stock solutions, creating new ATPS compositions quickly, allowing a rapid screening of conditions for the partition to occur. Once a new set of loading rates is imposed, the microfluidic approach only requires 4 minutes so that the concentrations within the microchannel to stabilize and the process only uses a few microliters of the solutions in that timeframe. For each ATPS system, five compositions were chosen as the points to determine the partitions coefficients. The PEG, dextran and phosphate concentration of the ATPS within the microchannel varied between 13.0% to 20.8% (w/w) of PEG, 11.6% to 16.6% (w/w) of phosphate and 13.5% to 17.5% (w/w) of dextran.

The five chosen points only required about 30 minutes to gather the relevant data and less than a milliliter of the stock solutions. In comparison, the macroscale approach can take up to a day and requires a minimum of tens of milliliters of solutions. Additionally, the use of image processing software for the K_p determination without physically separating the phases means that automation of the process is possible.

7 Electrical field assisted ATPS partition in a microfluidic platform

One of the advantages of microfluidics is the ease of integration of multiple processes. In this chapter, the microfluidic ATPS extraction developed in the previous chapters was integrated with electrophoresis, another separation technique. Electrophoresis is a technique to separate particles in a fluid based on the application of an electrical field (Lindblad, 2009). This technique was chosen due to the already existing evidence of its success when applied together with ATPS extraction (Munchow, et al., 2006) (Hahn, et al. 2011) (Munchow, et al., 2006).

The work presented in this chapter is the integration of electrodes into a microfluidic platform and the implementation of an electrical field on a ATPS extraction to test the effect of the electrical field. The electrodes were prepared by depositing, patterning and etching metallic films on a glass substrate that would be used to seal the PDMS microfluidic platform. The Al electrodes are etched without a gap between them so that the gap can be defined after the sealing process by flowing Al etchant in the microchannel allowing a self-aligned process. ATPS composed of PEG/dextran and PEG/phosphate were prepared in test tubes. The FITC marked biomolecules were mixed in the ATPS and then the ATPS phases were separated using a syringe. The phases were then inserted in the microfluidic platform and, when appropriate, a voltage differential was applied to the electrodes so that a uniform electrical field forms between them. Fluorescent microscopy was then used at the end of the microchannel to track the FITC-marked molecules to ascertain the effect of the electrical field.

7.1 Electrode etching in the microfluidic platform

A simple approach to apply the electrodes to the microfluidic platform was used (Figure 7.1): the electrodes were made of aluminum on top of a glass substrate, using the same method described previously in section 3.2.1 to fabricate the aluminum masks, and then this glass substrate with the aluminum electrodes was used to seal the microchannel replacing the PDMS slab or glass surface described in section 3.3.

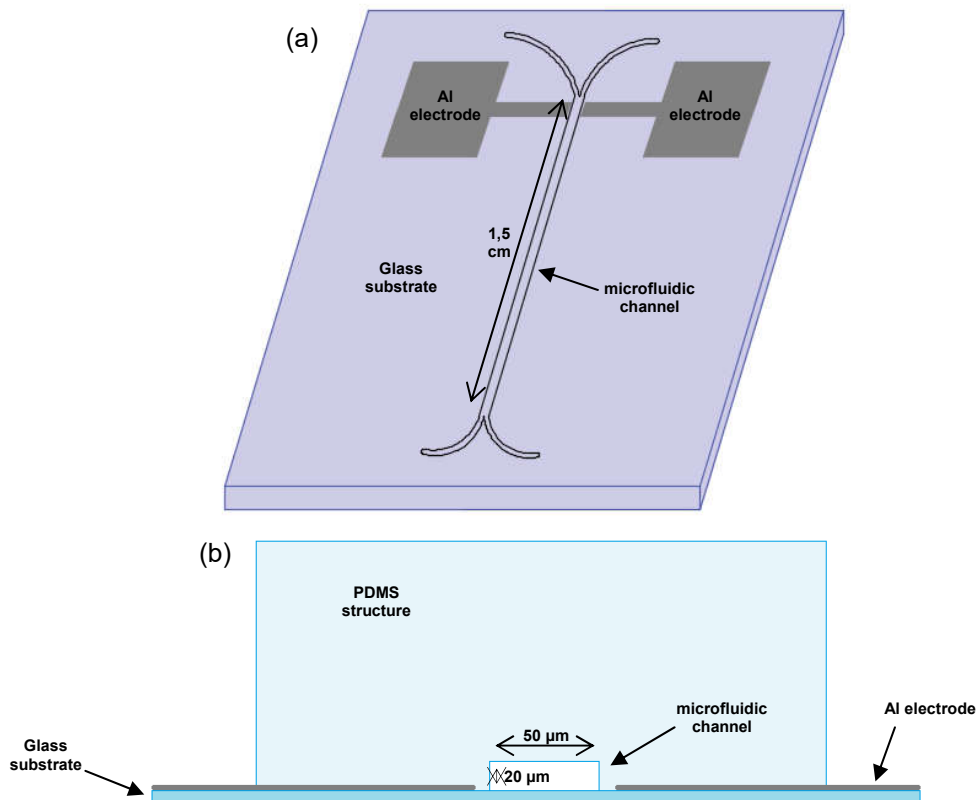


Figure 7.1 - (a) schematic representation of the electrode placement in the microfluidic platform. The light blue is the glass substrate while the gray is the aluminum electrodes. The location for the microchannel is highlighted by black lines. (b) Transversal schematic view of the microchannel at the site where the Al electrodes are present.

However aligning the microchannel with the electrode gap properly is not a simple task, considering that a microchannel is usually from tens to hundreds of micrometers and the gap would have to be only slightly bigger than the microchannel to allow the close proximity of the electrodes to the microchannel. Initially, both the glass substrate and the PDMS with the embossed microchannel would have alignment marks to aid the alignment process. However, at the micro-scale, it was difficult to make the alignment manually with repeatability. So a self-aligned method was developed.

The aluminum electrodes would be patterned without a gap, and the glass was to be used to seal the PDMS structure. Afterwards, an Al etchant solution was loaded in the microchannel at a rate of 3 $\mu\text{L}/\text{min}$ to etch the gap between the electrodes as is stated in section 3.3. Once the gap forms, the flow of Al etch is stopped and then mili-Q water is then loaded in the microchannel at a rate of 5 $\mu\text{L}/\text{min}$ to wash the Al etchant from the microchannel and thus end the etching process. With this method, the alignment of the microchannel could be made with precision and reproducibly. Also, since the strength of the electrical field is inversely proportional to the width of the electrodes, the width of the microchannel was significantly reduced from previous experiments (Figure 7.2).



Figure 7.2 - Image obtained by microscopy of the microfluidic platform with aluminum electrodes. The micrograph was obtained where the microchannel meets the aluminum electrodes and after the etching of the gap. The microchannel has a width of 50 μm , a height of 20 μm and a length of 3 cm. The black portion is the opaque aluminum.

However, the etching of the gap in the Al electrodes after the sealing process brings a new difficulty. Since the etching of the Al is isotropic, it is important to fully etch the thickness of the electrode while stopping before the etching increases significantly the distance between the electrodes. Therefore a better way to track the etching was adopted. By tracking the resistance between the two sides of the electrodes with a voltmeter, it is possible to follow the etch of the gap.

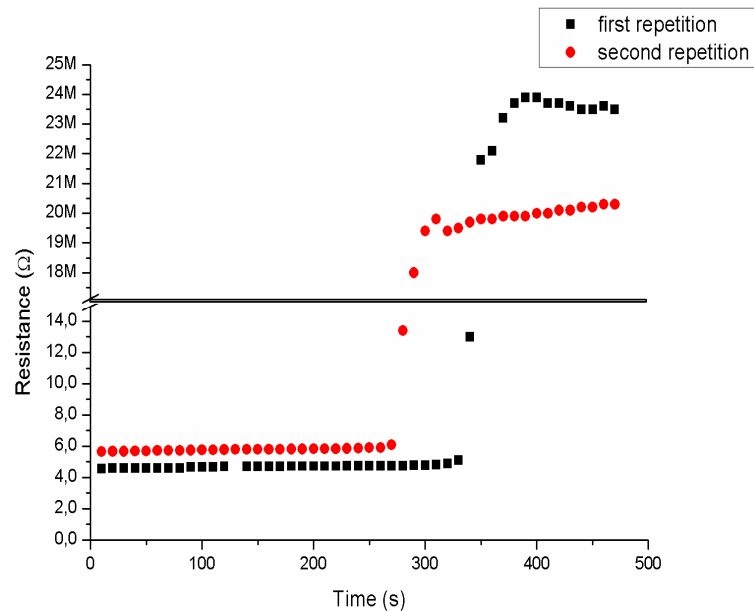


Figure 7.3 - Graphical representation of the measured resistance during the gap etching procedure. Time 0 corresponds to the moment where the Al etchant was inserted in the microfluidic channel.

In Figure 7.3 it is observable that the resistance begins at a very low value and that it experiences a sudden and very large increase after some time. The low resistance values at the beginning of the graph is due to the fact that at this point the aluminum electrodes are still

connected and the resistivity of aluminum is only of $2.65 \times 10^{-8} \Omega/m$. When the etch of the gap is complete, the two electrodes are no longer connected, producing an open circuit and causes the increase in the resistance measured. When the increase in resistance is observed, milli-Q water is loaded into the microchannel to wash the Al etchant from the microchannel.

The next step was to insert an established ATPS in the microfluidic platform with electrodes and verify what, if any, would be the effect of the electrical field on the interface of the ATPS. However, once the electrical field was applied, another problem arose.

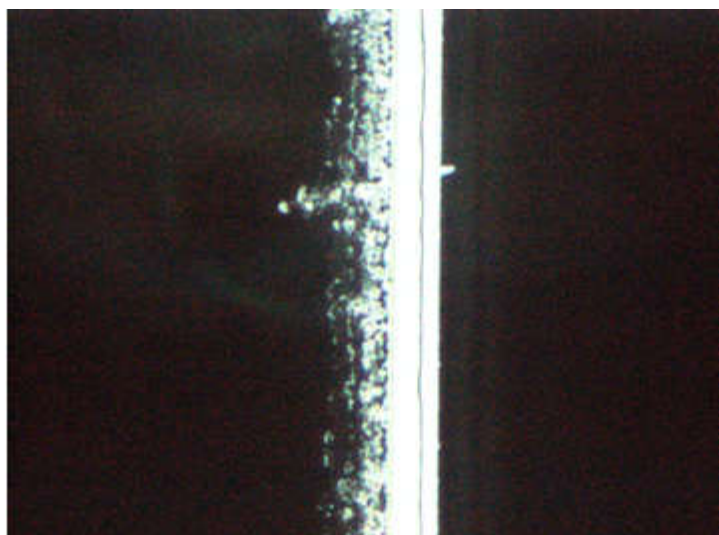


Figure 7.4 - Image obtained by microscopy of the microfluidic platform with deteriorated aluminum electrodes. The micrograph was obtained in the area in the middle of the aluminum electrodes and after the application of an electrical field for about 1 minute. The black portion is the opaque aluminum.

Figure 7.4 shows the effects of an experiment conducted by applying an electrical field to the ATPS interface within the microfluidic platform. In this experiment, the microfluidic platform had a 2 inlet and 2 outlet microchannel with $20 \mu m$ height, $50 \mu m$ width and 3 cm of length. A phosphate buffer and PEG ATPS was inserted in the microchannel. The gap of the electrodes had a width of $50 \mu m$. The ATPS was created by mixing PEG and phosphate in water to a final concentrations of 17,9% of PEG and 14,3% of phosphate buffer. After the phases separated, the phases were collected and each was the inserted in one of the microchannel inlets. The PEG-rich phase was inserted with a loading rate of $0.2 \mu L/min$ and the salt-rich phase was inserted with a loading rate of $0.5 \mu L/min$. The potential difference between electrodes was set at 10V, meaning that the electrical field in the microchannel had a force(E) of $200\ 000 V/m$. Once the electrical field was applied, the edges of the electrodes started to deteriorate almost immediately.

It is likely that this deterioration is due to the fact that the electrodes are in direct contact with the solution at the edge of the microchannel and when the electrical field is applied electrolysis occurs, damaging the electrodes. As such, the gap between the electrodes must be slightly larger than the width of the microchannel and the edges of the electrodes cannot be inside the microchannel. The solution to this situation was to allow the etch of the gap additional

time so that the aluminum would overetch. This would cause the edge of the aluminum to recede from the microchannel.

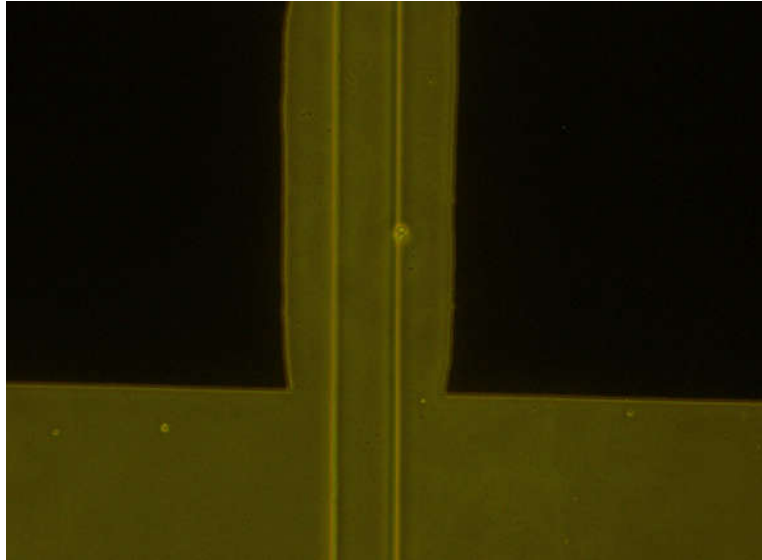


Figure 7.5 - Image obtained by microscopy of the microfluidic platform with aluminum electrodes. The micrograph was obtained where the microchannel meets the aluminum electrodes and after the etching of the gap. The microchannel has a width of $50\ \mu\text{m}$, a height of $20\ \mu\text{m}$ and a length of 3 cm. The black portion is the opaque aluminum. The etching process was allowed to continue for 30 seconds after the resistance increase.

Figure 7.5 shows a microchannel where the etching process was allowed to continue for 30 seconds after the resistance increase. It is possible to clearly see that the edges of the Al electrodes have receded away from the microchannel about $22.4\ \mu\text{m}$ on the right side and $20.5\ \mu\text{m}$ on the left side. While the process works as intended, it is also clear that the time needed for the overetch is also important. In Figure 7.5, an overetch of 30 seconds leads to the gap between the electrodes being nearly the triple of the width of the microchannel, which is much more than needed.

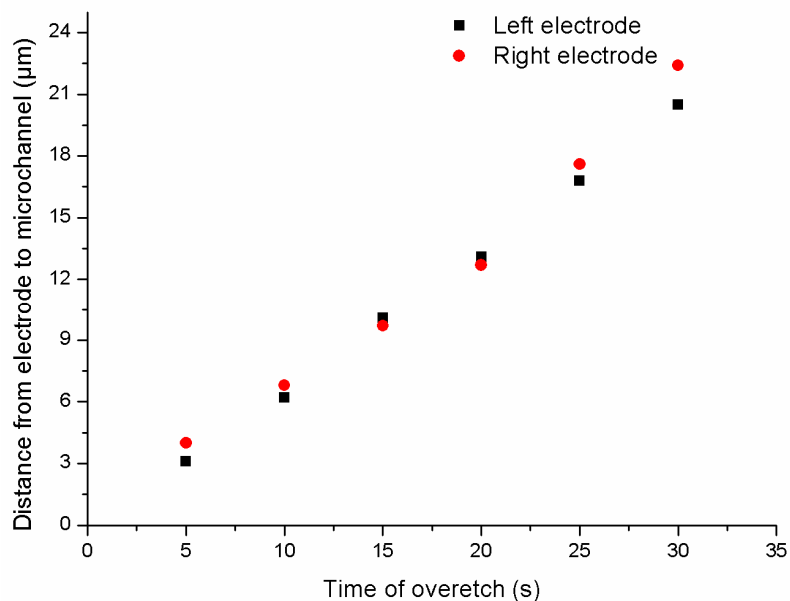


Figure 7.6 - Graphical representation of the influence of time on the overetch distance. Time 0 corresponds to the time when the resistance increase occurs signifying that the gap between the electrodes has formed.

By observing Figure 7.6 it is easy to understand the effect of time on the Al overetch observed. The final step needed for this method is ensuring that there is no fluid in contact with the electrode. By the end of the overetch step, there is still fluid in contact with the Al, otherwise there would be no overetch. To isolate the Al from the fluid we carried out a procedure similar to the sealing procedure which is detailed in section 3.2.3. First the Al etchant is washed away with milli-Q water and afterwards air is flowed to remove the liquid inside the microchannel. A heating step at 110° C is conducted to evaporate any remaining water. Afterwards the microfluidic platform is put into the oxygen plasma chamber and exposed to UV light. Pressure was applied to the top of the PDMS structure and, afterwards, placed in a hot plate at 110°C to aid the bonding process. This method, described in detail in section 3.3 reseals the area between the electrode and the microchannel thus isolating the electrodes from the fluids in the microchannel. From experiments performed it was discovered that this method did not work perfectly when the overetch duration was of 5 and 10 seconds. Presumably the distance between the Al and the microchannel was too small for the resealing process. Therefore the chosen overetch duration was of 15 seconds. Which leads to an average gap between electrodes of 70 µm for the 50 µm width microchannel.

7.2 Effect of the electrical field on biomolecule partition.

The chosen ATPSs used for the experimentation were a PEG/phosphate ATPS and a PEG/dextran ATPS. The PEG/phosphate ATPS was composed by 14.5% of PEG and 11.7% of phosphate and the PEG/dextran ATPS was composed by 15.8% of PEG and 9.5% of dextran. The biomolecules used for the experiments were insulin-FITC, IgG-FITC, BSA-FITC and ProA-FITC. In each case the biomolecules were dissolved in the ATPS system prior its insertion in the microfluidic platform and then the ATPS phases were separated and each was inserted into one of the two inlets of the microfluidic device.

For the PEG/phosphate ATPS, the results obtained presented a problem. As learned in section 4.1, the PEG-rich phase has a greater affinity for the PDMS wall than the phosphate-rich phase. The two inlet microchannel allows to insert both phases at the same time and, in the beginning of the microchannel, each phase would occupy one side of the microfluidic channel. However, as the fluids progressed through the microchannel, the phosphate-rich phase often would shift from its initial position in contact with one of the side PDMS wall to the center of the microchannel with the PEG-rich phase in both sides. In this situation, the phosphate-rich phase would oscillate constantly, which means that trying to use fluorescent microscopy, which requires large exposition times, was difficult.

Therefore, the testing for the PEG/phosphate ATPS was conducted in a three inlet microfluidic platform. The phosphate-rich phase would be inserted in the middle inlet with the

PEG-rich phase being inserted in both side inlets. Using this method, the oscillation observed in the phosphate-rich phase is not present anymore, allowing the use of fluorescent microscopy.

In this experiment it is expected that there will be two forces affecting the partition of the biomolecules. The affinity of the biomolecules towards each of the phases and the effect of the electrical field on the biomolecules. The affinity of the biomolecules to the ATPS phases is an effect that has already been discussed previously on this work. The effect of the electrical field is dependent on the charge of the biomolecules (Lyklema, 2000). If the biomolecules have a negative charge then the biomolecules will be attracted towards the positive electrode and if the biomolecules have a positive charge then the attraction will be towards the negative electrode. In the event of neutral biomolecules, then the electrical field should have no effect. The experiments conducted were always performed at pH 7. At this pH, the biomolecules considered are all negatively charged.

Due to the directionality of the electrical field, the position of the phases in the microfluidic channel and the position of each electrode is essential for understanding the effect of the electrical field.

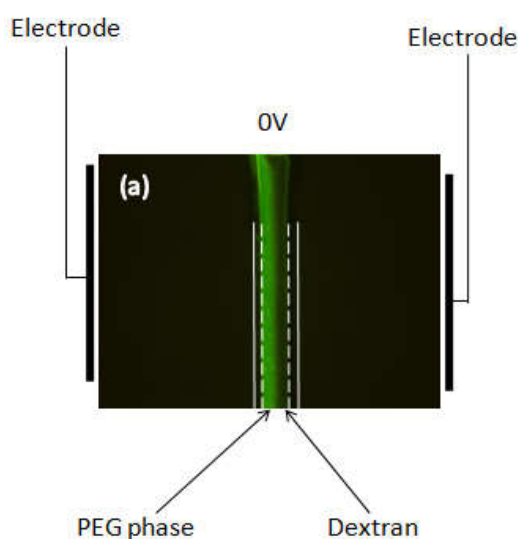


Figure 7.7 - Schematic of the setup used for testing the effect of the electrical field in biomolecule partition in the PEG/dextran ATPS. (a) fluorescent microscopy image of the end of the microchannel. The dashed white lines represent the position of the microchannel walls. The white solid line represents the position of the electrodes edge.

Figure 7.7 shows a schematic of the setup for the experiments with the various biomolecules. The setup was always maintained with the PEG-rich phase inserted in the left side of the microchannel and the dextran inserted in the right side of the microchannel.

Table 7.1 - Variation of biomolecules K_p when subjected to an electrical field. The second row indicates the position of negative and positive electrodes.

Phase position	PEG-rich phase		Dextran-rich phase			
	+/-		0	-/+		
E (kV/m)	570	285	0	285	570	
K_p	Insulin	5.2	5.0	4.8	4.4	4.0
	ProA	1.7	1.5	1.2	0.9	0.7
	BSA	3.7	3.4	3.2	3.0	2.8
	IgG	5.9	5.8	5.6	5.4	5.2

Table 7.1 shows the effect of the electrical field in the K_p of several biomolecules. Considering the charge of the biomolecules at the pH at which the experiments were performed, it was expected that the biomolecules would be attracted by the positive electrode. Since the PEG-rich side was in the left side of the microchannel this means that when the positive electrode was on the left side, the biomolecules would be attracted to the PEG-rich phase meaning an increase in the K_p and when the positive electrode was on the right side, the biomolecules would be attracted to the dextran-rich phase meaning a decrease in the K_p . The experimental data agrees with what would be expected.

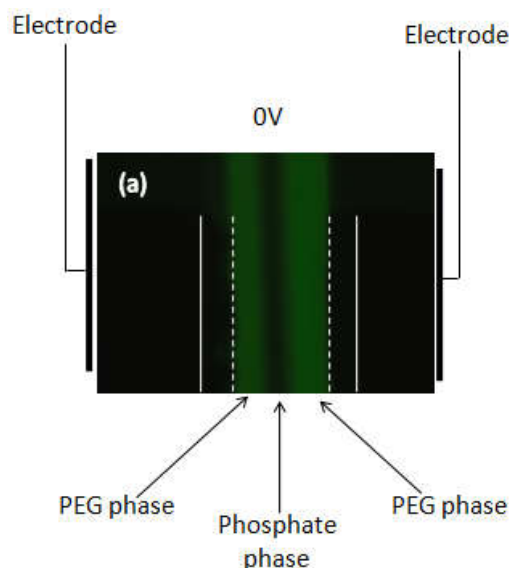


Figure 7.8 - Schematic of the setup used for testing the effect of the electrical field in biomolecule partition in the PEG/phosphate ATPS. (a) fluorescent microscopy image of the end of the microchannel. The dashed white lines represent the position of the microchannel walls. The white solid line represents the position of the electrodes edge.

In Figure 7.8, the setup shows a schematic of the setup for the experiments with the various biomolecules. The setup was always maintained with the PEG-rich phase inserted in the left side and the right side of the microchannel and the phosphate-rich phase inserted in the

middle of the microchannel. Using this system, the insulin-FITC was measured as a function of the electric field and presented in Figure 7.9 and 7.10.

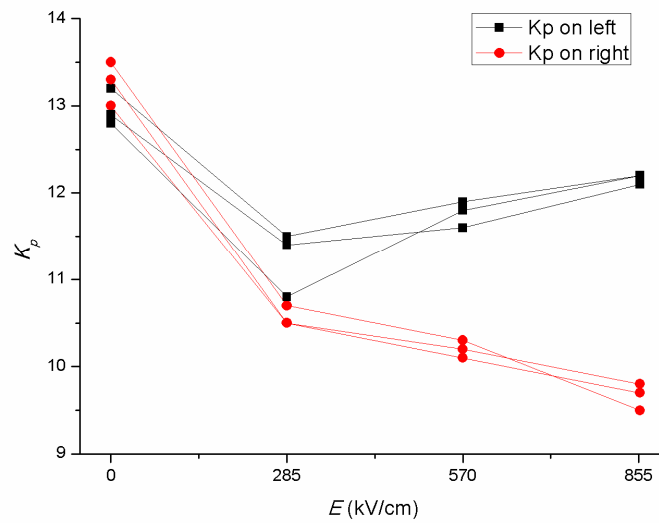


Figure 7.9 - Graphic representation of the K_p shift of insulin-FITC when under the effects of a electrical field (E). The results correspond to the partition coefficient when the positive electrode is on the left side.

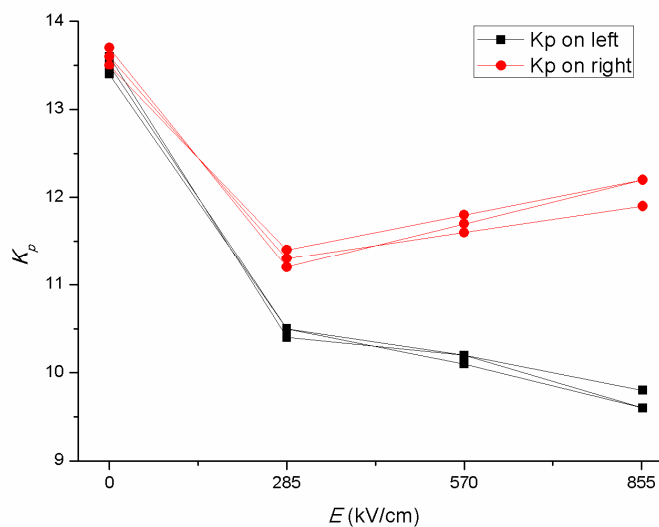


Figure 7.10 -Graphic representation of the K_p shift of insulin-FITC when under the effects of a electrical field (E). The results correspond to the partition coefficient when the positive electrode is on the right side.

Contrary to the case of the PEG/dextran ATPS, the PEG/phosphate ATPS has two interface within the microchannel and thus, we must consider the existence of two K_p . Similar with what happened with the PEG/dextran ATPS, it is expected that the insulin-FITC would be attracted to the positive electrode since insulin has a negative charge at pH 7. In Figure 7.9 and Figure 7.10, The K_p can be observed to drop significantly once the electrical field is applied but

afterwards the behavior becomes what would be expected. Ignoring the first point, the K_p of the interface behaves as expected. The K_p of the side of the positive electrode increases while the K_p of the side of the negative electrode decreases. The decrease of all K_p when the electrical field is applied can be explained by the migration of the biomolecules. When the electrical field is applied, The insulin in the PEG-rich phase that is near the negative electrode will move towards the other side of the microchannel, towards the PEG-rich phase close to the positive electrode. What possibly happens is that some of that insulin remains in the salt-rich phase. Considering that the concentration of insulin in the salt-rich phase is very low without the electrical field, then any small change of insulin concentration in the salt-rich phase would significantly affect the K_p value. Therefore, the small concentration increase of insulin in the salt-rich phase is enough to cause a significant decrease of K_p of both interfaces.

7.3 Conclusions

The proposed method of electrode implementation in the microfluidic platform proved to be successful. It was demonstrated that the aluminum electrodes without a gap between them could be etched into a glass surface and then the glass surface used to seal the PDMS microfluidic platform. The gap would then be etched by flowing Al etchant through the microchannel in the microfluidic platform. This allowed for a gap that is naturally perfectly aligned with the microchannel and it is also easy to follow the etching process by measuring the resistance between the electrodes. It is also possible to widen the gap beyond the microchannel in a somewhat controlled process by extending the etching time.

The applied electrical field had the expected effects by attracting the biomolecules tested, which were negatively charged at the fluids pH, towards the positive electrode. This effect was especially visible in the use of the PEG/phosphate ATPS, since there were two interfaces, one in each side of the microchannel.

8 Conclusions and future Perspectives

ATPS has, for a long time, already been established as a cost-effective method of separation. However, ATPS is still not a perfectly understood technique. The theoretical mechanisms by which a solution can separate into two or more phases are not fully known, which means that optimization of ATPS based extraction is still a time and cost-demanding empirical process. The introduction of ATPS to microfluidics can help reduce the time and cost needed by the optimization process. The work developed in this thesis had a general purpose to help understanding how can microATPS help with the optimization process.

A microfluidic device with a three inlets/three outlets design was fabricated using soft-lithography techniques based on PDMS and successfully demonstrated for the extraction of IgG with ATPS. It was possible to establish a stable, laminar flow of the two aqueous phases in the microfluidic network. Partition studies with FITC labeled IgG performed in PEG/phosphate ATPS showed a decrease of the fluorescence of the salt-rich phase, indicating partitioning of the IgG-PEG-rich phase, as observed in macro-scale experiments. Furthermore, it was demonstrated that the reduction to the microscale does not greatly affect the antibody extraction yield when compared with macroscale results, but it does reduce the operation time. A mathematical model was developed to simulate the partition behavior of the FITC-labeled antibody, showing good agreement with experimental results.

The ATPS chip developed for IgG extraction has great potential in biotechnology as an example of an application of microscale lab-on-a-chip devices as a generic technological platform capable of monitoring and optimizing the pharmaceutical production process, and, in particular, provides a demonstration of miniaturized downstream processing in the case of protein drugs such as therapeutic antibodies.

A microfluidic platform capable of determining ATPS formation was also successfully demonstrated. Using this device, a method to allow a rapid determination of the conditions leading the system to separate into two phases, when the conditions for phase separation are met, was developed. Moreover the data gathered was used to plot binodal curves which present similarities to the binodal curves determined using the turbidometric titration technique, the standard macroscale method. This method provides an easy, fast, inexpensive and continuous approach for the determination of the binodal curve, providing an alternative to the time-consuming traditional methods.

A microfluidic platform that can determine the partition coefficients of biomolecules in different ATPS with high speed and low material consumption was also developed. Moreover, the data gathered by this microfluidic approach are quantitatively similar to the data from the macroscale approach. This method provides an easy, fast, inexpensive and continuous

approach for the determination of partition coefficients, providing an alternative to the time-consuming traditional methods. In comparison, the macroscale approach can take up to a day and requires a minimum of tens of milliliters of solutions. Furthermore, since the microfluidics-based process uses image processing software to determine the partition coefficient within the microchannel without a need to separate the phases, this could allow for the automation of the process eliminating human error and further reducing the time required for the K_p screening process.

Combination of the microATPS extraction with electrophoresis showed that, beyond the partition caused by the ATPS, the electrical field has a visible effect on the partition coefficient and that is possible to control the force and direction of said effect allowing for an even greater customization of the partition process.

The application of ATPS to the recovery of biomolecules still requires a somewhat trial-and-error approach since the behavior of a given biomolecule in the partition environment is unique. This is due to the chemical and physical interactions related to surface hydrophobicity, charge, and size that are involved in the partitioning process and that gain particular importance in a microfluidic environment. Thus, the use ATPS in an integrated microfluidic system for microscale protein purification using an automated high-throughput platform for cell separation, biopharmaceuticals purification and analysis could potentially provide a means to speed up the process optimization of ATPS in downstream processing.

ATPS has proven to be an very versatile tool for separation. One of its greater drawbacks, that it generally cannot be continuous, is negated by the laminar flowing nature of microfluidics. The several works in this thesis have demonstrated the great potential and versatility that microATPS has. It is possible to miniaturize already established systems to have a continuous ATPS extraction. Also, the quick diffusion in microfluidics also allow for faster characterization of ATPS systems. Additionally, it was also possible to combine microATPS extraction with another technique (electrophoresis) to increase control over the partition.

With that said, there is still a lack of theoretical knowledge on the behavior of ATPS within a microfluidic channel, which means that most of the work that is developed currently is of an empirical nature. A systematic study of how ATPS behaves in laminar microfluidic flow and how the partition occurs in microfluidics, could help future work in this area. Furthermore, while there is a short study on the effect of the electrical field in microATPS extraction, a more complete and in depth study should be performed to ascertain the potential of these two techniques combined or the possibility that microATPS can be combined with other methods of separation.

9 Bibliography

Albertsson, A. "chapter 2: Aqueous Biphasic System. Properties and Applications in Bioseparations." In *Aqueous Biphasic Separations: Biomolecules to Metal Ions*, by A. Albertsson, 21-31. Springer Science & Business Media, 1995.

Azevedo, A. M., Gomes, A. G., Rosa, P. A. J., Ferreira, I. F., Pisco, A., and Aires-Barros, M. R. "Partitioning of human antibodies in polyethylene glycol–sodium citrate aqueous two-phase systems." *Separation and Purification Technologies*, 2009: 14-21.

Azevedo, A. M., Rosa, P. A. J., Ferreira, I. F., and Aires-Barros, M. R. "Optimization of aqueous two phase extraction of human antibodies". *Journal of biotechnology*, 2007: 2011 – 2021.

Azevedo, A. M., Rosa, P. A. J., Ferreira, I. F., and Aires-Barros, M. R. "Chromatography-free recovery of biopharmaceuticals through aqueous two phase processing". *Trends in Biotechnology*, 2009: 240 – 247.

Beebe, D., Mensing, G. and Walker, G. "Physics and applications of microfluidic in biology." *Annual Review Biomedical engineering*, 2002: 261-286.

Benavides, J., and Palomares, M. R. "Review, Practical experiences from the development of aqueous two phase processes for the recovery of high value biological products". *Journal of Chemical Technology and Biotechnology*, 2008: 133 – 142.

Bensch, M., Björn S., and Jürgen H.. "High Throughput Screening Techniques in Downstream Processing: Preparation, Characterization and Optimization of Aqueous Two Phase System". *Chemical Engineering Science*, 2007: 2011 – 2021.

Boer, A., Bruyneel, B., Krabbe, J., Lingeman, H., Niessen, W., and Irth, H. "A microfluidic-based enzymatic assay for bioactivity screening combined with capillary liquid chromatography and mass spectrometry." *Lab on a Chip*, 2005: 1286-1292.

Boxshall, K., Wu, M. H., Cui, Z., Cui, Z., Watts, J. F., and Baker, M. A. "Simple surface treatments to modify protein adsorption and cell attachment properties within a poly(dimethylsiloxane) micro-bioreactor". *SURFACE AND INTERFACE ANALYSIS*, 2006: 198-201.

Campos, C. D. M., Park, J. K., Neuzil, P., Silva, J. A. F., and Manz, A. "Membrane-free electroextraction using an aqueous two-phase system." *RSC advances*, 2014: 49485-49490.

Campos-Pinto, I., Espitia-Saloma, E., Rosa, S., Rito-Palomares, M., Aguilar, O., and Aires-Barros, M. R. "Integration of cell harvest with affinity-enhanced purification of monoclonal antibodies using aqueous two-phase systems with a dual tag ligand." *Separation and Purification Technology*, 2017: 129-134.

Cheng, X.; Irimia, D.; Dixon, M.; Sekin, K.; Demirci, U.; Zamir, L.; Tompkins, R.; Rodriguez, W.; Toner, M.. "A microfluidic device for practical label-free CD4+ T cell counting of HIV-infected subjects." *Lab on a Chip*, 2007: 170-178.

Cussler, E. L. *Diffusion: Mass Transfer In Fluid Systems, 3rd edition*. Cambridge University Press, 2009.

Diamond, A.D., and Hsu, J. T. "Aqueous Two-Phase Systems for Biomolecule Separation". *Advances in Biochemical Engineering, biotechnology*, 1992: 81 – 131.

Dong, Y., Zhang, F., Wang, Z., and Du, L. "Extraction and purification of recombinant human serum albumin from *Pichia pastoris* broths using aqueous two-phase system combined with hydrophobic interaction chromatography." *Journal Chromatography A*, 2012: 143-149.

Eggersgluess, J. K., Richter, M., Dieterle, M., and Strube, J. "Multi-stage aqueous two-phase extraction for the purification of monoclonal antibodies." *Chemical engineering technology*, 2014: 675-682.

Esmanhoto, E., and Kilikian, B. V. "ATPS applied to extraction of small molecules - polycetides - and simultaneous clarification of culture media with filamentous microorganisms." *Journal of chromatography B*, 2004: 139-143.

Frampton, J., Lai, D., Sriram, H., and Takayama, S. "Precisely targeted delivery of cells and biomolecules within microchannels using aqueous two-phase systems." *Biomedical microdevices*, 2011: 1043-1051.

Hahn, T., Munchow, G., and Hardt, S. "Electrophoretic transport of biomolecules across liquid-liquid interfaces." 2011: 1-8.

Hu, R.; Feng, X.; Chen, P.; Fu, M.; Chen, H.; Guo, L.; Bi-Feng, L. "Rapid, highly efficient extraction and purification of membrane proteins using a microfluidic continuous-flow based aqueous two-phase system". *journal of chromatography A*, 2007: 171-177.

Huang, F., Liao, C., and Lee, G. "An integrated microfluidic chip for DNA/RNA amplification, electrophoresis separation and on-line optical detection." *Electrophoresis*, 2006: 3297-3305.

Huang, Y., Meng, T., Guo, T., and Li, W. "Aqueous two-phase extraction for bovine serum albumin (BSA) with co-laminar flow in a simple coaxial capillary microfluidic device." *Microfluidics and Nanofluidics*, 2013: 483-491.

Huddleston, J., Veide, A., Köhler, K., Flanagan, J., Enfors, S., and Lyddiatt, A. "The molecular basis of partitioning in aqueous two-phase systems". *Trends in Biotechnology*, 1991: 381-388.

Huh, Y. S., Jeong, C. M., Chang, H. N., Lee, S. Y., Hong, W. H., and Park, T. J. "Rapid separation of bacteriorhodopsin using a laminar-flow extraction system in a microfluidic device". *BIOMICROFLUIDICS*, 2010.

Huh, Y. S., Jeong, C. M., Lee, E. Z., Park, H. S., and Hong, W. H. "Microfluidic extraction using two phase laminar flow for chemical and biological applications." *Korean Journal Chemical Engineering*, 2011: 633-642.

Jacinto, M., Soares, R., Azevedo, A., Chu, V., Conde, J. P., and Aires-Barros, M. R. "Optimization and miniaturization of aqueous two phase systems for the purification of recombinant human immunodeficiency virus-like particles from a CHO cell supernatant." *Separation and Purification Technology*, 2015: 27-35.

Kepka, C., J. Rhodin, R. Lemmens, F. Tjerneld, and P. Gustavsson. "Extraction of plasmid DNA from Escherichia coli cell lysate in a thermoseparating aqueous two-phase system." *Journal of chromatography A*, 2004, 23 ed.: 95-104.

Kruger, J., K. Singh, A. O'Neill, Jackson C., A. Morrison, and P. O'Brien. "Development of a microfluidic device for fluorescence activated cell sorting." *Journal of Micromechanics and Microengineering*, 2002.

Ladd Effio, C., L. Wenger, O. Otes, S. Oelmeier, R. Kneusel, and J. Hubbuch. "Downstream processing of virus-like particles: Single-stage and multi-stage aqueous two-phase extraction." *Journal of chromatography A*, 2015: 35-46.

Lei, Kin F. "Materials and Fabrication Techniques for Nano- and Microfluidic Devices." *Microfluidics in Detection Science: Lab-on-a-chip Technologies*, 2014: 1-28.

Lin, Y. K., C. W. Ooi, J. S. Tan, and P. L. Show. "Recovery of human interferon alpha-2b from recombinant Escherichia coli using alcohol/salt-based aqueous two-phase systems." *Separation and Purification Technologies*, 2013: 362-366.

Lindblad, Mark A. "Numerical studies on two phase flow electrophoresis". worcester polytechnic institute, 2009.

Lyklema, J. *Fundamentals of Interface and Colloid Science*. Academic Press, 2000.

Mark, S. W., M. L. Radomsky, K. J. Whaley, and R.A. Cone. "Antibody Diffusion in Human Cervical Mucus". *Biophysical Journal*, 1994: 508-515.

McDonald, J. Cooper; Duffy, David C.; Anderson, Janelle R.; Chiu, Daniel T.; Wu, Hongkai; Schueller, Olivier J. A.; Whitesides, George M. "Fabrication of microfluidic systems in poly(dimethylsiloxane)". *Electrophoresis*, 2000: 27-40.

Meagher, R. J., Y. K. Light, and A. K. Singh. "Rapid, continuous purification of proteins in a microfluidic device using genetically-engineered partition tags". *Lab on a chip*, 2008: 527–532.

Mehling, M., and S. Tay. "Microfluidic cell culture." *Current Opinion in Biotechnology*, 2014: 95-102.

Merchuk, J., B. Andrews, and J. Ansejo. "Aqueous two-phase systems for protein separation: studies on phase inversion." *Journal of chromatography B*, 1998: 285–293.

Munchow, G., S. Hardt, J. Kutter, and K. Drese. "Electrophoretic partitioning of proteins in two-phase microflows." *Lab on a Chip*, 2006: 98-102.

Munchow, G., S. Hardt, J.P. Kutter, and K.S. Drese. "Protein Transport and Concentration by Electrophoresis in Two-phase Microflows." *JALA*, 2006: 368–73.

Murphy, K., Paul T., and Mark W.. *Janeway's immunobiology 7th edition*. Garland Science, 2008.

Nam, K. H., W. J. Chang, H. Hong, S. M. Lim, D. I. Kim, and Y. M. Koo. "Continuous-flow fractionation of animal cells in microfluidic device using aqueous two-phase extraction". *Biomedical Microdevices*, 2005: 189-195.

Ng, H. S., C. P. Tan, M. N. Mokhtar, and S. Ibrahim. "Recovery of Bacillus cereus cyclodextrin glycosyltransferase and recycling of phase components in an aqueous two-phase system using thermoseparating polymer." *Separation and Purification Technologies*, 2012: 9-15.

Ooi, C. W., S. L. Hii, S. M. M. Kamal, A. Ariff, and T. C. Ling. "Extractive fermentation using aqueous two-phase systems for integrated production and purification of extracellular lipase derived from Burkholderia pseudomallei." *Processes in biochemistry*, 2011: 68-73.

Paegel, B., R. Blazej, and R. Mathies. "Microfluidic devices for DNA sequencing: sample preparation and electrophoretic analysis." *Current Opinion in Biotechnology*, 2003: 42-50.

Pereira, J. F. B., S. P. M. Ventura, F. A. Silva, and S. Shahriari. "Aqueous biphasic systems composed of ionic liquids and polymers: A platform for the purification of biomolecules." *Separation and Purification Technologies*, 2013: 83-89.

Pereira, J. F. B., V. C. Santos, H.-O. Johansson, and J. A. C. Teixeira. "A stable liquid-liquid extraction system for clavulanic acid using polymer-based aqueous two-phase systems." *Separation and Purification Technologies*, 2012: 441-450.

Pereira, J.; Vicente, F.; Santos-ebinuma, V.; Araújo, J.; Pessoa, A.; Freire, M.; Coutinho, J. "Extraction of tetracycline from fermentation broth using aqueous two-phase systems composed of polyethylene glycol and cholinium-based salts." *Process Biochemistry*, 2013: 716-722.

Prinz, A., J. Hönig, I. Schüttmann, H. Zorn, and T. Zeiner. "Separation and purification of laccases from two different fungi using aqueous two-phase extraction." *Process biochemistry*, 2014: 335-346.

Przybycien, T. M., N. S. Pujar, and L. M. Steele. "Alternative bioseparation operations: life beyond packed-bed". *Current Opinion in Biotechnology*, 2004: 469-478.

Purcell, E. M., and D. J. Morin. *Electricity and Magnetism*. Harvard: Cambridge University Press, 2013.

Qi, L., Y. Wang, Y. Li, and G. Zheng. "Microfluidic aqueous twophase extraction of bisphenol A using ionic liquid for high-performance liquid chromatography analysis." *Analytical and Bioanalytical chemistry*, 2015: 3617-3625.

Rämsch, C., L. Kleinlanghorst, E. Knieps, J. Thömmes, and M. Kula. "Aqueous two-phase systems containing urea: Influence of protein structure on protein partitioning." *Biotechnology and Bioengineering*, 2000: 83-90.

Reddy, V., and J. D. Zahna. "Interfacial stabilization of organic-aqueous two-phase microflows for a miniaturized DNA extraction module". *Journal of Colloid and Interface Science*, 2005: 158-165.

Rosa, P.A.J., A.M. Azevedo, S. Sommerfeld, M. Mutter, M.R. Aires-Barros, and W. Bäcker. "Application of aqueous two-phase systems to antibody purification: A multi-stage approach". *Journal of Biotechnology*, 2009: 306–313.

Rosa, P.A.J., A.M. Azevedo, S. Sommerfeld, M. Mutter, W. Backer, and M.R. Aires-Barros. "Continuous purification of antibodies from cell culture supernatant with aqueous two-phase systems: From concept to process." *Biotechnology Journal*, 2012: 352-362.

Rosa, P.A.J.; Azevedo, A.M.; Ferreira a, I.F.; Vries, J. de; Korporaal, R.; Verhoef, H.J.; Visser, T.J.; Aires-Barros, M.R. "Affinity partitioning of human antibodies in aqueous two-phase systems". *Journal of Chromatography A*, 2007, 1162 ed.: 103–113.

Schneider, C., W. Rasband, and Eliceiri K. "NIH Image to ImageJ: 25 years of image analysis." *Nature Methods*, 2012: 671-675.

Schoonen, J., V. Duinen, A. Oedit, P. Vulto, T. Hankemeier, and P. Lindenburg. "Continuous-Flow Microelectroextraction for Enrichment of Low Abundant Compounds." *Analytical chemistry*, 2014: 8048-8056.

Show, P. L., C. P. Tan, M. Shamsul Anuar, and A Ariff. "Extractive fermentation for improved production and recovery of lipase derived from *Burkholderia cepacia* using a thermoseparating polymer in aqueous two-phase systems." *Bioresources Technologies*, 2012: 226-233.

Shu, Y., M. Gao, X. Wang, and R Song. "Separation of curcuminoids using ionic liquid based aqueous two-phase system coupled with in situ dispersive liquid-liquid microextraction." *Talanta*, 2016: 6-12.

Shui, L., J. C. T. Eijkel, and A. Berg. "Multiphase flow in microfluidic systems – Control and applications of droplets and interfaces". *Advances in Colloid and Interface Science*, 2007: 35 – 49.

Sia, S. K., and G. M. Whitesides. "Microfluidic devices fabricated in poly(dimethylsiloxane) for biological studies". *Electrophoresis*, 2003: 3563–3576.

Silva, D., A. Azevedo, P. Fernandes, V. Chu, J. Conde, and M. Aires-Barros. "Design of a microfluidic platform for monoclonal antibody extraction using an aqueous two-phase system." *Journal of Chromatography A*, 2012: 1-7.

Silva, D., A. Azevedo, P. Fernandes, V. Chu, J. Conde, and M. Aires-Barros. "Determination of aqueous two phase system binodal curves using a microfluidic device." *Journal of Chromatography A*, 2014: 115-120.

Silva, D., A. Azevedo, P. Fernandes, V. Chu, J. Conde, and M. Aires-Barros. "Determination of partition coefficients of biomolecules in a microfluidic aqueous two phase system platform using fluorescence microscopy." *Journal of chromatography A*, 2017.

Silva, L. H. M., and W. Loh. "Sistemas Aquosos Bifásicos: Fundamentos e Aplicações Para Partição/Purificação de Proteínas". *Química Nova*, 2006: 1345-1351.

Soares, R. R., P. Novo, A. M. Azevedo, P. Fernandes, V. Chu, and R. Aires-Barros. "On-chip sample preparation and analyte quantification using a microfluidic aqueous two-phase extraction coupled with an immunoassay." *Lab-on-a-Chip*, 2014: 4284-4294.

Soares, R., A. Azevedo, J. Alstine, and M. Aires-Barros. "Partitioning in aqueous two-phase systems: Analysis of strengths, weaknesses, opportunities and threats." *Biotechnology Journal*, 2015: 1158–1169.

Soares, R., A. Azevedo, P. Fernandes, V. Chu, J. Conde, and M. Aires-Barros. "A simple method for point-of-need extraction, concentration and rapid multi-mycotoxin immunodetection in feeds using aqueous two-phase systems." *Journal of Chromatography A*, 2017: 15-24.

Soares, R., A. Azevedo, P. Fernandes, V. Chu, J. Conde, and M. Aires-Barros. "Aqueous two-phase systems for enhancing immunoassay sensitivity: Simultaneous concentration of mycotoxins and neutralization of matrix interference." *Journal of Chromatography A*, 2014: 67-76.

Soares, Ruben R. G., Silva, Daniel F. C., Fernandes, Pedro, Azevedo, Ana M., Chu, Virginia, Conde, João P., Aires-Barros, M. Raquel. "Miniaturization of aqueous two-phase extraction for biological applications: From micro-tubes to microchannels." *Biotechnology Journal*, 2016: 1-15.

Soohoo, J.R., and G.M. Walker. "Microfluidic aqueous two phase system for leukocyte concentration from whole blood". *Biomedical Microdevices*, 2009: 323-329.

Sousa, A.; Andrade, P.; Pirzgalska, R.; Galhoz, T.; Azevedo, A.; Silva, C.; Aires-Barros, M.; Cabral, J. "A novel method for human hematopoietic stem/progenitor cell isolation from umbilical cord blood based on immunoaffinity aqueous two-phase partitioning." *Biotechnology Letters*, 2011: 2373–2377.

Souza, R. L., S. P. M. Ventura, C. M. F. Soares, and J. A. P. Coutinho. "Lipase purification using ionic liquids as adjuvants in aqueous two-phase systems." *Green Chemistry*, 2015: 3026-3034.

Stichlmair, J., J. Schmidt, and R. Proplesch. "Electroextraction: a novel separation technique." *Chemical Engineering Science*, 1992: 3015-3022.

Stone, H. A., and S. Kim. "Microfluidics: Basic Issues, Applications, and Challenges." *AIChE Journal*, 2001: 1250-1254.

Theo, C., and W. Clark. "Electroextraction." *Applied Biochemistry and Biotechnology*, 1995: 143-157.

Tiselius, A., J. Porath, and Albertsson P. "Separation and Fractionation of Macromolecules and Particles." *Science*, 1963: 13-20.

Tsukamoto, M., S. Taira, S. Yamamura, Y. Morita, and N. Nagatani. "Cell separation by an aqueous two-phase system in a microfluidic device". *Analyst*, 2009: 1994–1998.

Weibel, D.B., W.R. DiLuzio, and G.M. Whitesides. "Microfabrication meets microbiology". *Nat Rev Micro*, 2007: 209-218.

Wiendahl, M., S. A. Oelmeier, F. Dimer, and J. Hubbuch. "Highthroughput screening-based selection and scale-up of aqueous two-phase systems for pDNA purification." *Journal of Separation Sciences*, 2012: 3197-3207.

Xia, Y., and G. M. Whitesides. "Soft Lithography." *Angew. Chem. Int. Ed.*, 1998: 550-575.

Yamada, M., V. Kasim, M. Nakashima, J. Edahiro, and M. Seki. "Continuous Cell Partitioning Using an Aqueous Two-Phase Flow System in Microfluidic Devices". *Biotechnology and Bioengineering, Biotechnology and Bioengineering*, 2004: 489-494.

Zhang, C., J. Xu, W. Ma, and W. Zheng. "PCR microfluidic devices for DNA amplification." *Biotechnology Advances*, 2006: 243-284.